Terahertz Micro-Doppler Radar for Detection and Characterization of Multicopters

by

Bharath Gundappa Kashyap

A Thesis Presented in Partial Fulfillment
of the Requirements for the Degree
Master of Science

Approved July 2018 by the
Graduate Supervisory Committee:

Georgios C. Trichopoulos, Chair
Constantine A. Balanis
James T. Aberle

ARIZONA STATE UNIVERSITY

August 2018

ABSTRACT

The micromotions (e.g. vibration, rotation, etc.,) of a target induce time-varying frequency modulations on the reflected signal, called the micro-Doppler modulations. Micro-Doppler modulations are target specific and may contain information needed to detect and characterize the target. Thus, unlike conventional Doppler radars, Fourier transform cannot be used for the analysis of these time dependent frequency modulations. While Doppler radars can detect the presence of a target and deduce if it is approaching or receding from the radar location, they cannot identify the target. Meaning, for a Doppler radar, a small commercial aircraft and a fighter plane when gliding at the same velocity exhibit similar radar signature. However, using a micro-Doppler radar, the time dependent frequency variations caused by the vibrational and rotational micromotions of the two aircrafts can be captured and analyzed to discern between them. Similarly, micro-Doppler signature can be used to distinguish a multicopter from a bird, a quadcopter from a hexacopter or a octacopter, a bus from a car or a truck and even one person from another. In all these scenarios, joint time-frequency transforms must be employed for the analysis of micro-Doppler variations, in order to extract the targets' features.

Due to ample bandwidth, THz radiation provides richer radar signals than the microwave systems. Thus, a Terahertz (THz) micro-Doppler radar is developed in this work for the detection and characterization of the micro-Doppler signatures of quadcopters. The radar is implemented as a continuous-wave (CW) radar in monostatic configuration and operates at a low-THz frequency of 270 GHz. A linear time-frequency transform, the short-time Fourier transform (STFT) is used for the analysis the micro-Doppler signature. The designed radar has been built and measurements are carried out

using a quadcopter to detect the micro-Doppler modulations caused by the rotation of its propellers. The spectrograms are obtained for a quadcopter hovering in front of the radar and analysis methods are developed for characterizing the frequency variations caused by the rotational and vibrational micromotions of the quadcopter. The proposed method can be effective for distinguishing the quadcopters from other flying targets like birds which lack the rotational micromotions.

To my mom, dad, sister and family

ACKNOWLEDGMENTS

I would like to express my deepest gratitude to Prof. Georgios C. Trichopoulos for skillful mentoring and attentive supervision throughout the duration of my thesis. Without his guidance and support this thesis would not have been possible.

I would like to thank my committee members, Prof. Constantine A. Balanis and Prof. James T. Aberle for their valuable suggestions.

I would also like to thank my lab colleagues Panagiotis Theophanopoulos, Yiran Cui, Mohammad Sakr and Sai Kiran Doaddalla for creating a pleasant working environment and for the quality discussions.

I would like to thank my friends, Subramanian Ramalingam, Manoj Babu and Shreyas Manjunath, whose support was instrumental to the success of this thesis.

Last but foremost, I would like to offer my special thanks to my mom, dad, sister and my entire family, for supporting me through all my endeavors.

TABLE OF CONTENTS

Page

CHAPTER Page

CHAPTER Page

LIST OF FIGURES

Figure Page

Figure Page

CHAPTER 1

INTRODUCTION

1.1 Motivation and Objectives

The ever-growing popularity of *multicopters*, more colloquially known as drones, owing to the ease of their operation, nonessential training, affordable prices and a plethora of applications for photography, gaming and leisure activities has led to their prevalence in the current world. They come in various sizes and shapes and in application-specific configurations. Although, most people use these *unmanned aerial vehicles* (UAVs) for relaxations and entertainment purposes, there are quite a few who misuse the capabilities of multicopters such as the smaller cross section, the excellent camera, the long operating ranges and the payload carrying abilities to perform illegal activities. The use of multicopters for illegal surveillance, harmful chemical/ biological agent disposal, trafficking drugs etc., have raised a lot of concerns. As such, it is high time that counter measures are developed for the detection of such aerial vehicles.

There are many methods for detection of multicopters, the prominent of which are the camera-based techniques and the radar-based techniques. Although camera-based techniques come with the possibilities such as clear images of the target which are easy to interpret, they cannot operate effectively in the presence of trees, rain, fog or during the night. On the other hand, all these requirements can be easily accomplished using radars which makes them more robust. Radars also have the capabilities of piercing thin walls, and longer range when compared to camera-based systems. Due to all these reasons, a radar-based system is employed in this research. The multicopters however, are

characterized as low visibility targets due to their small sizes. At the same time, their *radar cross section* is comparable to that of the birds and this makes their detection and distinction difficult using a conventional Doppler radar system. However, the radar return produced by each target is distinct form other and this feature can be used to distinguish birds from the multicopters. Multicopters are associated with a periodic rotational motion due to their propeller blades and a vibrational motion due the motors which cause time-varying frequency modulations on the backscattered echo signals from them. These additional modulations, which are not seen in the echo signals obtained from the birds, can be efficiently extracted by using a different type of radars called the micro-Doppler radars which are the extensions of the more commonly used Doppler radars. Although, the radar design is the same, the method of extracting the information from the radar return is what makes the micro-Doppler radar stand out. While Doppler radars use Fourier analysis to extract the frequency shift information, micro-Doppler radars use time-frequency analysis to extract the time dependent frequency variations. More details on the differences between the operation of Doppler and micro-Doppler radars along with the analysis methods used in each case will be discussed in the future chapters.

The second important problem that needs to be addressed when using the radar-based techniques is the detection of small – size multicopters with low cross section. High resolution is needed for extracting and segregating the micro-Doppler features due to rotation and vibration. This is a highly challenging task as the parts of the vehicle producing such returns are much smaller than the multicopter itself. It warrants the need for using higher frequencies. As such, this work focuses on designing a *terahertz* (THz) micro-Doppler radar system for detection of multicopters. A quadcopter has been used in this

work to demonstrate the procedure as they are most commonly occurring type of multicopters. The technique used here however, can be easily extended for other multicopters with different sizes and cross-sections.

1.2 Previous Work

Micro-Doppler radars are designed with the intent of exploiting the uniqueness of the radar returns in the form of time varying frequency modulations which are caused by the *micromotions* of the targets. The first occurrence of micro-Doppler phenomenon and its applications can be traced back to late 1990s when it was independently used in a coherent laser radar system and for studying radar returns from a walking person [1], [2]. Rotation, vibration, tumbling and coning motions are some of the commonly encountered motion characteristics in addition to the bulk translational motion of an object. Such additional motions are termed as micromotions. When an object in motion has such micromotions, it induces frequency modulations on the backscattered echo signal which appear as sidebands about the main Doppler shift from the target. This phenomenon is known as the *micro-Doppler effect* [2]. The micro-Doppler features are complementary to the existing Doppler shift information and thus aid in determining the characteristics of the target along with its detection. The most important distinction between Doppler radars and micro-Doppler radars is that the former depends on the time-invariant frequency shift information to detect the presence of a target, while the latter uses the time-varying frequency modulations for detecting as well as characterizing the target. While Fourier analysis is used in Doppler radars, time-frequency analysis techniques are used in micro-Doppler radars.

A very good introduction to the micro-Doppler effect and its applications is given in [2]. A detailed mathematical analysis and simulation study of various micromotions that

give raise to the micro-Doppler features are discussed in this work, along with formulas for vibration induced and rotation induced micro-Doppler modulations. A brief introduction to various time-frequency analysis schemes is included with an emphasis on the smoothed pseudo-Wigner Ville distribution method. A point scatterer model is utilized for demonstrating the basic micromotion dynamics. Many later researches concentrate on improving the resolution of the micro-Doppler feature using different time-frequency algorithms. Oscillating point targets that produce sinusoidal frequency modulations are studied in [3] using *synthetic aperture radars* (SAR) with high-resolution Cohen's class time-frequency methods. In [4], *Fourier – Bessel transforms* (FBT) are used in conjunction with the *fractional Fourier transform* (FrFT) to extract micro-Doppler features from rotating targets. A *quasi-maximum likelihood* (QML) based technique for parameter estimation of micro-Doppler signals is proposed in [5]. A two-stage method has been used here with *short-time Fourier Transform* (STFT) used in the first stage for rough parameter estimation and then QML based technique is used to refine those parameters. [6] presents the micro-Doppler analysis of ballistic targets. The precession and nutation of the warhead and the wobble of the decoys are used to distinguish one from the other. A method for extracting the micro-Doppler features from rotor blades of a helicopter using wavelet transform method is demonstrated in [7]. In [8], a simulation study is carried out for extracting the micro-Doppler modulations induced by the rotational motion of the propeller blades of a multicopter. Detailed description of multicopter features are given in this work along with a HFSS model of the propeller. *Singular value decomposition* (SVD) is used for feature extraction. Most of these works are focused towards operation in the microwave range. Recently however, the demand for higher resolution had led to the exploration of

higher frequencies by researchers. As such, new techniques for operating in the THz domain are being developed. One such approach is demonstrated in [9], where a W-band radar operating at 92 GHz is used extracting micro-Doppler features using STFT and for the automatic measurement of a stationary drone's blade length and its rotation rate.

Another important application of micro-Doppler effect is in the domain of gait analysis. Gait is the manner in which a person walks which again is unique for each human being. As such, this feature can be utilized for identification of human targets by extracting the micro-Doppler modulations induced by various parts of the body while walking. In [10], an ultra-wideband impulse radar is used with the *short-time state-space method* (STSSM) for extracting micro-Doppler features from a walking target. A *Boulic* model of human motion is used for carrying out the simulations and experimental data is cross-verified with the simulations. Wavelet transforms are used in conjunction with time-frequency analysis for extracting human micro-Doppler data in [7]. THz systems are being developed for human gait recognition as well as shown in [11]. The performance of a 292 GHz CW radar is compared with a 24 GHz CW radar to demonstrate the higher resolution and wide bandwidth features of such high frequency systems.

1.3 Scope of this Work

As seen from the literature review, most of the existing works focus on design and development of micro-Doppler radars in the microwave range. While many of them concentrate on the simulation studies, few attempt actual measurements. Although, there have been few high frequency systems in the recent years, the THz micro-Doppler systems for multicopter detection, still need a lot of research, and efficient methods are to be designed for extracting micro-Doppler features. As such, a THz micro-Doppler radar is

developed in this work for detecting and characterizing a quadcopter in flight. A 270 GHz CW Doppler radar in monostatic configuration and a DROCON X708W quadcopter are used to carry out the experiments in the low THz domain and results are presented. This research opens the opportunities for target characterization at higher frequencies with the advantage of higher resolution.

1.4 Outline of the Report

With this general introduction to micro-Doppler, radars and THz, the work now concentrates on combining the features of THz and Doppler radar with the micro-Doppler phenomenon to design a THz micro-Doppler radar. The remaining sections of the report are organized as follows. Chapter 2 introduces the THz and radar concepts. The description of each concept is associated with how it is employed in this work. The advantages and application of using THz and radar-based systems are also outlined in this chapter. Chapter 3 describes the working of THz micro-Doppler radar and gives an overview of multicopter features. Chapter 4 focuses on developing a theoretical analysis for characterizing the targets based on their micro-motions. A point scatterer model is used here to model the propellers of the multicopter and MATLAB is used to generate the expected micro-Doppler signature of the multicopter. Chapter 5 describes the experimental setup developed in this research for detecting micromotions and presents the measurement results obtained using the setup. Chapter 6 summarizes the work and presents avenues for future work.

CHAPTER 2

TERAHERTZ AND RADAR CONCEPTS

2.1 Introduction to Terahertz Technology

The region that lies between the microwave and the infrared regions in the electromagnetic spectrum is termed as the ‘terahertz (THz)’ band. The frequencies in the range, 0.3 THz to 3 THz, are commonly used to carry out operations in this band. These frequencies constitute the wavelengths from 1 mm to .1 mm, thus earning the name submillimeter-wave region for the THz band.

Although there is no clear distinction of where one region starts and the other ends, the frequencies ranging from 30 GHz to 300 GHz called the millimeter-wave region, and 3 THz to 30 THz called the far infrared region, are generally regarded as the immediate neighbors of the THz or the submillimeter-wave region. As such, many applications developed throughout the 0.1 THz to 10 THz frequency range are considered to be a part of the terahertz domain [12]. Though there has been extensive research in the microwave and optical domains, until quite recently, the terahertz region had remained one of the least explored portions of the electromagnetic spectrum. This can be primarily attributed to the technological shortcomings that were involved in the manufacture of efficient and compact THz sources and detectors employing the conventional electronic systems used to generate microwaves [13], [14]. The strong attenuation of the THz signals in the earth’s atmosphere turns out to be another major obstacle for the use of THz radiation for long-range commercial and military applications [15]. Owing to these reasons, the terahertz band is sometimes referred to as the ‘THz gap’ [13].

However, recent technological advancements have enabled the production of transceivers required for operation in the THz region, thus narrowing the so-called THz gap. The growing need for the short-range wide-band communications, high-resolution spectroscopy and remote sensing applications have peaked the interests of researchers in this area. The THz band along with other regions of the electromagnetic spectrum based on their frequency allocations is depicted in figure 2.1. [14].

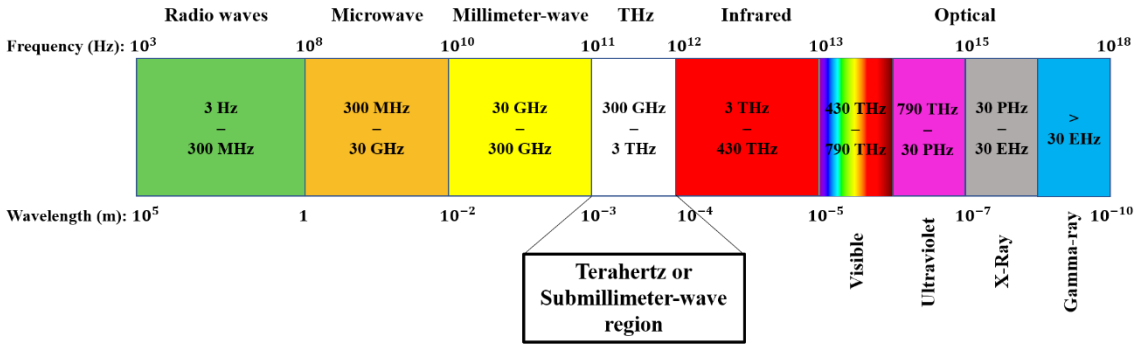

Figure 2.1. Electromagnetic Spectrum with Frequency Allocations for Different Bands.

This work focuses on utilizing a CW Doppler radar operating at a low-THz frequency of 270 GHz for detecting the micromotions of multicopters. This operation needs the generation of THz signals using a suitable method and the use of a suitable detector to decipher the received signals. The following section gives an abstract overview of various methods of THz generation and detection while highlighting the techniques employed in this work.

2.2 Terahertz Sources and Detectors

Terahertz radiation emitted as a part of black-body radiation by most bodies is the natural source of THz signals. Nevertheless, these signals usually have very low energy and cannot be used for practical applications. On the other hand, there are several methods that can be used for the generation of terahertz radiation artificially as well, and they are broadly

classified into two categories. The first method uses frequency down-conversion techniques for THz signal generation. *Optical rectification* and *difference frequency generation* (DFG) are some of the common techniques used in this scheme, where optical signals and femtosecond laser pulses are used to generate broadband THz pulses. *Backward wave oscillators* (BWOs), *free electron lasers* (FELs) *and quantum cascade lasers* (QCLs) are other useful sources for generating terahertz radiation [13].

The second method for generation of THz signals uses frequency up-conversion techniques A microwave signal known as the radio frequency (RF) signal, f_{RF} is first generated form a signal generator which is usually an oscillator. It is up-converted to the desired THz frequency using a series of frequency multiplier circuits incorporated in devices called frequency extenders. This work employs the frequency up-conversion technique for generating THz signals needed for the operation of THz micro-Doppler radar. A detailed description of the signal generation and frequency extender operation is given in chapter 3.

The detection techniques used in the THz realm are broadly classified into two categories. If both the amplitude and the phase of the field are measured by the detector, then it is a coherent detector. On the other hand, if the intensity of the field is measured by the detector, then it is an incoherent detector [13]. Coherent detectors are further classified as homodyne or heterodyne detectors while incoherent detectors are sub divided into power detection and photon detection schemes. A coherent source is usually coupled with a coherent detector while an incoherent source is usually coupled with an incoherent detector, but this might not always be the case [15]. Some of the commonly used coherent detection techniques include free space electro-optic (EO) sampling and sensing with

photoconductive antennas. In heterodyne detection, mixers are used to down convert the signals to an intermediate frequency. Incoherent detection techniques employ bolometers at cryogenic temperatures, Golay cells at room temperatures and pyroelectric detectors in applications involving dynamic temperature variations. In this work, a modified coherent heterodyne detection scheme is employed to down-convert the received THz signal to an intermediate microwave frequency of the order of MHz. However, instead of measuring the field, the intensity of the received power is measured and the micro-doppler features are extracted from it.

The source and the detector together with the target of interest, constitute the THz sensor system. Based on the distance between the source, target and the detector, the THz sensor system can be classified as remote sensor or point sensor.

2.3 Challenges and Advantages of using Terahertz Systems

Just as any other region of the electromagnetic spectrum, operation in the THz region is not free from impediments and presents its own unique challenges. The severe attenuation of the THz signals due to atmospheric absorption is one of the major shortcomings that limits the use of THz radiation for long distance communications such as radar applications. Water vapor is the dominant factor that causes the highly increased propagation losses in the THz region [15]. The smaller wavelength of the THz wave not only brings down the size of the antennas and guiding structures, but also the power handling capabilities of these devices. As a result, only low-power sources can be used for THz operation. This low-power signal upon transmission, undergoes additional propagation losses and loses more energy before reaching the detector. Such signals can be lost within the noise floor of the detector, and thus, extremely accurate detectors with

excellent dynamic range and phase noise characteristics are needed for operation in the THz realm. More accuracy implies costly fabrication techniques for ensuring the desired level of performance. Thus, the THz systems are usually very expensive making them less suitable for commercial applications. As the frequency increases, other materials like connectors, adapter etc., also become expensive and delicate making their handling arduous. They make THz testing a strenuous venture and introduce additional repeatability errors during the measurements which are very difficult to remove. Unlike microwave/millimeter-wave systems where thermal noise dominates or optical systems where shot noise dominates, THz systems are susceptible to both noises, depending on the nature of sensor, radiation and other factors [15]. All these variables effectively increase the noise floor of the detectors, thus act as an added bane to the THz operation.

Most of these problems are solvable with the current techniques and thus, THz operation is gaining an increased interest from the research community. THz band is characterized by smaller wavelengths when compared to microwave or millimeter-wave regions, leading to a reduction in the size of the antennas and wave-guiding structures used in the THz realm, thus, making the system more compact. It also enables the design of large arrays that effectively occupy smaller physical area while offering the advantages of higher directivity, smaller beamwidth and better efficiency which is highly advantageous for short-range radar applications. The smaller wavelength of the THz devices also gives raise to higher spatial resolution than the microwave/ millimeter wave devices. This is the main encouragement for THz imaging systems. Unlike X-rays, THz radiation is non-ionizing. This makes it safe and better suited for biological imaging applications. Although the microwave signals are also non-ionizing, the benefit of higher resolution offered by the

THz radiation gives it an edge over the microwave signals. THz can penetrate most of the non-conducting materials like clothing, plastic, thin walls, paper etc., which are opaque to the optical signals. They also operate using line-of-sight propagation making them suitable for high resolution imaging radars. THz systems are very useful for broadband spectroscopy, remote sensing and non-destructive sensing applications. THz signals do not suffer from the problem of interference from other devices owing to their wide bandwidth and lesser number of devices as compared to microwave/ millimeter wave systems.

2.4 Applications of Terahertz Technology

The principal motivation for any research is the applications and benefits that can be obtained from the techniques and systems designed. As such this section lists some of the important applications of the THz technology.

2.4.1 Defense and Security Applications

The intermolecular vibrations of molecules in many chemical and biological compounds, including explosives have distinct spectroscopic fingerprints characterizing their rotational and vibrational modes in the THz range, and thus provide information which is not available in any other part of the electromagnetic spectrum [16]. In addition, THz can penetrate most of the common materials like clothing, leather, plastic, wood etc., which are opaque to optical signals. These properties of the THz radiation make THz imaging highly convenient for detecting hidden weapons, explosives, and illicit drugs [17]. The higher resolution offered by THz signals makes their use highly advantageous in short range radars. As shown in this work, the increased resolution greatly improves the detection of various micro-motions of quadcopters in flight, which can be extremely cumbersome with low frequency systems.

2.4.2 Biomedical Applications

THz radiation has energy levels of the order of few millielectron volts which make it non-ionizing and thus, harmless to human DNA and tissues. Thus, THz is advantageous for biological imaging when compared to X-rays. THz time domain spectroscopy which is also known as THz pulsed imaging finds applications in the detection and characterization of cancer tissues [18] and for generating multi-dimensional images for detecting thermal and chemical distribution of injected solutions inside the body [19].

2.4.3 Industrial Applications

Owing to the ability of the THz radiation in penetrating dielectric materials, THz imaging can be used in non-destructive sensing applications to detect defects in sealed packages like ICs, which are usually made of dielectrics [13], to detect leaky IV bags and for the measurement of thickness of plastic bottles, hoses and tubes [20].

2.4.4 Communication

Although, the high atmospheric attenuation and scattering of the THz radiation makes its usage impractical for long range communications, it can be effectively used for short range in-house wireless communications enabling high data rates up to terabits per second (Tbps) [21]. Such THz access points also can be installed at the places of high data consumption such as metro stations, stadiums and airports. The lossy nature of THz radiation can also be exploited by using it in the security-sensitive communications in both military and commercial scenarios [22].

2.4.5 Remote Sensing

THz systems, together with optical and infrared sensors are used for observing and measuring precipitation, humidity, water vapor and ice cloud profiles. It is usually done

using passive detectors in geostationary orbits. Radio astronomy has been another major driver of THz technology. The dust clouds in the galaxies and around stars have distinct signatures in the THz region. Thus, THz spectrum provides useful information about the characteristics of such dust clouds, their age and aid in collecting necessary information needed for understanding the origins of the universe. THz sensors are also used in the observation of asteroids, comets, satellites and other planetary bodies [23].

There are many other applications of THz spectroscopy, imaging and sensing that are being developed every day in the fields of medicine, scientific research, space and terrestrial operations, military and industries. The so-called THz gap has been reducing and continues to do so with each new technology that gets introduced!

2.5 Introduction to Radars

Before delving into the concept of micro-Doppler phenomenon and its utilization in radar-based detection techniques, it is prudent to have a quick description of some of the basic radar concepts and how they are going to be adopted in this work. RADAR (or more colloquially, radar), the acronym for RAdio Detection And Ranging, is an electromagnetic system that uses radio waves for detection and location of targets. The term RADAR was coined by the United States Navy in 1940 [24]. The two most basic functional requirements of a radar are to detect the presence of a target and to measure its range [25]. Other important functionalities include, the measurement of target angles and target velocities using Doppler [26]. Radars offer numerous advantages when compared to optical and infrared systems as they are capable of operating in all kinds of weather conditions at both short and long ranges [25]. They also have the ability to penetrate walls, clothing etc., which makes them suitable for numerous applications.

2.6 A Brief History

A demonstration by Heinrich Hertz in the late 1880s, providing experimental verification of James Clerk Maxwell's theory of electromagnetism showed that the radio waves can be reflected off metallic objects. This can be considered as one of the earliest developments in the field of radar communications. Several independent researches followed this, but the work of German physicist, Christian Hulsmeyer in the early 1900s wherein he used radio waves to detect metallic targets using a device which he developed called the 'telemobilioscope', marks as the first basic model of a radar system [24].

Further developments in radar technology were carried out in secret by different countries around the world, during the period of world wars, particularly the world war II. The discovery of the utility of the cavity magnetron as a microwave generator revolutionized the radar technology in the late 1930s. The German Freya radar and Seetakt radar, the British Chain Home (CH) radar and the US XAF radar can be considered as some of the important early radars [24].

2.7 Radar Block Diagram

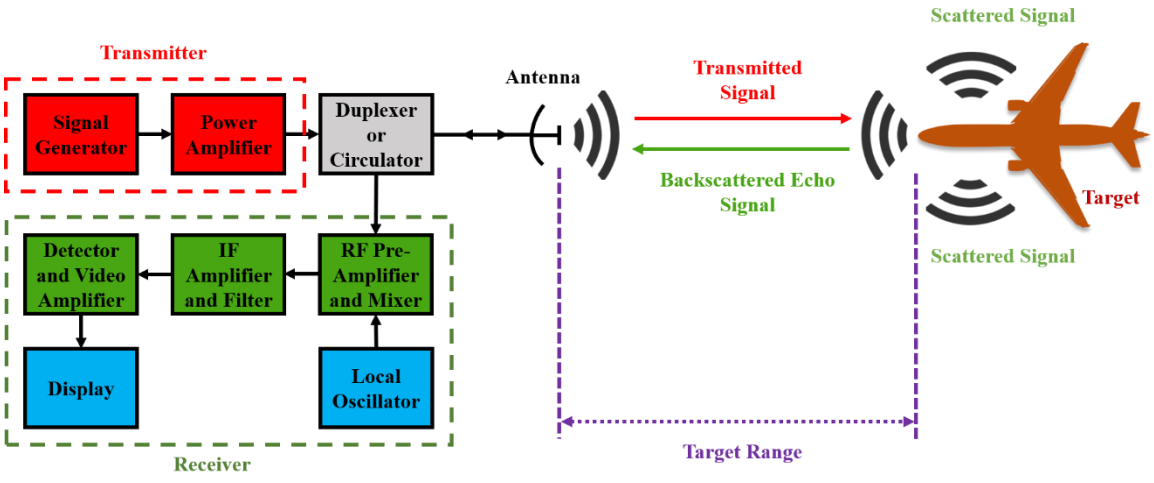

Figure 2.2. Block Diagram of a Simple Radar.

The block diagram of a simple radar system with its basic operating principle is shown in figure 2.2. The signal generated by the signal generator is amplified to the desired level by a power amplifier in the transmitter. The radar antenna radiates this electromagnetic signal into space. As the signal propagates through space, a part of it is intercepted by a reflecting object, often called the target. This signal is reradiated in different directions by the target. A part of this reflected echo signal is returned to the radar antenna which delivers it to the receiver for processing [27]. The received echo signal is usually a weak signal. Thus, it needs to be amplified without adding additional noise. This is done using a low noise pre-amplifier before down-converting it to an IF frequency using a mixer. Then the signal is further amplified and filtered to remove undesired harmonics and displayed on a screen. A duplexer or a circulator is used between the transmitter and the receiver to provide isolation between the signals transmitted and received by the radar antenna. The interaction of the transmitted electromagnetic signal with the target changes the properties of the signal. These changes are unique to each target. Thus, the received echo signal not only indicates the presence of a target, but also contains information about the characteristics of the target. Using adequate amplification, filtering and signal processing techniques, the target characteristics can be deciphered.

The important parameters in the design of a radar system include the available area, required power and bandwidth and the expected range of the target from the radar. Several external parameters also affect the radar's performance like the target cross section or radar cross section, which determines the reflectivity of the target, external noise and interference due to other radiators, undesirable echo signals from stationary objects, propagation losses and so on [27].

2.8 Doppler Effect in Radars

The radar receives echo signals from various types of reflecting objects such as aircrafts, ships, missiles, vehicles, people, land, sea, buildings, mountains and so on. Some of these are stationary while some or not. So, it is necessary have a mechanism to separate the moving targets from the stationary ones, which generate echo signals often termed as 'clutter' [13-15]. This is where Doppler effect finds its application. When a target travels at a constant velocity with respect to the radar (or if the radar moves with respect to the target, or if both move), there exists a relative motion between the target and the radar. It causes the reflected signal from the target to be shifted in frequency, proportional to the target's (or radar's) velocity. This is known as the Doppler effect [2], and the magnitude of the frequency change, is known as the Doppler frequency shift or simply Doppler shift [28]. There will be an increase in the frequency of the reflected signal as compared to the transmitted signal, if the target motion is towards the radar, and a decrease in the frequency of the reflected signal if the target motion is away from the radar. Thus, the difference between the frequency of the transmitted and the received signals not only indicates the presence of the target but also gives a measure of its relative velocity with respect to the radar. As such, the Doppler frequency shift, 'f_d', as a function of the operating frequency, f_0 and the radial velocity of the target, $v_r = vcos\theta$ is given by,

$$f_d = \frac{2f_0 vcos\theta}{c} = \frac{2vcos\theta}{\lambda} = \frac{2v_r}{\lambda} \text{ Hz} \tag{2.1}$$

where

c is the speed of light in free space

λ is the operating wavelength = $\frac{c}{f_0}$ m

Figure 2.3 shows the geometry of a stationary monostatic radar with a moving target. If the target directly approaches or goes away from the radar, then $\theta = 0^0$, making $\cos\theta = 1$ and the Doppler frequency shift reduces to,

$$f_d = \frac{2vf_0}{c} = \frac{2v}{\lambda} \text{ Hz} \tag{2.2}$$

In the limiting case, when the target motion is perpendicular to the direction of the incident radar signal, no frequency shift will be observed as $\theta = 90^0$ makes $\cos\theta = 0$, and thus, $f_d = 0$. The radar utilized in this work combines the principles of Doppler effect in radars with the micro-Doppler phenomenon to accomplish the goal of detecting and characterizing the multicopter's micro-motions.

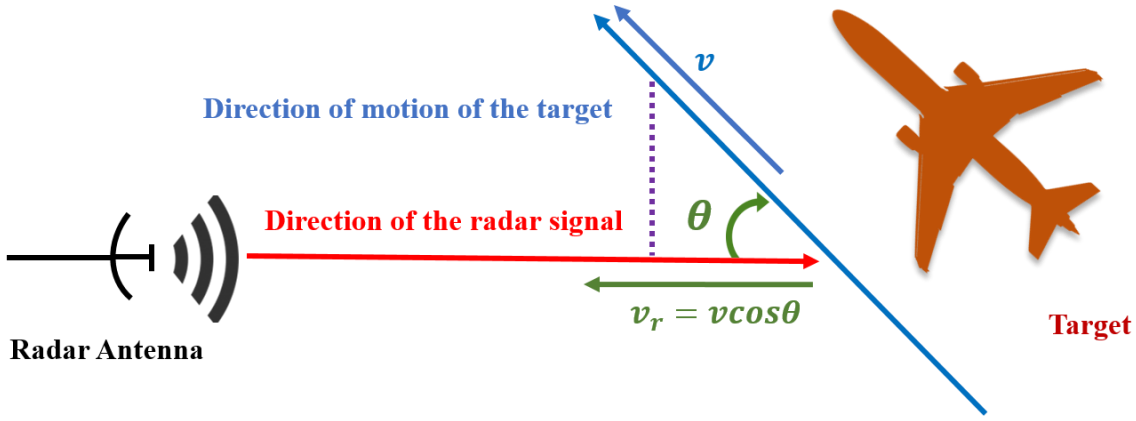

Figure 2.3. A Simple Stationary Monostatic Radar with a Moving Target.

2.9 Types of Radars

There are many ways to classify radars based on their design, configuration, operation and applications. This section gives an overview of different radar categories, and highlights the type of the radar chosen for this work. The reason for choosing the particular radar configuration is also elucidated along with the description of each configuration. The first

classification is based on the antenna architecture, which broadly categorizes the radars into three types.

- Monostatic radar
- Bistatic radar
- Multistatic radar

2.9.1 Monostatic Radar

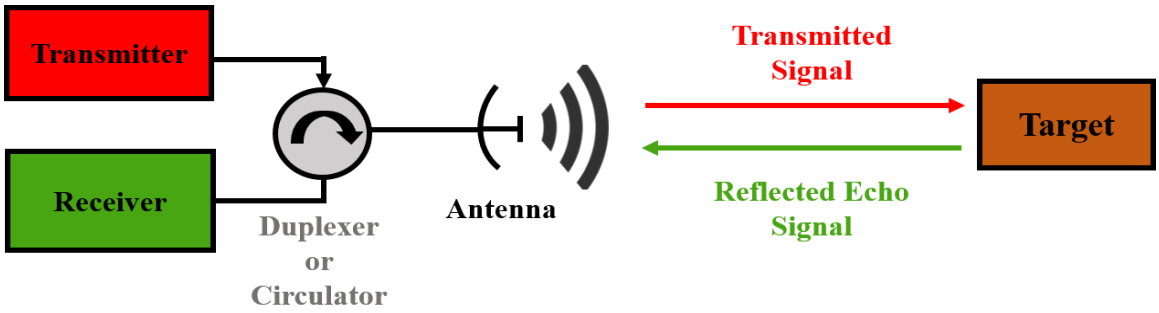

Figure 2.4. Monostatic Radar Configuration.

A simple monostatic radar architecture is shown in figure 2.4. A monostatic radar configuration is one in which a single antenna is used for both transmission and reception. In some cases, separate transmitting and receiving antennas may be employed. However, when done so, for the arrangement to be considered monostatic, the antennas must be in the proximity of each other such that the angles formed by the radar signal to the target is same for both antennas [29]. In general, most pulsed radar systems utilize the single antenna model while almost all continuous-wave (CW) models use separate antennas as they need the continuous signal transmission for their operation. The major concern with monostatic configuration is the isolation between the transmitting and receiving sections. A duplexer or circulator is used to provide this isolation. An additional switch can be used in the receiver section to further improve the isolation at the cost of increasing the noise

figure. Thus, it is only used in applications where the received echo signals are not very weak. When two separate antennas are used for transmission and reception, the coupling between the antennas also becomes a challenging problem. Highly directional arrays, horn antennas [30], leaky-wave antennas [31] etc., with very narrow beamwidth must be designed for such scenarios. The coupling effect can also be greatly reduced by the use of electromagnetic band-gap (EBG) surfaces [32]. This method is especially useful in the design of planar antennas.

In this research, a simple CW Doppler radar in monostatic configuration is used with two separate highly directional horn antennas. The antennas have a very narrow *half power beamwidth* (HPBW) of 10^0 and a high gain of 26 dB. It is ensured that the antennas are close to each other such that the angle that the radar signal forms with the direction of motion of the target is same for both transmitting and receiving antennas.

2.9.2 Bistatic Radar

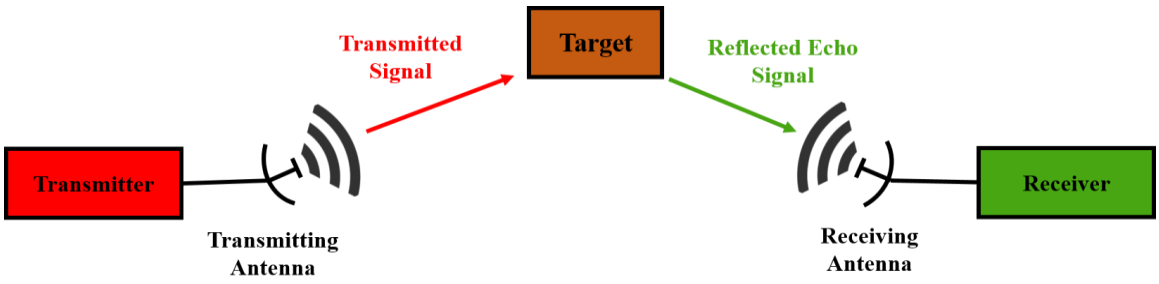

Figure 2.5. Bistatic Radar Configuration.

A simple bistatic radar architecture is shown in figure 2.5. A bistatic radar configuration is one in which two different antennas are used for transmission and reception. Another requirement is that these two antennas must be separated by some distance in such a way that the ranges or angles to the target are different [29]. Because of this inherent separation between the transmitting and receiving antennas, the bistatic radars do not suffer from the

problems of coupling between the antennas as well as the need of isolation between the transmitting and receiving sections. Although bistatic configuration offers inherent advantages, they come at the cost of complex and expensive architecture. This is one of the main reasons for no considering such a system in this research.

2.9.3 Multistatic Radar

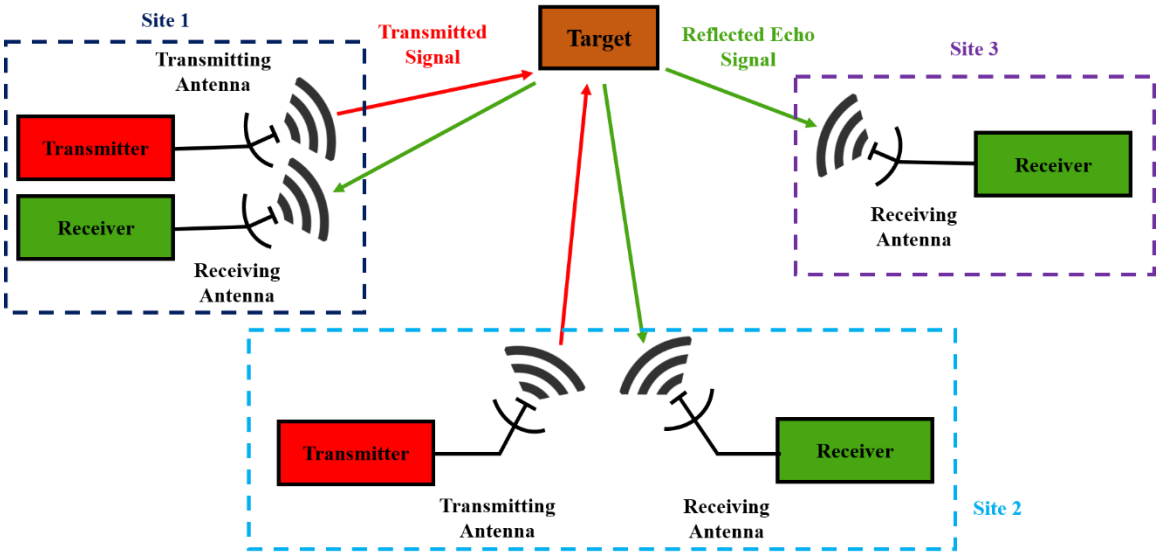

Figure 2.6. Multistatic Radar Configuration.

A multistatic radar configuration is one in which multiple antennas in monostatic, bistatic or passive receiver-only configurations share a surveillance area. The spatial diversity offered by the multistatic radar system gives it the ability to view a target from multiple perspectives, which increases the amount of information available from a target when compared to individual monostatic or bistatic systems, thus enhancing the radar's ability to detect, track and identify the target [33]. A simple multistatic radar system is shown in figure 2.6 with monostatic, bistatic and passive receiver-only systems. However, these kinds of systems are generally used for large-scale commercial or government applications and thus out of the scope of this work.

Based on the type of the signal used for communication, the radars can be classified into two different categories.

- Pulse radar
- Continuous-wave (CW) radar

A CW radar is used in this work and the next section describes its design and operating principles. Pulse radars are not considered in this work and thus are out of the scope of discussion here.

2.9.4 Continuous-wave (CW) Radar

A continuous-wave (CW) radar uses a sinusoidal signal of some constant frequency that is transmitted continuously from the transmitting antenna. A separate receiving antenna is usually used to receive the reflected echo signals from targets. CW radar operation is predominantly based on the Doppler shift detection. The weak echo signal is shifted in frequency by an amount, $\pm f_d$ based on the direction of motion and the velocity of the target. A positive Doppler shift, $+f_d$ indicates that the target is approaching the radar. Thus, the received echo signal will have a higher frequency compared to the transmitted signal. On the other hand, a negative Doppler shift, $-f_d$ indicates that the target is going away from the radar. This makes the received echo signal to be at a lower frequency than the transmitted signal. Thus, by comparing the frequencies of transmitted and reflected signals, the radial velocity and the direction of motion of the target can be detected in a CW radar.

The operation of a simple CW radar is shown in figure 2.7. Although the CW radar operation is not always as simple as depicted here, it gives the general idea of operation of a CW radar system. In practical scenarios however, the received echo signal will never be a single frequency signal like the transmitted signal as it will be a composite of the

reflections from target as well as stationary and slow-moving clutter. At the same time, it might be difficult to detect the weak echo signal in the presence of various noise sources. Thus, proper amplification, signal processing and filtering techniques are needed to extract the frequency information that is critical to the operation of CW radar. Since the transmitter is always transmitting, CW radars almost always use a separate antenna for receiving the echo signals. Thus, there should be very good synchronization between the transmitter and receiver. This continuous transmission in CW radars is however advantageous compared to some pulse radar schemes that employ low pulse repetition frequencies, as it does not suffer from the problem of blind speeds.

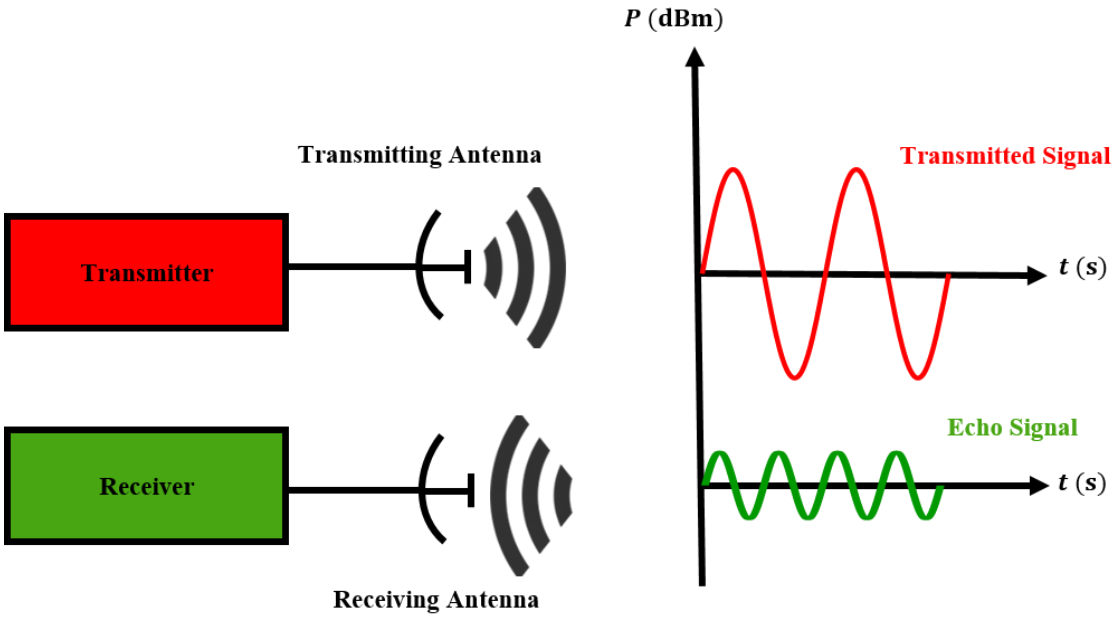

Figure 2.7. Continuous-wave (CW) Radar System.

The major shortcoming of a continuous-wave radar is its inability to measure the target's range. This is again attributed to the feature of continuous transmission of radar signal. The continuous transmission does not allow the CW radars to have 'listening time' as seen in pulse radars. Thus, it is impossible to measure the range using a simple CW radar

system. To overcome this problem, the transmitted sinusoidal signal can be modulated leading to a *Frequency-modulated continuous-wave* (FM-CW) radar. As the frequency changes with respect to time, a FM-CW radar has the time information that is not available for the simple CW radar. Although this type of measurement works well with stationary targets, it is difficult to obtain accurate results for moving targets. Hence, FM-CW radars are usually used in applications that require measuring range to fixed targets such as aircraft altimeters which are used to measure the height of the aircraft above the ground [34].

A simple CW radar has been used in this work owing to its simplicity of operation, lower cost and requirement of less architecture as compared to pulsed radars. The goal here is to develop a proof of concept for detection of micro-motions at THz frequencies and it is sensible to first approach the problem with simpler but effective practices so that more robust techniques can be employed in the future. In addition, as the focus of the research is on detecting the micro-motions of the multicopter within a pre-determined range in order to characterize it, and not on the measurement of its range, it is justified to utilize a simple CW radar. A FM-CW radar cannot be used for the obvious reason that the target considered is not a stationary one.

2.9.5 Other Radar Types

There are many other methods of classifying radars based on their operation, configuration and applications. Some of the important and commonly encountered radar systems are listed below [27].

- Tracking radar
- Imaging radar
- Synthetic Aperture radar (SAR)

- Inverse Synthetic Aperture radar (ISAR)
- Weather radar
- Surveillance radar
- Guidance radar
- Weapons control radar

All these radars can be designed either as pulse or continuous-wave radars using monostatic or bistatic architectures, based on the specific scenarios in which they are used.

2.10 Friis Transmission Equation and Radar Range Equation

The signals transmitted from a radar antenna get attenuated as they propagate through the atmosphere. This reduces the power of the signal such that, when observed from a sufficient distance from the transmitting antenna, the total power reduces to 0. Friis transmission equation gives the amount of power available at a particular distance from the antenna. The radar range equation is useful for obtaining the range of a target from the radar, as such, it determines the maximum distance at which the targets can be successfully detected [27]. These two equations are generally used in the design and analysis of radar systems [30].

The received power, P_r by an antenna places at some distance, R from the transmitting antenna as given by Friis transmission equation is [30],

$$P_r = e_t e_r (1 - |\Gamma_t|^2)(1 - |\Gamma_r|^2) G_t G_r |\hat{\rho}_t \cdot \hat{\rho}_r|^2 P_t \left(\frac{\lambda}{4\pi R}\right)^2 \tag{2.3}$$

where

e_t is the efficiency of the transmitting antenna

e_r is the efficiency of the receiving antenna

$(1-|\Gamma_t|^2), (1-|\Gamma_r|^2)$ are the reflection efficiencies of the transmitting and the receiving antennas respectively

G_t, G_r are the gains of the transmitting and the receiving antennas respectively

$|\hat{\rho}_t \cdot \hat{\rho}_r|^2$ is the polarization loss factor (PLF)

$\hat{\rho}_t, \hat{\rho}_r$ are the polarization unit vectors of the transmitting and the receiving antennas respectively

P_t is the transmitted power

λ is the operating wavelength

The radar range equation used to determine the range of the target from the radar as a function of radar characteristics is given by [13 - 15], [30],

$$P_r = \frac{\sigma}{4\pi} e_t e_r (1-|\Gamma_t|^2)(1-|\Gamma_r|^2) G_t G_r |\hat{\rho}_t \cdot \hat{\rho}_r|^2 P_t \sigma \left(\frac{\lambda}{4\pi R_1 R_2}\right)^2 \quad (2.4)$$

where

σ is the radar cross section (RCS) or echo area

R_1 is the distance from the transmitting antenna to the target

R_2 is the distance from the target to the receiving antenna

If the transmitter and receiver are equidistant from the target, the above equation becomes,

$$P_r = \frac{\sigma}{4\pi} e_t e_r (1-|\Gamma_t|^2)(1-|\Gamma_r|^2) G_t G_r |\hat{\rho}_t \cdot \hat{\rho}_r|^2 P_t \left(\frac{\lambda}{4\pi R^2}\right)^2 \quad (2.5)$$

Rearranging the terms, a more commonly used form of the radar range equation can be obtained as,

$$R = \left[e_t e_r (1-|\Gamma_t|^2)(1-|\Gamma_r|^2) |\hat{\rho}_t \cdot \hat{\rho}_r|^2 \left(\frac{\lambda}{4\pi}\right)^2 \frac{\sigma P_t G_t G_r}{4\pi P_r} \right]^{\frac{1}{4}} \quad (2.6)$$

Further, if a monostatic radar configuration is used, the above equation reduces to,

$$R = \left[e(1-|\Gamma|^2) \left(\frac{\lambda}{4\pi}\right)^2 \frac{\sigma P_t G}{4\pi P_r} \right]^{\frac{1}{4}} \quad (2.7)$$

In this work, since a CW radar is used, it is not possible to measure the range of the target. Thus, a predetermined range is selected for operation is calculated using the radar range equation, based on the maximum power capability of the transmission system.

2.11 Radar Cross Section (RCS)

A new quantity, known as the radar cross section (RCS) or the echo area, σ has been introduced in (2.4) to (2.7). This is a very important far-field parameter that determines the visibility of the target to the radar. The RCS of a target is defined as, "the area intercepting that amount of power which, when scattered isotropically, produces at the receiver a density which is equal to that scattered by the actual target" [30], and is given by,

$$\sigma = \lim_{R \to \infty} \left[4\pi R^2 \frac{W_s}{W_i} \right] \tag{2.8}$$

where

R is the distance from the observation point

W_i is the incident power density

W_s is the scattered power density

When the transmitter and the receiver are in the monostatic configuration, a monostatic RCS is used, and when they are in bistatic configuration, a bistatic RCS is used. RCS is intensively used in the design of stealth targets as reducing the RCS reduces the target's visibility to the radar. The RCS of a target is represented as an area in square meters (m^2) or decibel per square meter (dBsm). The RCS of a target can be minimized by shaping the target and/or using certain materials that trap the incident energy and dissipate it either as heat or in undesired directions. Thus, using round corners and avoiding flat and concave surfaces, the RCS can be reduced [30].

2.12 Applications of Radar

Radars find applications in almost all aspects of our lives. Some of the major applications are listed here.

2.12.1 Defense and Security Applications

Radars were initially developed for this purpose. Today, they are an integral part of air, sea and land based military operations. High resolution imaging radars such as SARs and surveillance radars are used for reconnaissance purposes in the battlefields. Weapons control radars and tracking radars are used to track missiles and aircrafts and provide positional information of the targets to aid in the deployment of counter measures against them. Guidance radars are used to guide the missiles to their targets [25], [27]. Another major application of radars is counter-surveillance. Radars can be used to detect incoming missiles, enemy aircrafts and unmanned aerial vehicles such as multicopters. Both short-range and long-range radars can be used for this purpose. This work focuses on the design of a short-range counter-surveillance radar which can be used to detect quadcopters, or in general any multicopter in flight.

2.12.2 Aircraft Safety and Air Traffic Control (ATC)

Radars are used to monitor the air traffic and ensure the aircraft and passenger safety in all the airports around the world. Airport surveillance radars (ASR) are used to observe the air traffic and weather in the vicinity of the airports. Air route surveillance radars (ARSR) are used to monitor and control air traffic between airports. Major airports have an additional radar called the air surface detection equipment (ASDE) for observing and controlling aircraft and vehicular traffic on ground [25], [27]. Radars are also used in aircrafts for navigation control, communication with nearby airports and to monitor weather conditions.

Altimeters equipped with FM-CW radars are used to keep track of the altitude of the aircraft during the flight [25].

2.12.3 Remote Sensing

Remote sensing applications include monitoring the environment. Radars are used for weather observation, planetary observation and terrestrial mapping applications [14].

2.12.4 Law Enforcement and Vehicular Safety

CW Doppler radars are commonly used by the law enforcement authorities to monitor the vehicular traffic and enforce speed limits in cities and on the highways. Radars are currently used in almost all the latest vehicles for collision avoidance, lane assistance backup sensor and blind spot monitoring applications. Radars also form the basis for autonomous driving applications.

2.12.5 Other Applications

Radars find applications in many other fields like spacecraft safety, ship safety, for speed and distance measurement in industry and sports, for monitoring insect and bird movements, for oil and gas exploration and so on.

CHAPTER 3

TERAHERTZ MICRO-DOPPLER RADAR DESIGN

3.1 Terahertz Micro-Doppler Radar

The electromagnetic signal emitted by a radar undergoes different changes upon interaction with different targets. Thus, the backscattered signal from each target contains unique information about the characteristics of each target. If the target moves at constant velocity, the frequency shift induced by its relative motion with respect to the radar can be obtained using the principles of Doppler effect as discussed in section 2.8. Most of the current radar systems depend on Doppler effect to identify targets and their properties like direction of motion and range. Although the Doppler radars can detect the presence of the targets and deduce if they are approaching or receding from the radar, they are incapable of identifying the targets and characterizing their features. In the current scenario with the increased air traffic, it is crucial to have mechanism to distinguish different targets in order to avoid undesired results.

However, to achieve this goal of discriminating different targets, additional information is needed. As it turns out, most of the targets encountered by the radars have mechanical vibrations, rotations, coning and/or tumbling motions in addition to their translational motion. These are termed as ‘micro-motions’ and they induce time-varying frequency modulations on the reflected signal which appear as sidebands about the Doppler frequency shift. This phenomenon is known as micro-Doppler effect [2]. Micro-Doppler modulations caused by various targets are different from each other. For example, the modulations caused by the engine vibrations of a car and a bus are distinct from each other.

Similarly, the modulations due to rotational motions of the bicycle wheels, helicopter blades and the propellers of an aircraft are different from each other. Further, the modulations due to the propellers of a passenger plane are distinct from that of a fighter jet. Thus, the micro-Doppler effect provides the necessary additional information required to characterize the targets.

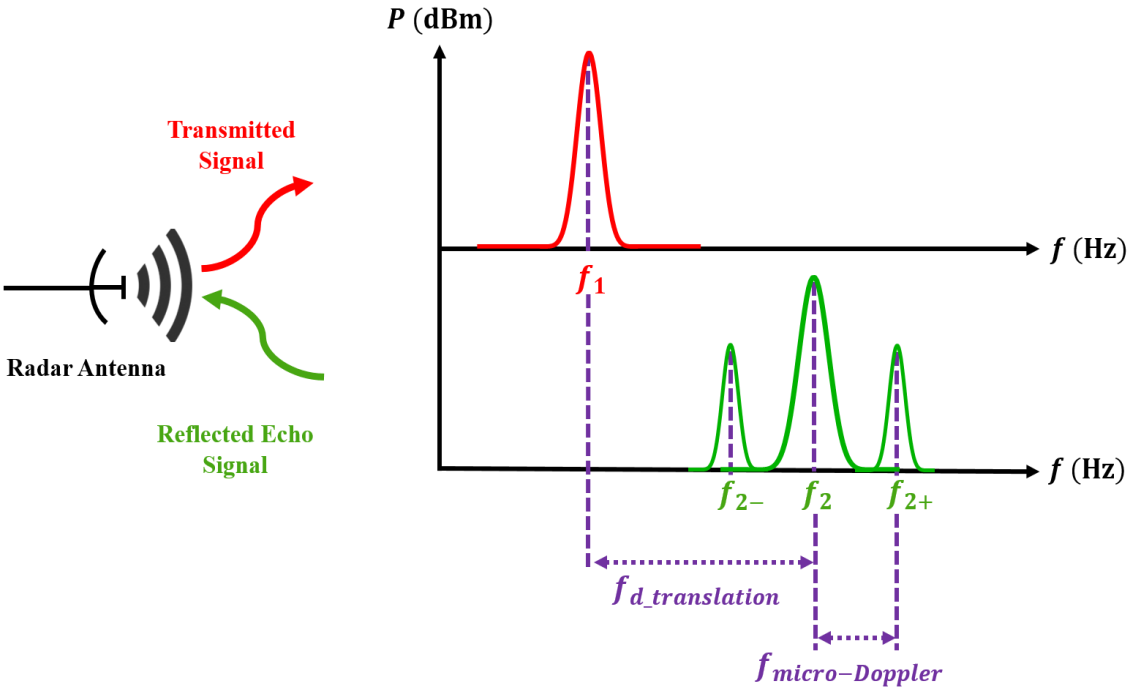

Figure 3.1. Radar Returns from a Target with Micromotions.

Figure 2.1 shows the working of a micro-Doppler radar when the target with micromotions intercepts a radar signal. A rotational micromotion from a quadcopter is considered for demonstration. The quadcopter is assumed to be approaching the radar, thus there is an increase in the frequency of the reflected echo signal. This frequency shift due to the translational motion of the quadcopter is called $f_{d\_translation}$. The rotational motion of its blades causes additional frequency components to appear as sidebands along the main Doppler shifted signal. The magnitude of the variation of these additional frequency

components determines the frequency shift due to micromotions and is denoted by, $f_{micro-Doppler}$. If the quadcopter is receding from the radar, then the entire frequency shift profile will be seen at the lower end of the frequency spectrum. The figure shown here is just to demonstrate the basic idea of how the micromotions modulate the reflected signal. In real life scenarios however, many signals due to multiple reflections from various parts of the target will be superimposed on top of each other and more complex analysis methods must be employed to extract the micro-Doppler features.

3.2 System Design

In this work, a low-THz micro-Doppler radar operating on continuous-wave (CW) Doppler radar principles is developed. A monostatic or more accurately, a pseudo-monostatic radar configuration is chosen for operation with two separate highly directional horn antennas, one for transmitting the signal to the target and the other for receiving the echo signals from it. Two separate antennas are chosen to avoid the use of isolating devices such as a circulator or a duplexer. Operation in THz comes with restrictions on the maximum power handling capabilities of the components. As such, only low power signals can be transmitted from the transmitter. This is coupled with the propagation losses along the path from the radar to the target and from the target back to the radar. Thus, the radar returns from the target are much lower in power. Since, circulators are passive devices they lead to additional loss of the signal power. As it will be shown later, the received signals have a maximum power of around -85 dBm and thus, the usage of two separate antennas and omission of additional isolation devices are justified. Continuous-wave radar is chosen because of the ease of generating the signals and the simplicity of designing the system as compared to pulse radar systems.

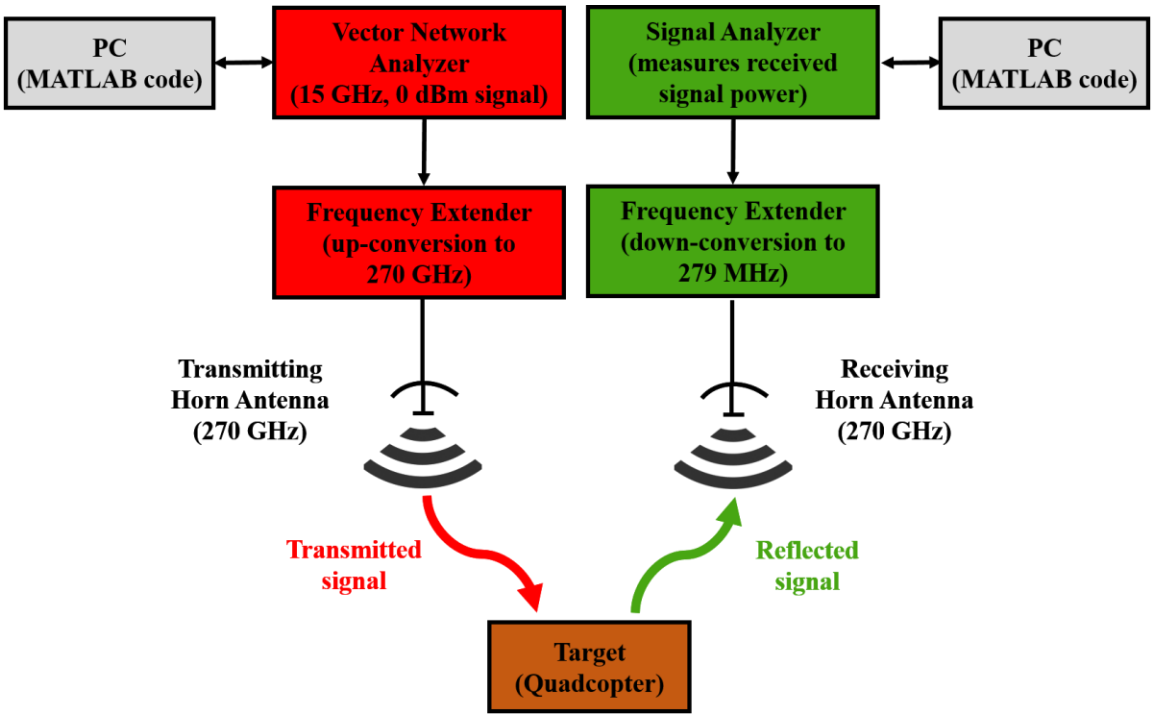

Figure 3.2. THz Micro-Doppler Radar System.

The design workflow of the THz micro-Doppler radar system used in this research is shown in figure 3.2. The vector network analyzer (VNA) is used as the signal source instead of a signal generator because of its better phase noise characteristics. Also, two separate signals at different frequencies are needed for operation; one is the radio frequency (RF) signal and the other is the local oscillator (LO) signal. So, instead of using two separate signal generators, it is easier to use two ports of the VNA. A 15 GHz RF signal is generated by the VNA and fed to the RF input of the frequency extender. It is passed through a series of frequency multipliers which multiply the signal by x18 to generate a 270 GHz signal. This 270 GHz signal is supplied to the transmitting horn antenna. It is also mixed with the local oscillator signal of 14.9845 GHz, that is fed to the LO input of the frequency extender, and used as the reference signal. The transmitted signal when intercepted by the quadcopter, gets scattered in different directions. Some part of it is also

backscattered towards the radar. This backscattered echo signal is received by the receiving horn antenna and fed to the frequency extender on the receiver side. The second frequency extender is also fed with the same LO signal through its LO input. Then the 270 GHz signal is mixed with the LO signal and is down-converted to an intermediate frequency (IF) signal of 279 MHz. This signal is supplied to the signal analyzer for display. A separate signal analyzer is used for displaying the received signals as it is easier to calibrate the signal analyzer for power measurements when compared to VNA. Also, since VNA is used as the signal source, its oscillator is made to generate a single frequency signal. So, the received signal is also measured at a single frequency. However, in order to capture the frequency shift, the oscillator must sweep a certain frequency band equal to the sampling interval. This makes the sweep time longer, and thus, the measurements slower if the VNA is used. Since the goal here is to measure the power of the received signal and not the fields or S-parameters, it is possible to use a vector signal analyzer instead of a VNA. The signal analyzer also provides the advantage of shorter sweep time as compared to VNA, and reduces the additional time and effort needed for calibration of the VNA. This entire process is repeated several times for a desired period of time to capture the frequency variations caused by the target during that time interval. The process is also automated by exploiting the remote-control feature in the VNA and the signal analyzer. This is done using the *Standard Commands for Programmable Instruments* (SCPI) commands in MATLAB. The computer and the VNA/ signal analyzer are connected together using the ethernet cables. The interface is achieved using virtual instrument software architecture (VISA) standard employing the TCP/IP protocol. Once the connection is established, the desired parameters are set using the SCPI commands in both VNA and signal analyzer and

measurements are carried out. The functions of each of the components in the radar system are described in detail in the following sections.

3.2.1 Vector Network Analyzer (VNA)

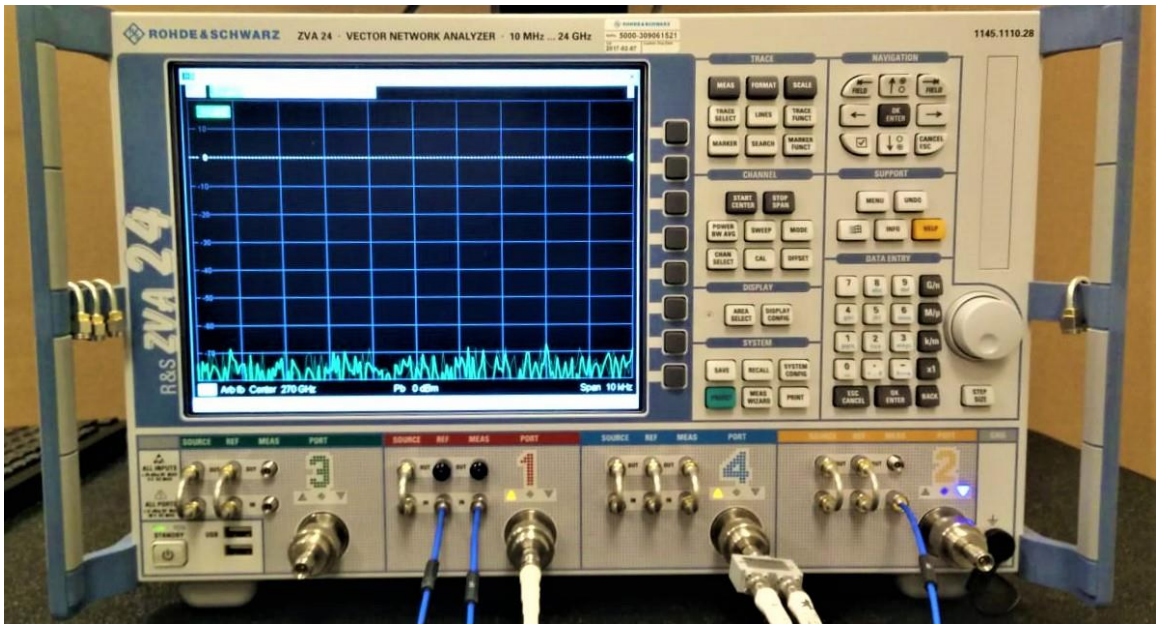

Figure 3.3. Rhode and Schwarz ZVA 24 VNA.

Rhode and Schwarz ZVA 24 VNA shown in figure 3.3 is used in this work as the signal source. It consists of 4 ports and 4 internal sources, and is capable of operating in the frequency range of 10 MHz to 24 GHz with a frequency resolution of 1 Hz. This enables the generation of the desired single tone continuous-wave signal using this VNA. The VNA exhibits an excellent dynamic range better than 130 dB with a noise floor of -110 dBm. All these features, increase the accuracy of measurements. However, the ZVA 24 does not have the ability to independently control the resolution bandwidth (RBW) and the video bandwidth (VBW) [35]. The ratio of RBW to VBW is set constant at 1:1, and called the measurement bandwidth. This results in an increase of sweep time which is given by,

$$t_{sweep} = \frac{span}{RBW \cdot VBW} = \frac{span}{(measurement\ bandwidth)^2} \tag{3.1}$$

Since, the ratio is 1:1, the sweep time increases as a function of the square of the measurement bandwidth, thus making the measurement process slow. In contrast, the signal analyzers have the ability to control the RBW and the VBW independently, and thus, the sweep time can be reduced. In this research, port 1 is used as the RF signal source and connected to the frequency extender on the transmitter side. Port 4 is used as the LO signal source and connected to both the frequency extenders.

3.2.2 Frequency Extenders

In this work, the THz signal is generated by the frequency up-conversion technique and this section is dedicated to describing the process. Two frequency extenders from Virginia Diodes Inc. are used in this research, one for up-conversion in the transmitter which is a transceiver module and the other for down-conversion in the receiver which is a receive-only module. They are capable of operating in the frequency range of 220 – 330 GHz. A single transceiver module can be used for both transmission and reception, however, as two separate antennas are used in this work, both frequency extender modules are employed for frequency conversions. The block diagram of the transceiver module is shown in figure 3.4 [36]. It consists of two inputs, two outputs and a power cord connection. The 15 GHz RF signal is frequency multiplied to produce the 270 GHz signal. The extenders can be supplied with a maximum power of 10 dBm and are capable of an output power of -6 dBm (approximately 250 μW). The isolator is used to block the signals that leak back into the transmitter. The directional coupler couples this 270 GHz signal to a mixer, where it is mixed with the LO signal to form the 279 MHz reference signal. The signal coupled to the second directional coupler is passed on to the antenna. The signal received from the antenna is coupled to the second mixer where it is mixed with the same

LO signal to obtain the measured signal at 279 MHz. Since the same LO signal is used for down-conversion, a high phase coherence is achieved.

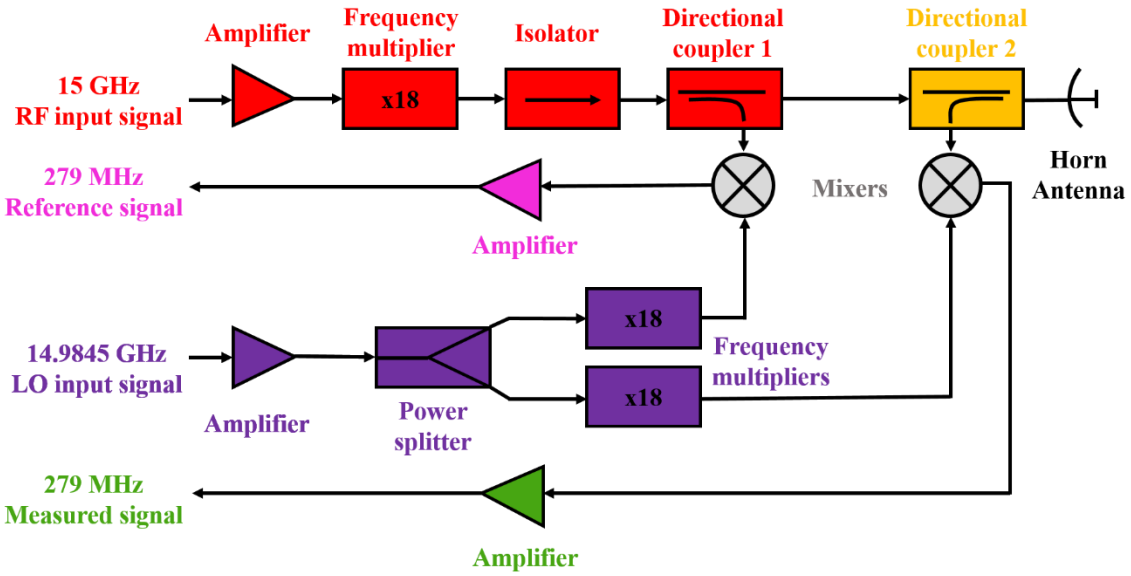

Figure 3.4. Block Diagram of Frequency Extender Transceiver Module.

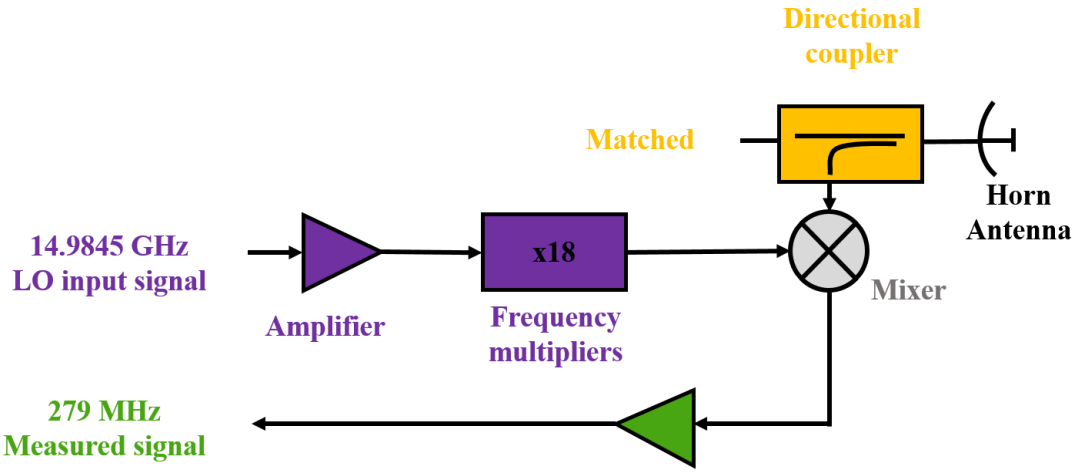

Figure 3.5. Block Diagram of Frequency Extender Receive-only Module.

Figure 3.5 shows the block diagram of receive-only frequency extender module [36]. It consists of a single input and a single output, along with the power cord connection. The operation here is exactly same as in the receiver section of the transceiver module. The

LO signal is mixed with the received signal to obtain the measured signal at an IF of 279 MHz. Since, the same LO signal is fed to this module as well, similar phase coherence characteristics are achieved. Figure 3.6, shows the frequency extenders used in this research with all the input and outputs labelled.

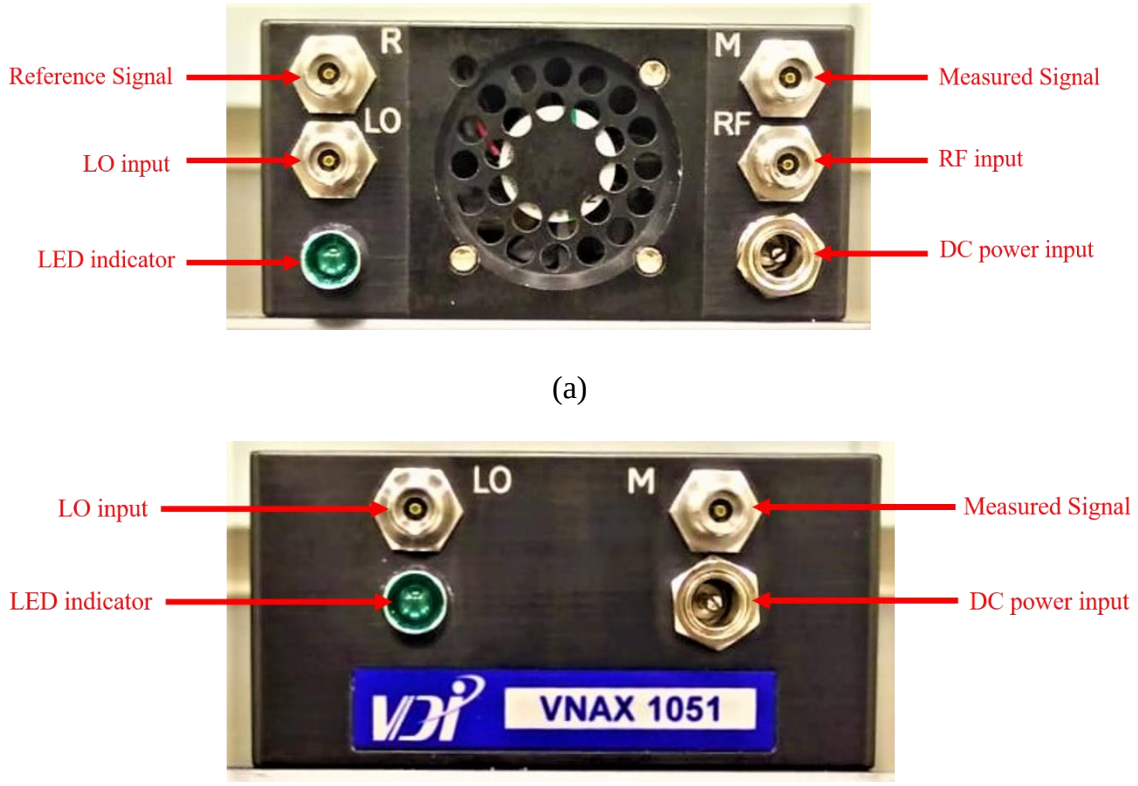

Figure 3.6. Frequency Extenders (a) Transceiver Module, and (b) Receive-only Module.

3.2.3 Signal Analyzer

Keysight MXA X-series signal analyzer 9020A is used in this work for the measurement and display of the echo signals returned from the target. The analyzer operates in the 10 Hz to 8.4 GHz band with excellent phase noise characteristics of -114 dBc/Hz at 10 kHz offset and an amplitude accuracy of ± 0.23 dB. This high accuracy combined with the ease of coding the analyzer for remote control applications makes it ideal for this research. It

also has the ability to control the RBW and VBW independently, a feature which helps in reducing the sweep time, and thus enabling faster acquisition of data. The signal analyzer used in this work is shown in figure 3.7.

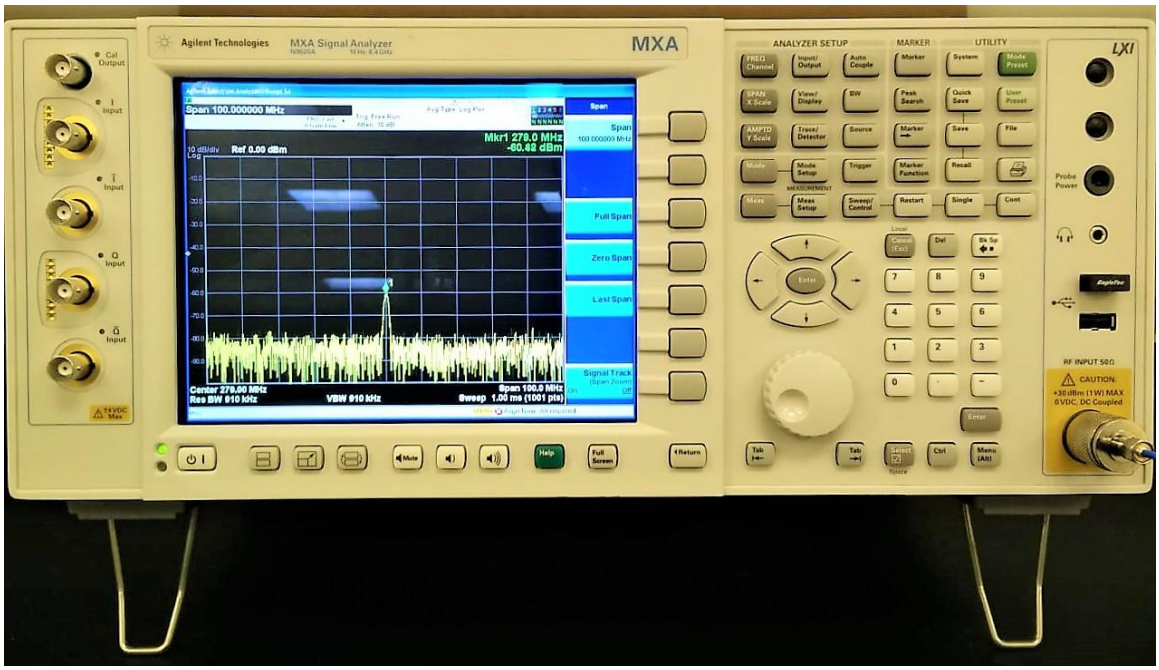

Figure 3.7. Keysight MXA X-series Signal Analyzer N9020A.

3.2.4 Horn Antenna

Two WR – 3.4 (frequency range 220 – 325 GHz) horn antennas from Virginia Diodes Inc. are used in this work. They are connected to the frequency extenders and made to operate at a center frequency of 270 GHz. Due to the high frequency of operation, coaxial connectors cannot be used to supply power to the antennas and thus, waveguide based connectors are used in the frequency extenders. The antennas are designed as diagonal horn antennas with a length of 56 mm and an aperture diameter of 5.6 mm. The horns are highly directional with a half power beamwidth of 10^0 and a gain of 26 dB. The front and side views of the horns are shown in figure 3.8.

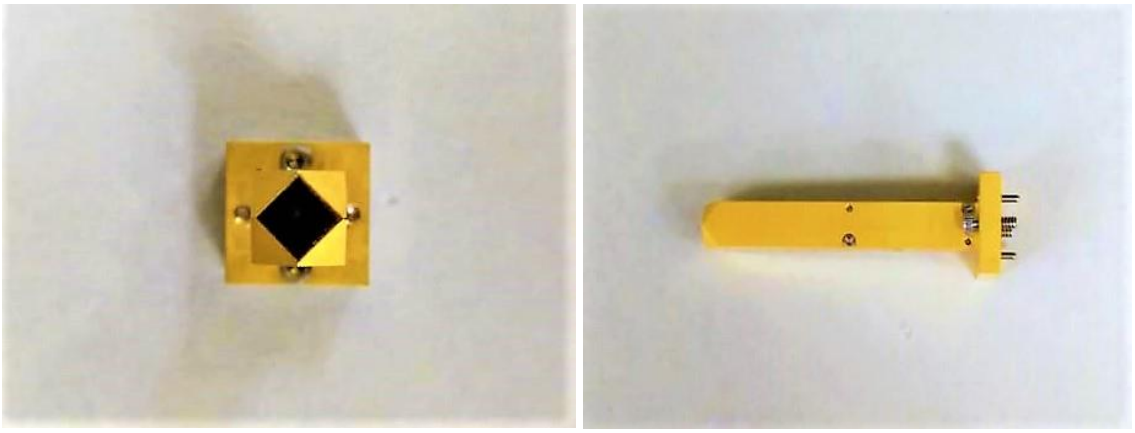

(a) (b)

Figure 3.8. WR – 3.4 Horn Antenna (a) Front View, and (b) Side View.

All these components are put together as shown in figure 2.2 to form the THz micro-Doppler radar system. The final component in the design of the radar is the target, which is a quadcopter. The next section is dedicated to describing it features and operation.

3.3 Introduction to Multicopters

A multicopter (also known as *multirotor*) is an aerial vehicle that uses more than two rotor blades for flight. The fixed-wing aircrafts and the single or double rotor helicopters were some of the first aerial vehicles mainly used for either military or commercial purposes. However, the launch of multicopters, unlocked an entire new arena of applications for aerial photography, gaming and other recreational activities. The demand for multicopters, more colloquially known as ‘drones’ has grown exponentially ever since. Although the initial versions of multicopters were sold separately and needed to be assembled by some professionals, the recent ones come in *ready-to-fly* configurations. These multicopters are controlled using a remote and require very little or no training for their operation. These developments can be attributed to the advances in the field of aviation technology which have made the design and fabrication of multicopters almost effortless for the unmanned

aerial vehicle (UAV) manufacturers. Thus, the ease of operation and the ready-to-fly architecture, combined with the affordable purchase- and maintenance prices, are considered as some of the important reasons for the increased popularity of multicopters in today's scenario.

Multicopters are used for a variety of purposes including photography, surveillance, racing, as small payload carriers, and so on. However, their ease of availability has also led to their misuse. They are used as means for illegal surveillance, illicit trafficking activities as well as to deploy dangerous chemical and biological agents remotely [8]. This has necessitated the need for developing methods to detect drones, especially when they are in flight. The most common methods employed for target detection can be broadly classified into optical techniques and radar-based techniques. Among these, the radar-based techniques are more robust than the optical techniques as they do not require ambient lighting conditions for their operation, can perform well in all weather conditions and have the ability to penetrate walls, fog, rain, wood, clothing and many dielectrics which are opaque to optical signals. Hence, a radar-based detection technique is employed in this work for detection and characterization of multicopters.

3.4 Multicopter Features

Multicopters are the aerial vehicles with the capability of vertical take-off and landing (VTOL). This is attributed to the placement of propellers on the top of the mulitcopters' body which is called the fuselage. Generally, multicopters have three, four, six or eight propellers and are called tricopters, quadcopters, hexacopters and octacopters respectively. Each propeller of the multicopter usually consists either two or three blades. Higher number of blades can also be designed as in aircrafts; however, they are very uncommon.

Among all the multicopters, quadcopters are the most popular ones. Quadcopters are further classified into three categories based on the arrangement of their propellers; X4-, +4- and H4-configurations [8] as shown in figure 3.9.

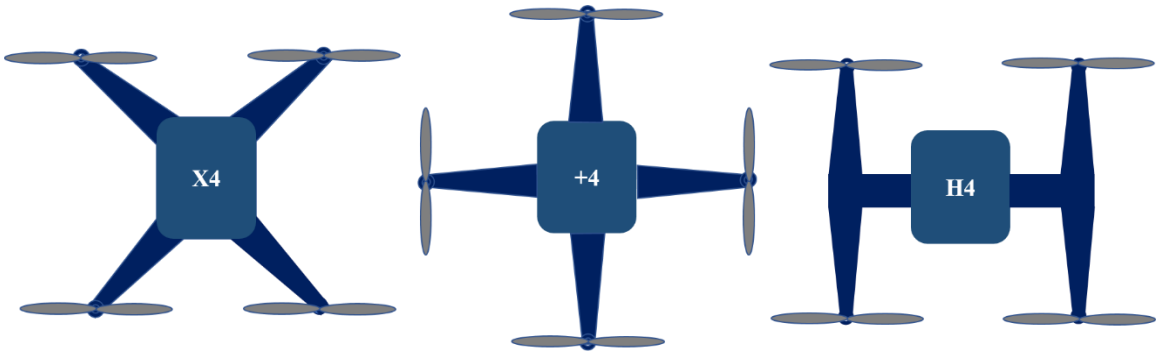

(a) (b) (c)

Figure 3.9. Arrangements of Propellers in Quadcopters: (a) X4 Configuration, (b) +4 Configuration, and (c) H4 Configuration [8].

The X4 configuration is the most commonly used quadcopter configuration. In a quadcopter, two pairs of propellers rotate in the clockwise (CW) direction and the remaining two pairs rotate in the counter-clockwise direction (CCW), with opposite pair of propellers rotating in the same direction. This mechanism aids in maintaining the orientation of the quadcopter while hovering [8].

Propellers in most of the general-purpose quadcopters are usually made from plastics. Propellers can also be made from metal, wood and carbon-fiber. Propeller length which is called the ‘diameter’ of the propeller is the diameter of the circle it forms while rotating. It can vary with the size of the quadcopters. Longer diameters lead to higher tip velocities even with lower rotational speeds to achieve the required thrust for lift off. Thus, shorter diameter propellers need to rotate at higher speeds than the longer ones, to generate the required thrust or the lift force. The propellers are designed in a curved shape in such a

way that the leading edge of their blades have a lower radius of curvature than the trailing edge. The curved shape increases the *attack angle*, the angle at which the blades cut through the air, and also helps in the vertical take-off. Although propellers can be designed so that the pitch of propellers can be varied dynamically, most of the commonly used multicopters are designed as fixed pitch propellers. The quadcopter used in this research is also built with a fixed pitch propeller. The radius of curvature is also higher near the central hub of the propeller and decreases towards its tips. The speed of the rotation increases from the center of the propeller to the tip and thus, the maximum speed of a propeller depends on its tip velocity. If the propeller rotates at x rpm, then the angular velocity of the propeller is given as,

$$\omega = x \cdot \frac{2\pi}{60} \text{ radians/s} \tag{3.2}$$

and the corresponding linear tip velocity, v_{tip} is given by,

$$v_{tip} = \omega \cdot r \tag{3.3}$$

where

r is the length of each blade of the propeller, also known as the radius of the propeller

Multicopters have very low cross section and operate at a lower altitude when compared to the aircrafts or helicopters. They also move at much lower speeds than the aircrafts. The placement of the propellers on the top of the multicopter body partially or completely masks them from the radars operating from the ground level, thereby masking the micro-Doppler modulations caused by the rotation of the blades. All these features of the multicopters makes their detection difficult using a radar-based system. However, as the multicopters glide, they tilt towards the direction of their motion, exposing the

propellers to the radar, and this property can be utilized for detecting the rotational micro-Doppler modulations induced by the blades. The second major challenge in the detection of multicopters is offered by the birds, which have a cross section comparable to that of the multicopters. However, the micro-Doppler modulations induced by their wingbeat is much less when compared to that of the multicopters. This is because the received signals from the birds are modulated by their wingbeat frequency which is in the range of 0 for large birds that glide to about 20 Hz for small birds [37]. This is much less than the rotational speeds of the propeller blades which is usually much greater than 50 Hz.

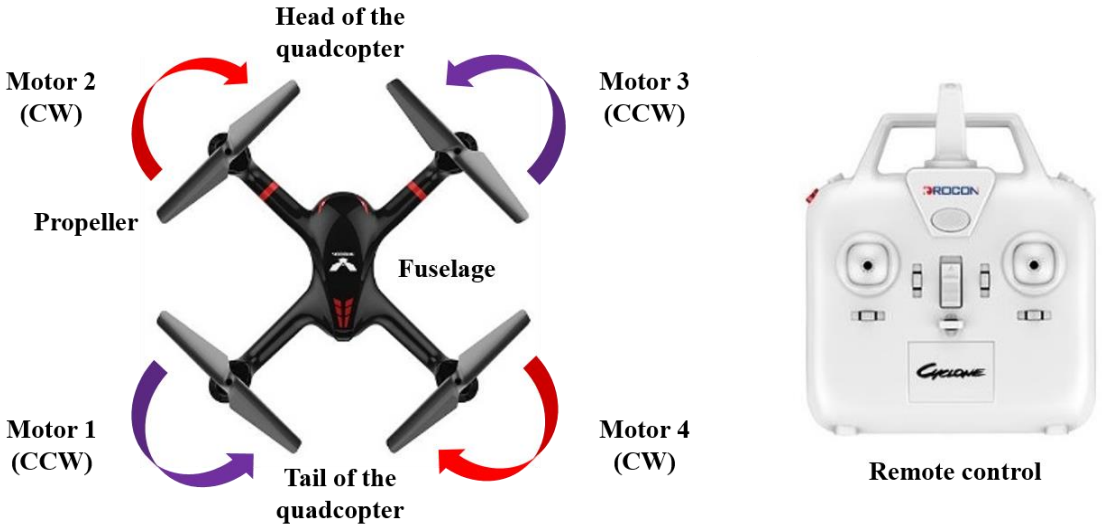

Figure 3.10. (a) X708W Quadcopter used in this Research, and (b) Remote Control used to Operate the Quadcopter.

A Drocon cyclone – X708W quadcopter as shown in figure 3.10 (a) is used in this work. It comes as a pre-assembled package and has four two-blade propellers, with each propeller having a diameter of 138 mm. The fuselage length is 310.5 mm and the height of the quadcopter is 60 mm. It uses a Li-polymer battery with voltage and current ratings of

3.7V and 550 mAh respectively. The body of the X708W quadcopter and its propellers are made from plastic and thus is very light and suitable for leisure activities and photography. The bottom left and the top right motors rotate in the counter-clockwise (CCW) direction, while the top left and the bottom right motors rotate in the clockwise (CW) direction. The quadcopter can be controlled using a remote and operates in the *industrial, scientific and medical* (ISM) band of 2.4 GHz.

CHAPTER 4

ANALYSIS OF MIRCO-DOPPLER SIGNATURES

4.1 Introduction

When a target moves at a constant velocity, it induces a Doppler frequency shift on the reflected signal proportional to its velocity and this frequency shift is time-invariant. It can be extracted using Fourier analysis, which decomposes the signal into individual frequency components. While the Fourier transform efficiently extracts the magnitude and phase of individual frequencies, it cannot deduce the order in which the frequency shifts are happening, i.e., it cannot extract the instantaneous frequency information. On the other hand, the micromotions of the target induce time-varying frequency modulations which appear as sidebands about the Doppler shifted signal, and form the micro-Doppler signature of the target. As these modulations change with time, it is not possible to use the Fourier transform to extract the micro-Doppler features. Thus, joint time-frequency transforms are needed for the analysis of micro-Doppler signatures.

In time-frequency analysis, the available spectrum is divided into short time intervals and Fourier transforms are obtained for each of these intervals. This gives a representation of the frequency shift information varying as a function of time. There are many techniques used in the joint time-frequency domain for extracting the micro-Doppler features and are broadly divided into Linear and Bilinear techniques. *Short-time Fourier transform* (STFT) and *Gabor transform* are the most commonly used linear transforms. Linear techniques are easier to compute but lack resolution. Bilinear transforms on the other hand, have a higher resolution, but suffer from the problems of cross-term

interference and are more complex to analyze. *Cohen's class*, *Wigner-Ville* distribution, *Choi-Williams* distribution and *Rihaczek* distribution are some of the commonly used bilinear techniques. The cross-term problems in bilinear techniques such as Wigner-Ville distribution, can be reduced using filtering techniques to form smoothed pseudo Wigner-Ville distribution [2]. However, this work concentrates on using a simple linear time-frequency transform for the analysis of micro-Doppler features. The most important requirements of any time-frequency transform are listed below.

- It must have high resolution in both time and frequency, so that it can efficiently characterize both the temporal and the spectral behavior of the analyzed signal
- It must not have any cross-term interference.

The time-frequency transforms must also not consume a lot for time for analysis so that they can be used for real-life applications.

4.2 Short-Time Fourier Transform

In this work, the STFT is considered for analysis. STFT is the simplest and the most commonly used linear time-frequency transform. The time-frequency representation of the square of the magnitude of STFT is known as the *spectrogram* of the signal. Since STFT is a linear transform, its resolution is lower, but it does not suffer from the cross-term interference problem. STFT also offers the advantages of low computational time and gives a good physical intuition of the analysis. The short-time Fourier transform operates by taking a signal and dividing it into shorter intervals of equal length in time-domain. It then computes the Fourier transform for each interval separately and adds them together to give the time-frequency representation of the frequency variations. The signals are divided in time using a *window function*, which is multiplied to the original signal to get a portion of

the signal at a desired instance. A window function is a mathematical function that has a ‘zero’ value outside a specific interval. Many types of windowing functions can be used such as the rectangular window, triangular window, gaussian window, hann window and hamming window of which gaussian and hamming windows are widely used ones. The size of the window function determines the resolution of the analyzed signal in the time-frequency domain. A larger window size gives a better resolution in frequency domain as more points are available for applying Fourier transform, but it reduces the resolution in temporal domain as the window covers a large time interval. Conversely, a smaller window size gives a better resolution in temporal domain, but lowers the resolution in frequency domain due to overlapping frequency components. This is attributed to the *uncertainty principle*, according to which it is impossible achieve arbitrary resolution in both time and frequency at the same time. The uncertainty here is not in the inherent resolution of the signal, but the information available at some arbitrary interval of time or frequency, due to the choice of window size [38]. So, it is not possible to have very small or very large windows and an optimum window size must be chosen based on the application, to achieve the desired resolution. Higher resolution in both time and frequency can be achieved by using overlapping windows. Generally, up to 50% overlapping windows are commonly used in the STFT based techniques. This work also employs 50% overlapping windows. Similar to short-time Fourier transform, short-frequency time transform can also be used in time-frequency analysis, where the signal is divided into short frequency intervals and the variations in time are analyzed using time transforms. However, it is not considered here as the goal here is to capture the variations in frequency caused by micromotions over a certain time interval.

As the value of the window function is zero outside a certain chosen interval, multiplying it with the signal to be analyzed, gives a localized short interval signal corresponding to the size of the window used. This multiplication effectively leaves the original signal unchanged around the time, t, as the window function is chosen to have its peak value at t, while the remaining portion of the signal goes to zero at that instant. Mathematically, if $h(t)$ is the window function centered at time, t, and $s(\tau)$ is the time domain signal containing the time dependent frequency variations, then the product of the two signals used for obtaining the Fourier transform is given by [38],

$$s_t(\tau) = s(\tau) \cdot h(\tau - t) \tag{4.1}$$

where

t is the fixed time at which the signal needs to be analyzed

τ is called the running time

The Fourier transform, $S_t(\omega)$ of this modified signal is given by [29],

$$S_t(\omega) = \frac{1}{\sqrt{2\pi}} \int e^{-j\omega\tau} s_t(\tau)\, d\tau \tag{4.2}$$

or,
$$S_t(\omega) = \frac{1}{\sqrt{2\pi}} \int e^{-j\omega\tau} s(\tau)\, h(\tau - t)\, d\tau \tag{4.3}$$

The window is slid through the original signal, forming short segments of the modified signal and Fourier transform is calculated for each of these segments. A 50% overlap between adjacent windows is used here to improve the accuracy of the analysis. All these segments are put together to obtain the time-frequency representation of the analyzed signal. The spectrogram represents the power of the magnitude of the STFT signal, $P_{STFT}(t, \omega)$ which is obtained as [38],

$$P_{STFT}(t,\omega) = |S_t(\omega)|^2 = \left|\frac{1}{\sqrt{2\pi}}\int e^{-j\omega\tau} s(\tau)\, h(\tau - t)\, d\tau\right|^2 \tag{4.4}$$

In this work, since the power of the received signal is measured instead of the fields, the squaring is not needed and the STFT data directly gives the spectrogram of the signal.

4.3 Vibrational and Rotational Micro-Doppler

When a quadcopter hovers at a height, it has two important micromotions which induce micro-Doppler variations: the vibrational micromotion due to the motors and the rotational micromotion due to the propellers. When observed from a certain distance, the micro-Doppler modulation induced by rotation is dominant as compared to the vibrational micro-Doppler. So, this work mainly concentrates on detecting the quadcopter utilizing the rotation induced micro-Doppler features. Along with rotational motion of the blades, the quadcopter can move back and forth or sideways, or have a precession motion, as shown in figure 4.1, and these motions also induce micro-Doppler modulations. However, these modulations vary much slowly in time and can be easily visualized when compared to the micro-Doppler modulation induced by rotational micromotions.

(a) (b) (c)

Figure 4.1. Different Motions a Quadcopter can have while Hovering (as seen from the Top): (a) Back and Forth Motion, (b) Sideways Motion, and (c) Precession Motion.

The micro-Doppler induced by periodic motion of targets changes only the phase of the reflected signal. For a linearly vibrating or a rotating target, if the direction of the vibration or rotation is along the direction of the incident radar signal, then the phase change is maximum and hence the frequency change is maximum. On the other hand, if the target vibration or rotation is orthogonal to the direction of the radar signal then the phase change and the corresponding frequency change are zero and thus the micro-Doppler variations cannot be detected. The micro-Doppler modulations induced by vibration or rotation depend on the rate at which the target vibrates or rotates, the operating frequency, and the angle between the direction of vibration or rotation and the direction of the incident radar signal. The induced frequency modulation will be perceived as a change of phase of the received signal.

Consider a target is vibrating at a rate equal to an angular frequency of ω_v, with a maximum amplitude of vibration equal to D_v. Then, the maximum frequency shift induced by the micro-Doppler due to vibrational micromotion as seen by a radar with an operating wavelength of λ is given by [2],

$$f_{micro-Doppler\_vibration} = \frac{2}{\lambda} D_v \omega_v \tag{4.5}$$

where

$$\omega_v = 2\pi f_v \tag{4.6}$$

f_v is the frequency of vibration

If the operating frequency is $f_0 = \frac{c}{\lambda}$, then the maximum micro-Doppler induced frequency shift is given by [2],

$$f_{micro-Doppler\_vibration} = \frac{4\pi f_0 \, f_v \, D_v}{c} \tag{4.7}$$

The back and forth motion due to vibration induces a sinusoidal modulation on this frequency shift over a duration of time, t, which is given by [2],

$$f_{micro-Doppler\_vibration} = \frac{4\pi f_0 \, f_v \, D_v}{c} \cos(2\pi f_v t) \tag{4.8}$$

The above equations represent the situation when the target is directly in front of the antenna. But, this might not be the case always and the target may be located at a certain height such that its periodic motion forms an angle between 0^0 and 90^0 with respect to the radar signal. In such conditions, the angular information must be considered for frequency shift calculations. In this work however, owing to the reasons of low-power system and narrow beamwidth of the antenna, the target is positioned directly in front of the antenna and thus, the analysis for additional angular modulations is not considered.

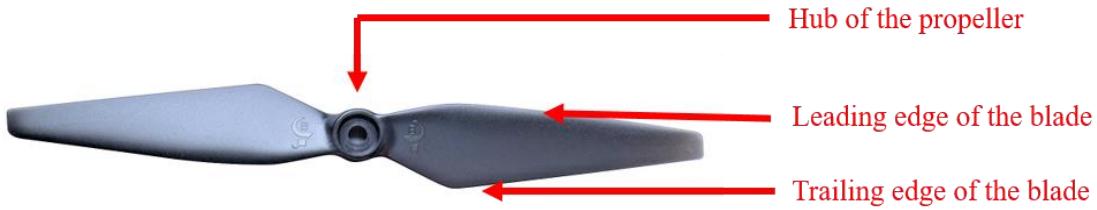

Figure 4.2. A Single Propeller of the Quadcopter used in this Research.

A single propeller with two blades as shown in figure 4.2 is considered for the analysis of the rotation induced micro-Doppler modulation. The leading edge has the lowest radius of curvature and cuts through the air to generate thrust. A point scatterer model of the single propeller is used to analyze the micro-Doppler variations caused by the rotation of the blades. At first, only three points will be considered; one for the central hub of the propeller and the other two for the tips of each of the two blades. Since the maximum frequency shift corresponds to the tip velocity, it is necessary to calculate the tip velocity

of the blades. In this analysis, the blades are assumed to be rotating at a rate of 1000 rpm. Then the angular velocity of the blades is,

$$\omega = 1000 \cdot \frac{2\pi}{60} = 104.7198 \text{ radians/s} \tag{4.9}$$

With the blade lengths of 69 mm, the corresponding tip velocity is given by,

$$v_{tip} = \omega \cdot r = 104.7198 \cdot 69 \cdot 10^{-3} = 7.2257 \text{ m/s} \tag{4.10}$$

At an operating frequency of 270 GHz, this velocity gives a maximum frequency shift of,

$$max(f_{micro-Doppler\_rotation}) = \frac{2f_0 v_{tip}}{c} = 13.0063 \text{ kHz} \tag{4.11}$$

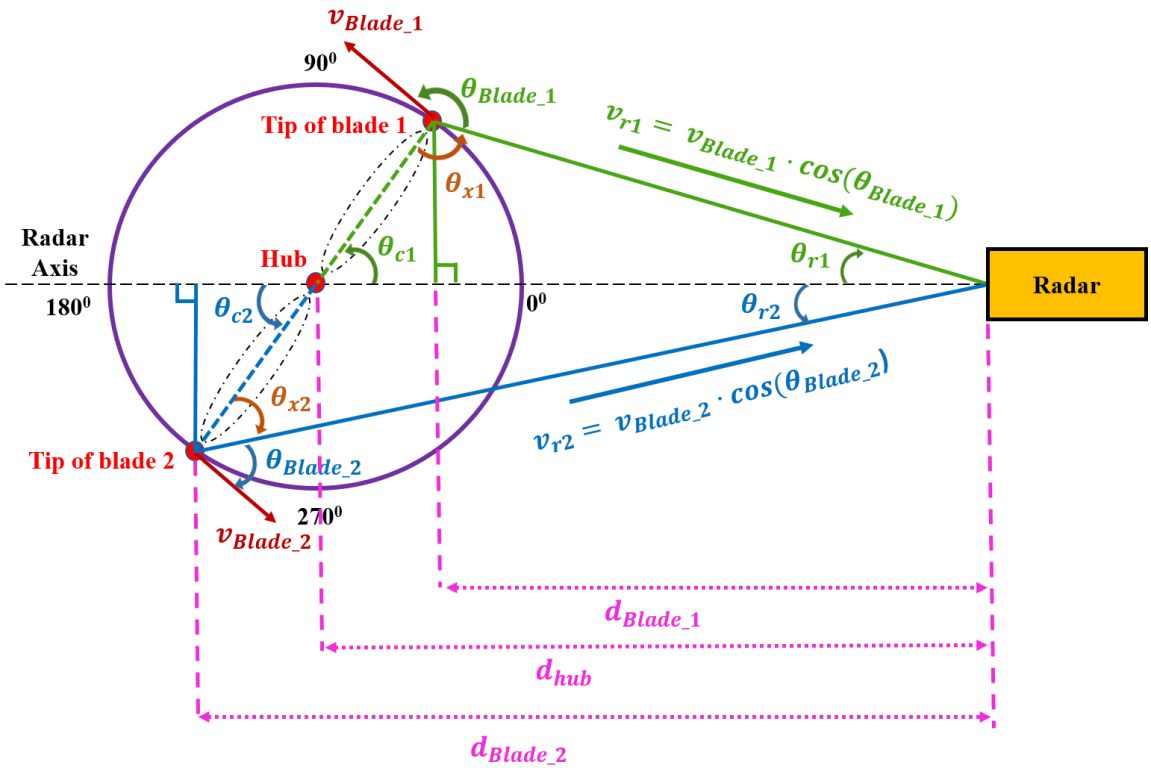

Figure 4.3. Model used for Analysis of Instantaneous Frequency Shift Produced by a Single Propeller with two Blades, using a Point Scatterer Model. Only the Tips of the Blades and the Hub of the Propeller are Considered.

The instantaneous frequency shift at any point during this rotation can be calculated using the model shown in the figure 4.3. Since the blades are assumed to rotate at 1000 rpm or 16.6667 rps, they need 0.06 seconds (60 ms) to complete 1 rotation. Thus, the blades complete a rotation in 6^0 angular increments every millisecond as they follow a circular path. The instantaneous angles between the radar and the two blades which are called here as the radar angles are denoted by θ_{r1} and θ_{r2} respectively. These angles can be obtained by first finding the horizontal distances of the blade tips from the radar. The horizontal distances are the projections of the blade tips onto the radar axis. Thus, d_{Blade_1} is the horizontal distance of the tip of the first blade from the radar. Similarly, d_{Blade_2} and d_{Hub} are the distances of the tip of the second blade and the hub respectively from the radar. θ_{c1} and θ_{c2} are the central angular increments at which the blades rotate and since, the blades on the same axis, $\theta_{c1} = \theta_{c2}$. So, at any instant of time, the central angle and the radar angle are known. To find the required angle between the incident radar signal and the direction of motion of the blade tips given by the velocity vectors, $v_{Blade_1}$and v_{Blade_2}, the two arbitrary angles formed by the propeller body with the direction of the incident radar signal must be first found. These two angles represented by θ_{x1} and θ_{x2} are calculated as,

$$\theta_{x1} = 180^0 - \theta_{r1} - \theta_{c1} \tag{4.12}$$

$$\theta_{x2} = 180^0 - \theta_{r2} - (180^0 - \theta_{c2}) \tag{4.13}$$

It must be noted that the two velocity vectors, $v_{Blade_1}$and v_{Blade_2} are tangential to the circle that the blades traverse. From θ_{x1} and θ_{x2}, the two angles between the incident radar signal and the direction of motion of the tip of the blades is calculated as,

$$\theta_{Blade\_1} = 360^0 - \theta_{x1} - 90^0 \tag{4.14}$$

$$\theta_{Blade\_2} = 90^0 - \theta_{x2} \tag{4.15}$$

where

θ_{Blade_1} and θ_{Blade_2} are the angles between the direction of the incident radar signal and the direction of motion of the tips of blade 1 and blade 2 respectively

Finally, the radial velocities in the direction of the radar signal are obtained as,

$$v_{r1} = v_{Blade\_1} \cdot \cos(\theta_{Blade\_1}) \tag{4.16}$$

$$v_{r2} = v_{Blade\_2} \cdot \cos(\theta_{Blade\_2}) \tag{4.17}$$

where

v_{r1} and v_{r2} are the radial velocities of the tips of blade 1 and blade 2 respectively in the direction of the radar signal

As the blades rotate, each of these radial velocities are used to calculate the time dependent frequency shift caused by the rotational micromotion. These frequency shifts dues to the two blades denoted by $f_{micro-Doppler\_rotation1}$ and $f_{micro-Doppler\_rotation2}$ are given by,

$$f_{micro-Doppler\_rotation1} = \frac{2v_{r1}f_0}{c} \tag{4.18}$$

$$f_{micro-Doppler\_rotation2} = \frac{2v_{r2}f_0}{c} \tag{4.19}$$

Considering a single blade tip, the maximum frequency shift is obtained when the blade tip is at 90^0 or 270^0, and minimum shift is obtained when the blade tip is at 0^0 or 180^0. This is because when the blade tip is at 90^0 or 270^0, the angle between the direction of the radar signal and the velocity vector is close to 0^0, and since $cos0 = 1$, a maximum frequency shift is obtained. On the other hand, when the blade tip is 0^0 or 180^0, the velocity vector is perpendicular to the direction of the radar signal and thus, a minimum frequency

shift is obtained which is zero. If a_1, a_2, a_3, and a_4 correspond to the position of the blade tip at 0^0, 90^0, 180^0 and 270^0 respectively, then each of these points are represented on the sinusoidal frequency modulation as shown in figure 4.4.

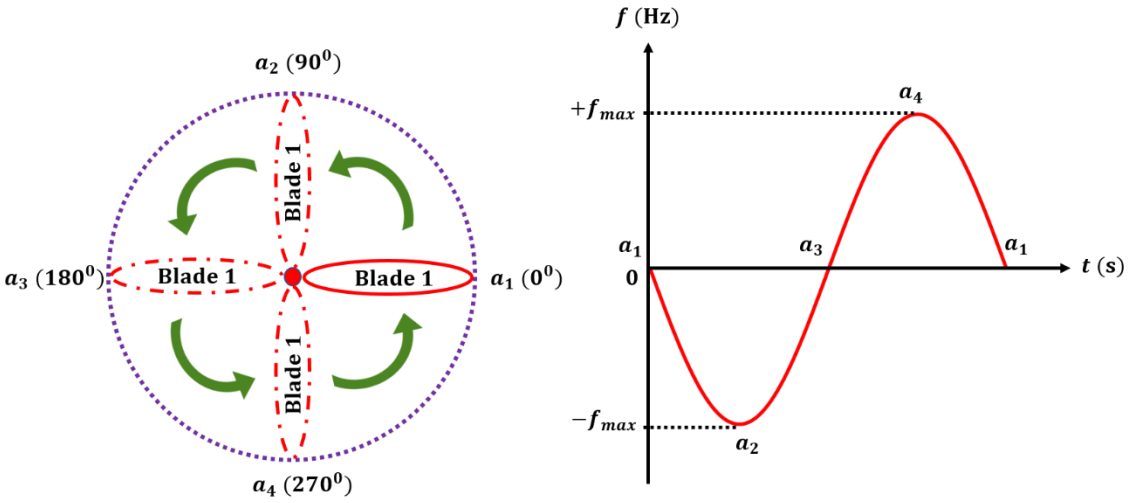

Figure 4.4. Variation of frequency Shift as a Function of Position and Time.

The motion of blade 1 in the four quadrants and its effect on the frequency shift is explained as follows. At a_1, the velocity vector is perpendicular to the radar signal and thus, the frequency shift is 0. As, the blade tip moves towards a_2, it is going away from the radar, but the angle between the radar signal and the velocity vector decreases. Thus, the frequency shift is negative, and it reaches a maximum value of $-f_{max}$ at a_2. As it moves from a_2 to a_3, the blade is still going away from the radar and the angle between the radar signal and the velocity vector is also increasing. As a result, the frequency shift is still negative, and it is decreasing as well. At a_3, the frequency shift again becomes 0. The motion from a_3 to a_4 is associated with decrease in both the distance from the radar and the angle between the radar signal and the velocity vector. This causes the frequency shift to be positive and it reaches a maximum value of $+f_{max}$ at a_4. Finally, as the blade moves

from a_4 back to a_1, the distance from the radar is still decreasing, while the angle between the radar signal and the velocity vector increases. Thus, the frequency shift still remains positive, but decreases. At a_1, the frequency shift goes back to 0. When both the blades are considered together along with the hub, the frequency shift from the tips of the two blades follow opposite trends, which means, when the frequency shift from the tip of blade 1 traces the negative half cycle of the sine wave, the frequency shift from the tip of the blade 2 traces the positive half cycle of the sine wave. However, since the hub always remains at the same place, the frequency shift obtained from it is always 0.

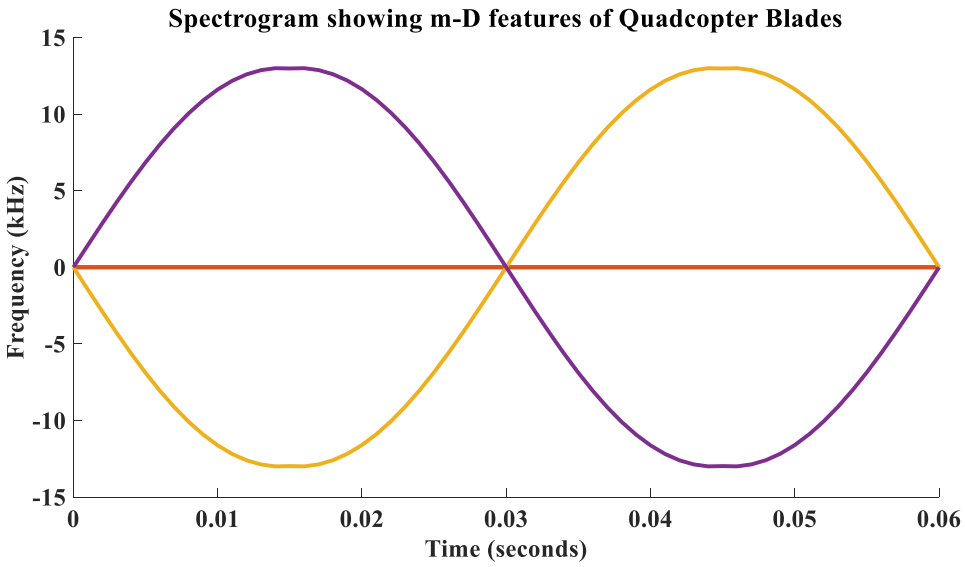

Figure 4.5. Spectrogram of the Rotation Induced Micro-Doppler Modulation using Point Scatterer Model with 3 Points.

A Matlab code is developed to trace the motion of the blades as they rotate on their axis. The sinusoidally modulated frequency shift obtained by the rotating blades is plotted in figure 4.5. The yellow curve corresponds to micro-Doppler modulations from the blade tip 1, the blue curve corresponds to the micro-Doppler modulations from the blade tip 2 and the brown line is due to the constant reflections from the hub of the propeller. Here,

only 3 points are considered for the point scatterer model and the micro-Doppler modulation corresponding to only one rotation is plotted. From figure 4.5, the maximum frequency shift obtained is 13 kHz. If the number of points are increased, the frequency shifts due to reflections from different parts of the blade can be seen. One such plot considering 31 points is plotted for a longer duration of time of 0.6 s is potted in figure 4.6.

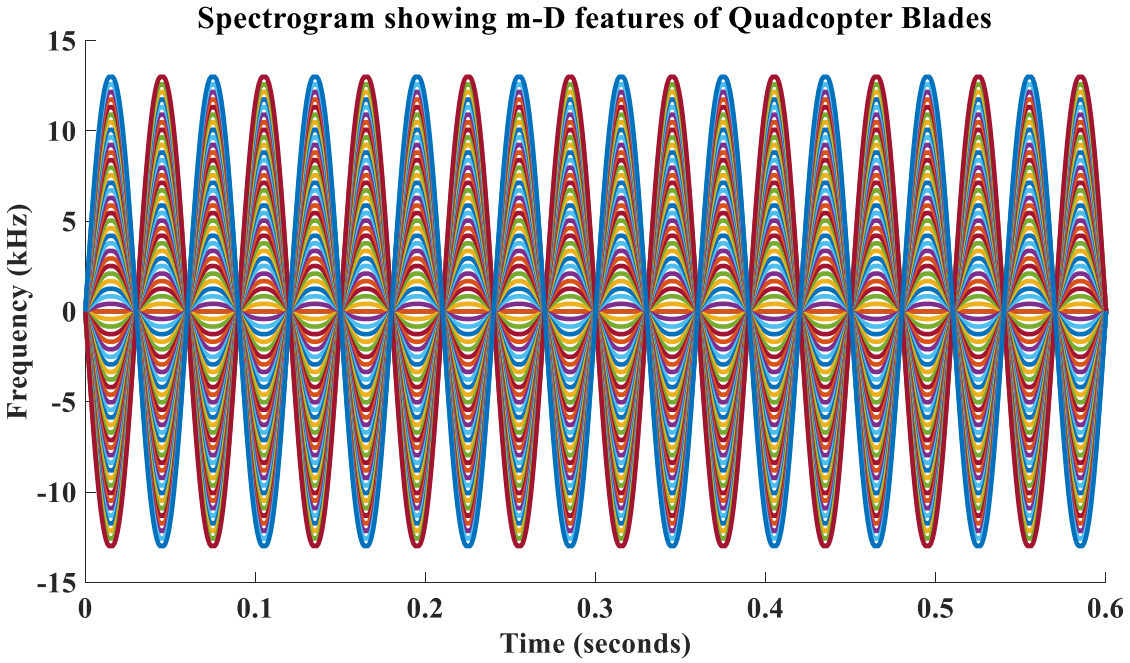

Figure 4.6. Spectrogram of the Rotation Induced Micro-Doppler Modulation using Point Scatterer Model with 31 Points.

Although it is not possible to detect the micro-Doppler modulations induced by vibration at long distances, the back and forth motion of the quadcopter while hovering can be considered as a slow vibration with a large amplitude. If this back and forth motion of the quadcopter body alone is modeled using the point scatterer model, the frequency modulation induced by this motion can be plotted. Here, the entire body can be considered as a single point as the frequency shift obtained by the whole body of the quadcopter will

be the same. Here the quadcopter has a maximum displacement, D_v of 0.5 m as it moves back and forth in front of the radar. However, the motion happens at a slow rate of 0.2 Hz, and thus the maximum frequency shift that can be obtained is,

$$f_{micro-Doppler\_vibration} = \frac{4\pi f_0 \, f_v D_v}{c} = 1.131 \text{ kHz} \tag{4.20}$$

This frequency modulation varies over time between +1.131 kHz and -1.131 kHz as governed by (4.8), when the quadcopter moves back and forth and is shown in figure 4.7.

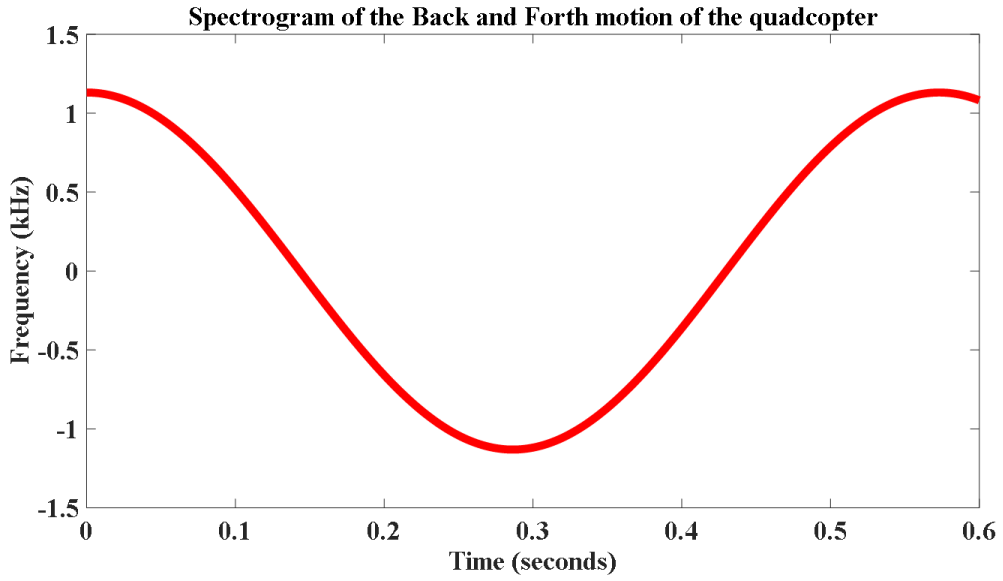

Figure 4.7. Micro-Doppler Variation due to Back and Forth Motion of the Quadcopter.

The precession motion of the quadcopter will also have a similar micro-Doppler modulation. However, the sideways motion will not be associated with any modulations as it is orthogonal to the direction of the incident radar signal.

As a final step, the back and forth motion of the quadcopter shall be combined with the rotational motion of the blades. Still a single propeller model is used and the micro-Doppler modulation caused by the rotational motion together with the back and forth motion is plotted in figure 4.8.

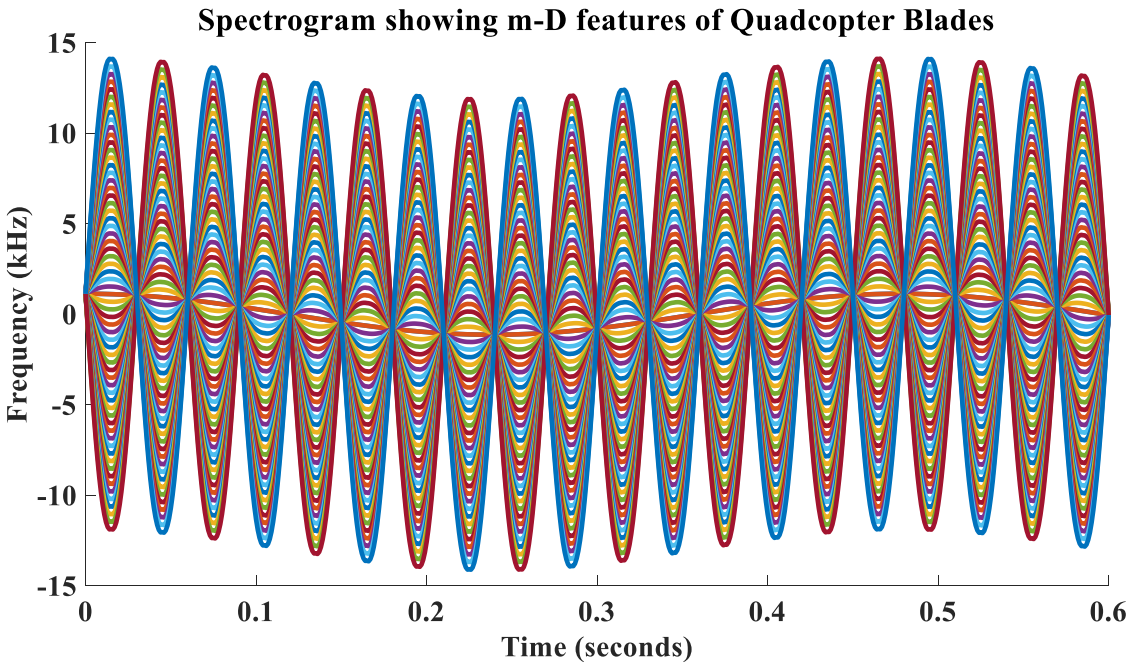

Figure 4.8. Micro-Doppler Modulation caused by Rotation of Blades Together with Back and Forth Motion of the Quadcopter covering a Distance of 0.5 m.

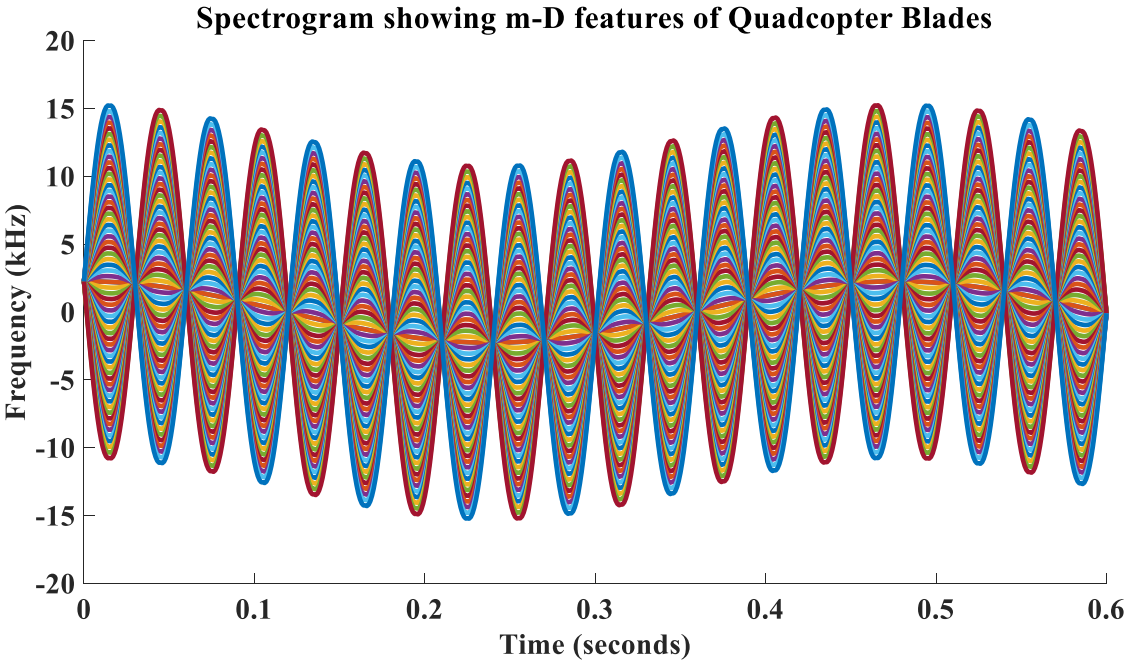

Figure 4.9. Micro-Doppler Modulation caused by Rotation of Blades Together with Back and Forth Motion of the Quadcopter covering a Distance of 1 m.

Although the variation in amplitude can be seen in the plot of figure 4.8, it is small compared to the frequency shift obtained by rotation. Hence, only a small modulation is seen due to the back and forth motion. However, if the maximum displacement due to back and forth motion is further increased such that the quadcopter hovers back and forth over a distance of 1m instead of 0.5 m, a more pronounced effect of this motion on the micro-Doppler modulation can be seen as shown in figure 4.9.

The analysis in this section considers ideal conditions with only a single propeller model. However, in real life situations, the scenario is more complex. When all four propellers are considered, there will be multiple reflections which can cause signal losses. Additionally, in the analysis, material used for the blades and the quadcopter body are not considered. In general, most of the quadcopters are made of plastics or carbon fiber, which are not as reflective as conducting materials. This results in the further loss of received signal power especially from the tips of the blade which have very low radar cross sections. Also, it would be difficult to include the multipath propagation losses here. Because of all these reasons, the ideal frequency shift values have been obtained and plotted in this section. In the next section, measurements will be conducted using real quadcopters and it will be shown how these problems appear in practical scenarios.

CHAPTER 5

MEASUREMENT SETUP AND RESULTS

In this chapter, the measurement setups used to obtain the micro-Doppler frequency modulations induced by the vibrational and the rotational micromotions associated with the quadcopter operation. At first, the vibrational micromotion due to the motors in the quadcopter is measured. It is followed by the rotational micromotions from the propellers of a stationary quadcopter. Finally, the micro-Doppler modulations obtained from the quadcopter hovering in front of the radar is detailed. The back and forth, precession and the sideways motions are some of the common motion traits of a quadcopter in flight. Thus, the micro-Doppler modulations caused by these three motions are measured and analyzed together with the propeller rotation.

The THz micro-Doppler radar setup used for measurements is shown in figure 5.1. The RF signal and the LO signals from the two ports of the vector network analyzer (VNA) are fed into the RF and LO inputs of the transmitting frequency extender using coaxial cables. Here the RF signal is upconverted to 270 GHz and transmitted by the transmitting horn antenna. The reflected signals from the quadcopter are received by the receiving horn antenna, down converted to an IF of 279 MHz and displayed on the signal analyzer. This process is repeated for a duration of 6 seconds, with each measurement sweep taking 60 ms. All the data is accumulated by the Matlab code which controls the entire measurement process and a spectrogram showing the micro-Doppler frequency variations over time is plotted. Short-time Fourier transform is used with 50% overlapping windows for obtaining the time-frequency plot.

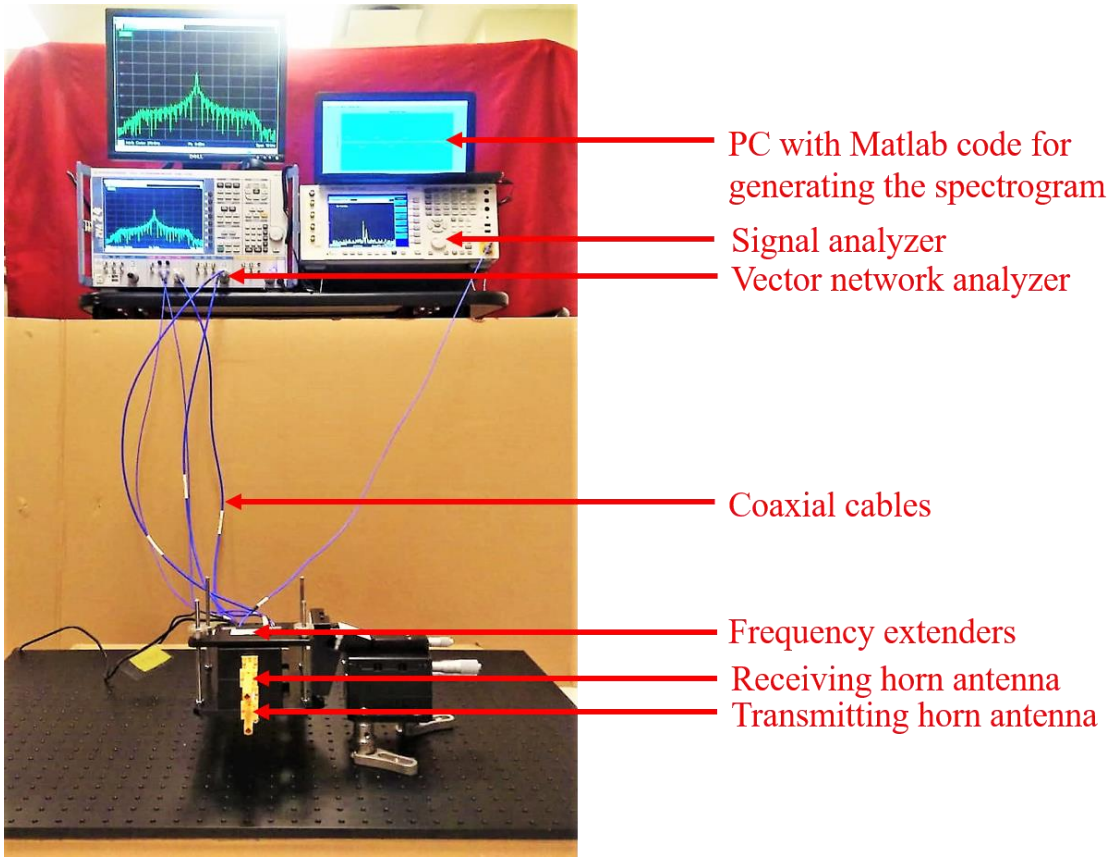

Figure 5.1. THz Micro-Doppler Radar Setup used for Measurements.

5.1 Vibration Induced Micro-Doppler Modulations

Since the vibration induced micro-Doppler modulations can only be observed at close distances, the measurement distances have been restricted to be within 0.5 m from the radar. This is also useful in focusing onto the bottom part of the quadcopter's fuselage, which has the highest vibration and the largest RCS. Two measurement distances are considered; 0.2 m and 0.4 m and the spectrograms of the micro-Doppler modulations are obtained for each case. The maximum power transmitted from the radar is -6dBm. This signal when intercepted by the quadcopter, gets reflected and returns to the radar. During this course, it further loses power and thus, the maximum received power is of the order of -100 dBm for a stationary quadcopter, and about -80 to -90 dBm for a vibrating quadcopter.

The horn antenna has a half-power beamwidth of 10^0. For any particular distance of interest, the *field of view* (FoV) depends on this beamwidth as shown in figure 5.2.

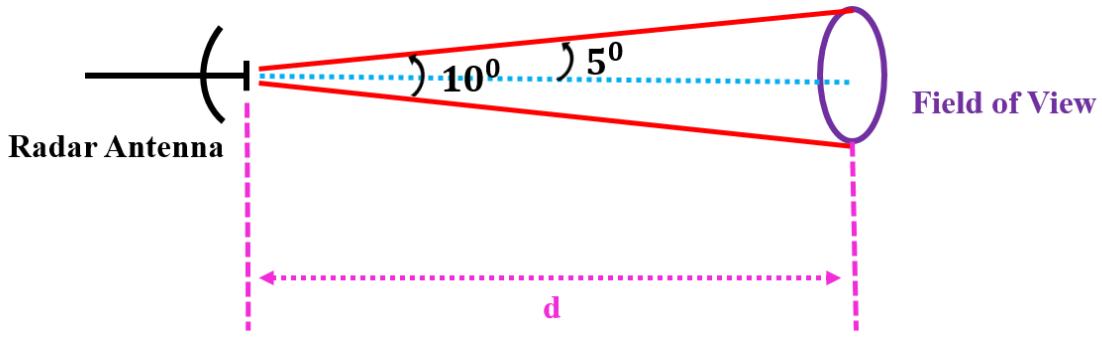

Figure 5.2. Half-power Beamwidth and Field of View of the Horn Antenna.

For a distance, $d = 0.2$ m, the diameter of the FoV is calculated to be 35 mm, and for $d = 0.4$ m, it is 70 mm. These two FoVs are ideal to focus only on the vibrating bottom part of the quadcopter masking the propellers from view. The arrangement used for measuring the vibrations is shown in figure 5.3. The quadcopter is placed vertically facing the radar so that the FoV is restricted to the region shown in yellow in the figure. At first, a measurement is taken for the case when quadcopter is off and then for the case when the rotors are turned on to account for vibrations. The spectrograms look identical for both the distances when the quadcopter is off. It is seen as a single straight line which represents the peak of the received signal that is not shifted in frequency through-out the entire duration of 6 seconds. However, when the quadcopter is turned on, the number of components in the spectrogram increases. The strong central line is still seen due to the low SNR of the received signal. However, the spectral components decrease as the distance increases. This is due to the fact that the signal undergoes a higher loss as the distance increases. As a result, it becomes difficult observe the micro-Doppler modulation due to vibrations. Figure 5.4 shows the typical spectrum for the stationary quadcopter with blades

off and in figure 5.5, the corresponding spectrogram of the quadcopter with blades off is shown. They are followed by the spectrograms of the quadcopter with blades on at 0.2 m and 0.4 m respectively in 5.6 (a) and (b).

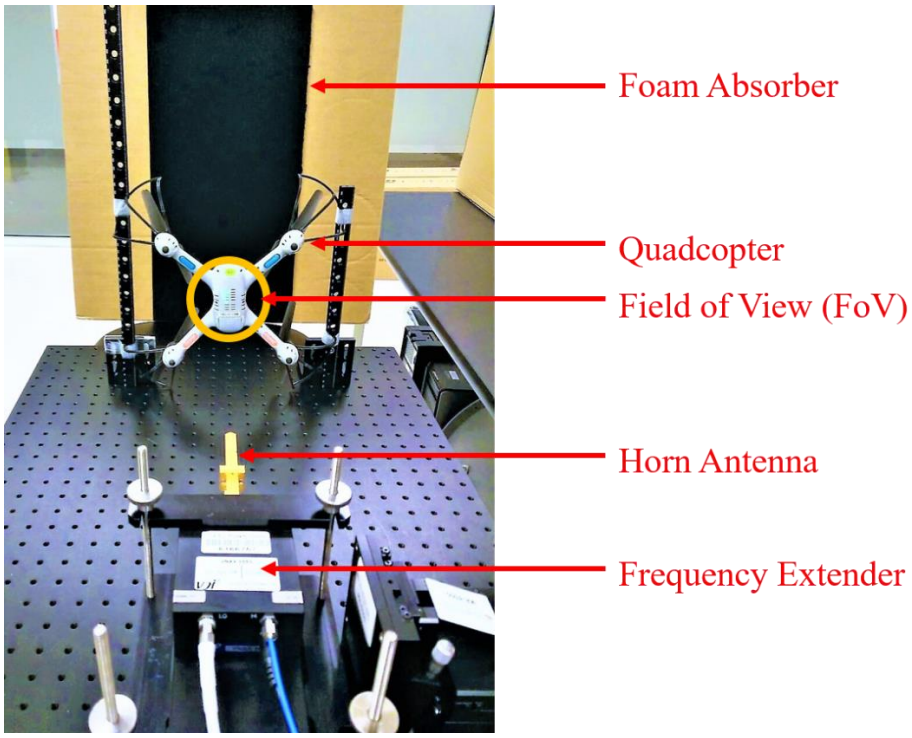

Figure 5.3. Arrangement used for Measuring Vibrations from Quadcopter.

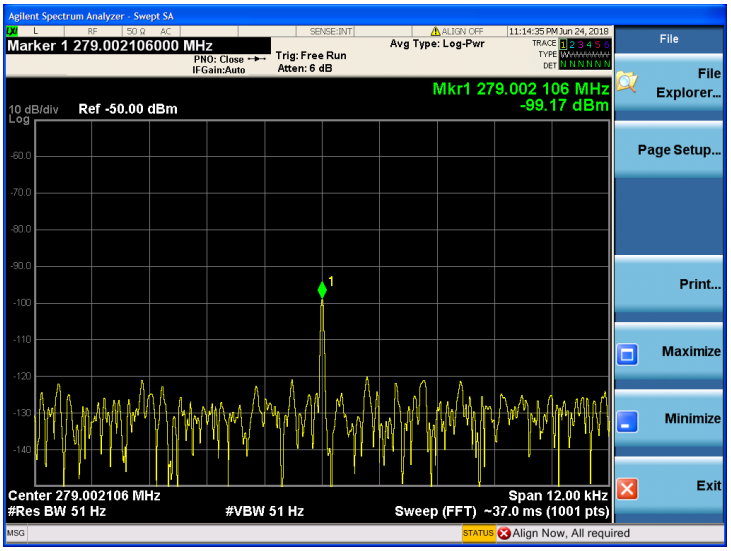

Figure 5.4. Spectrum of a Stationary Quadcopter with Blades off.

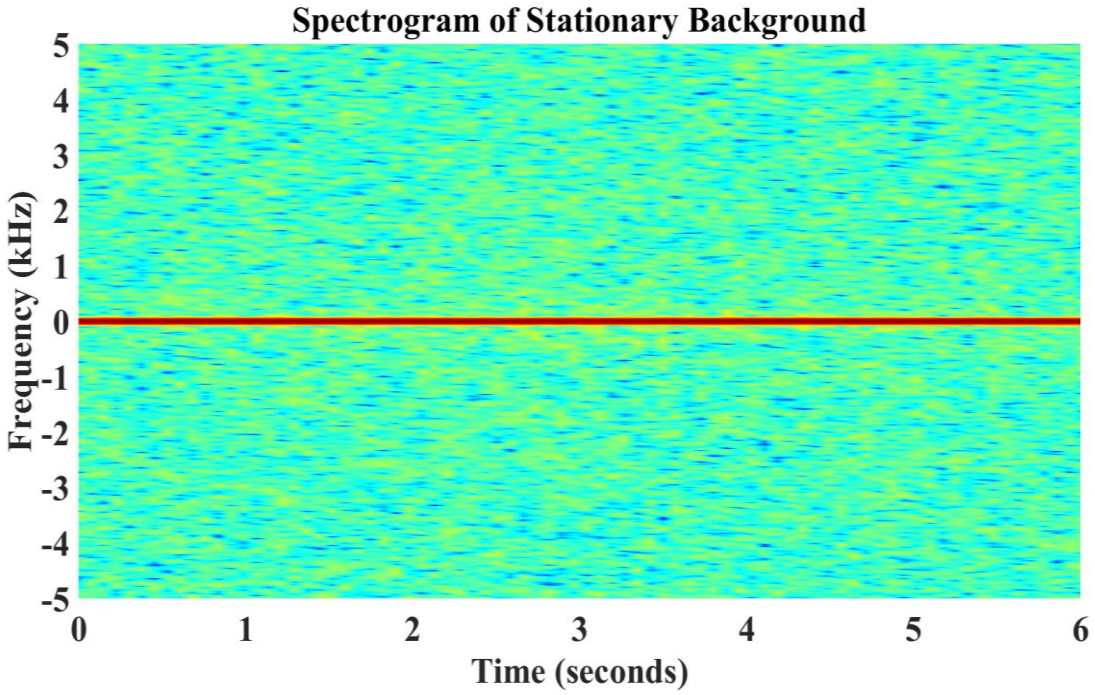

Figure 5.5. Spectrogram of the Stationary Quadcopter with Propellers Turned off. Since the Quadcopter remains Stationary, the Frequency Shift is Zero, and thus, a Single Line is seen that Corresponds to Received Signal at 279 MHz for the Entire Duration of 6s.

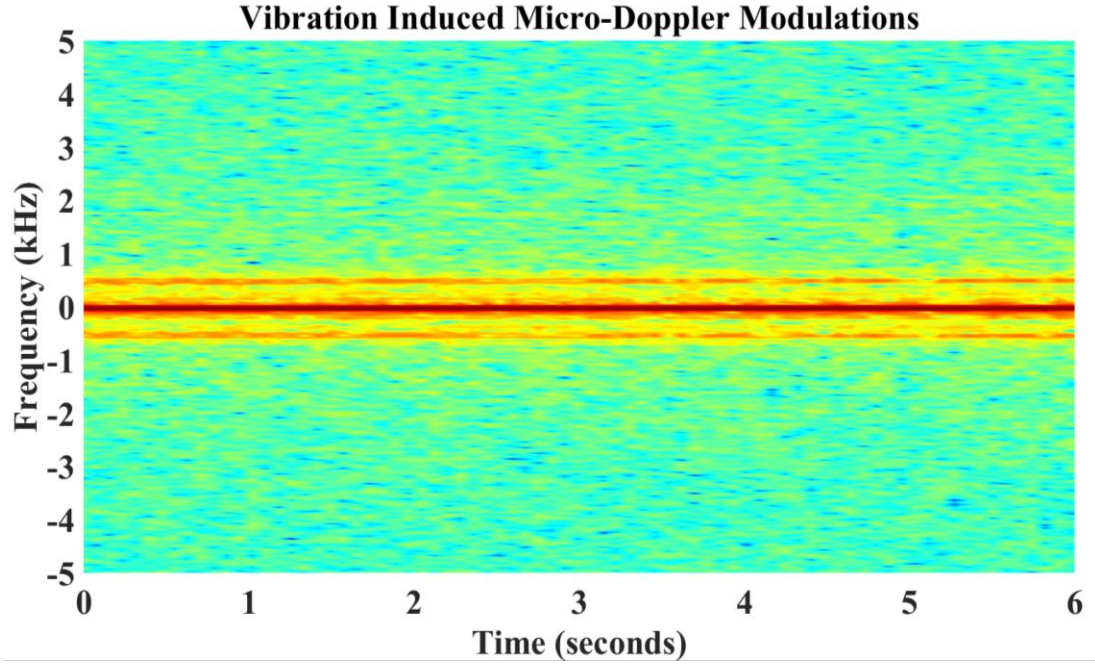

(a)

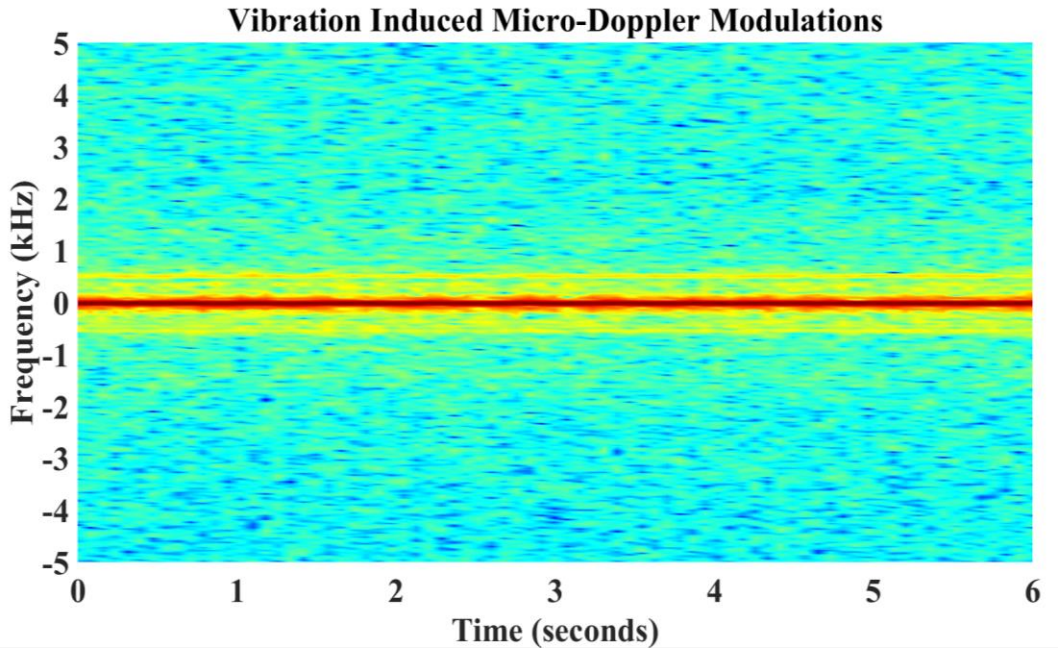

(b)

Figure 5.6. Spectrogram of the Vibration Induced Micro-Doppler with Propellers Turned on at a Distance of (a) 0.2 m, and (b) 0.4 m from the radar

To extract the micro-Doppler modulations induced by vibration, the simple STFT technique used in this research is not sufficient as it lacks the required resolution, and thus, more complex analysis methods like bilinear transforms, wavelet transforms, Wigner-Ville distribution etc., must be employed. This has not been included in this work, and will be considered in the future. However, by looking at the spectrum it is very clear that the amplitude of the received signal decreases as the distance from the radar increases.

5.2 Rotational Micro-Doppler from Stationary Quadcopter

To obtain the micro-Doppler modulations induced by rotation, the quadcopter is placed horizontally at a distance of 1.5 m, such that the propellers are directly facing the antenna. The arrangement used for measurement is shown in the figure 5.7. The four different configurations in which the quadcopter is used are shown in figures 5.8 (a), (b), (c) and (d).

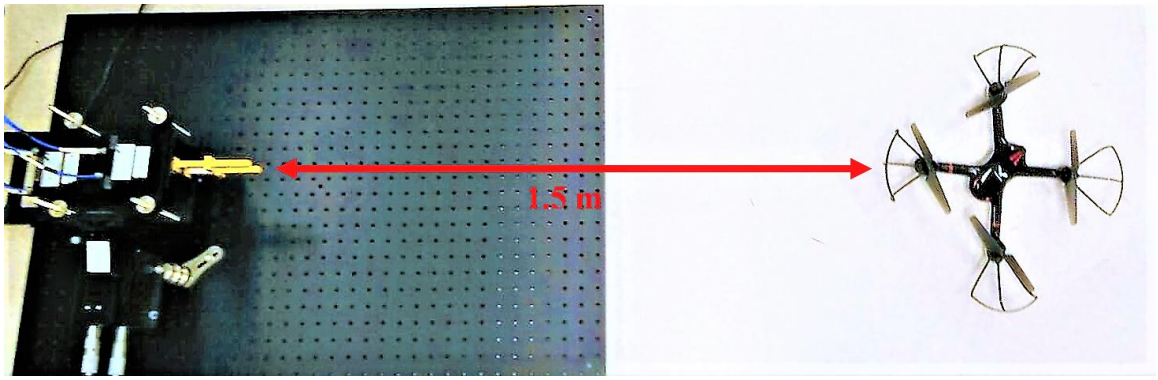

Figure 5.7. Top view of the Setup for Measuring Rotation Induced Micro-Doppler with the Quadcopter placed at a Distance of 1.5m from the Radar.

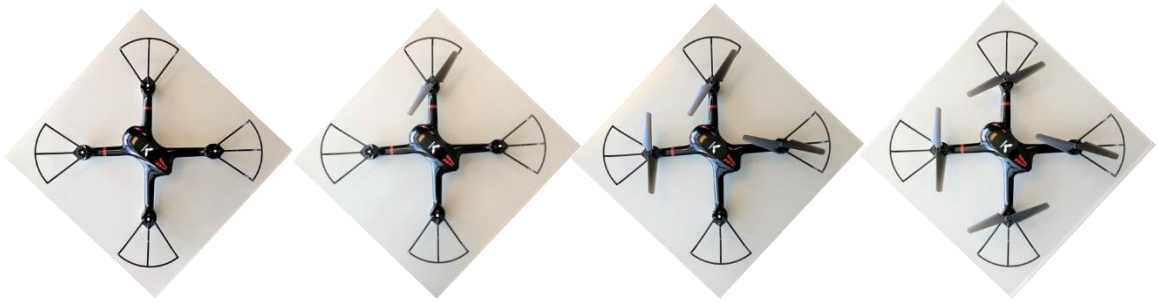

(a) (b) (c) (d)

Figure 5.8. Top view of the Quadcopter with (a) No Propeller, (b) One Propeller, (c) Three Propellers, and (d) Four Propellers used for Measurements.

When all the blades are removed, the micro-Doppler variations are only due to the vibration of motors. However, as seen in figure 5.9 (a), due to the increased distance, the vibrations are not detectable and the spectrogram for this case is same as that of the situation when the quadcopter is turned off (figure 5.5). This confirms that as the distance increases, it becomes difficult to capture micro-Doppler variations due to vibration. When the front propeller alone is used the spectrogram is as shown in figure 5.9 (b). As the propellers are increased, the spectral content increases as seen in the subsequent figures 5.9 (c) and 5.9 (d). However, it is not easily discernible as the reflections are dominated by the

front propeller of the quadcopter as compared to the other propellers. Again, this can be rectified by extracting the micro-Doppler features using more complex time-frequency transforms as in [2], [4], [7], and [10], which will be considered in the future works.

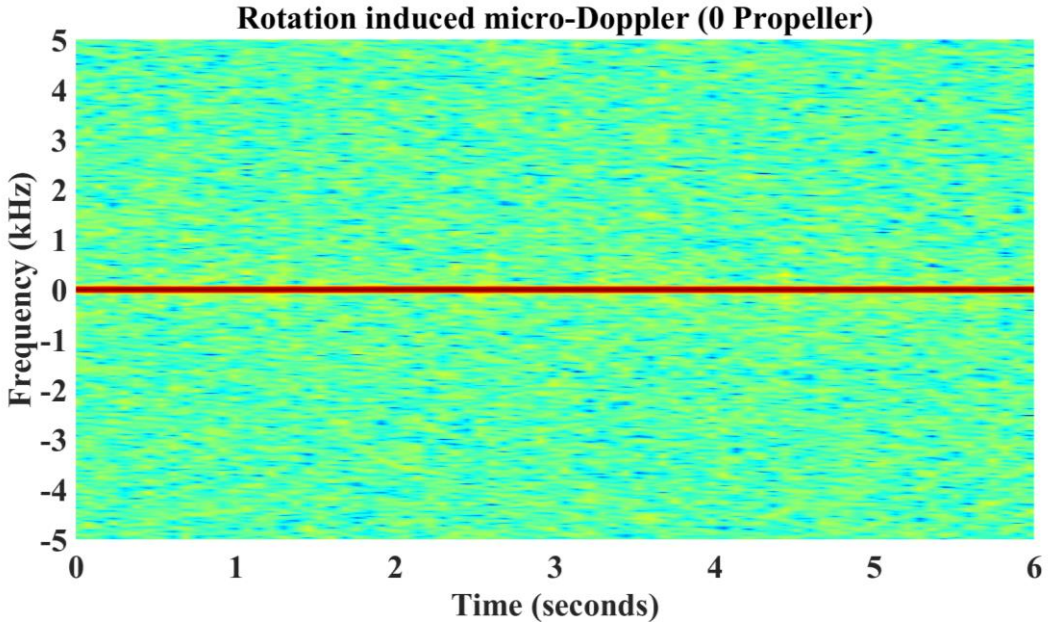

(a)

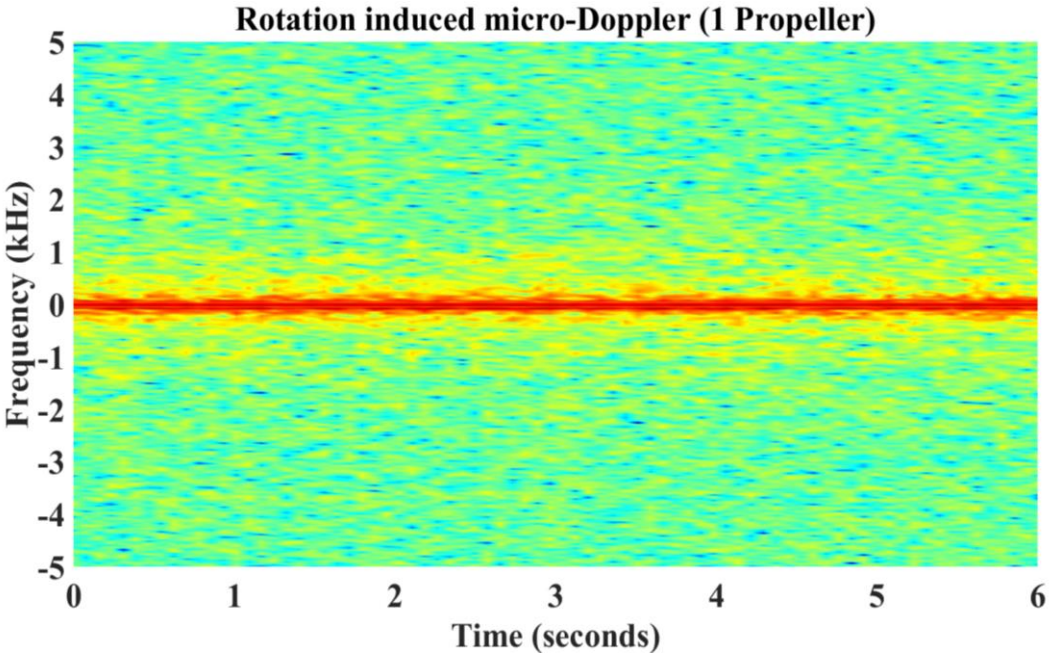

(b)

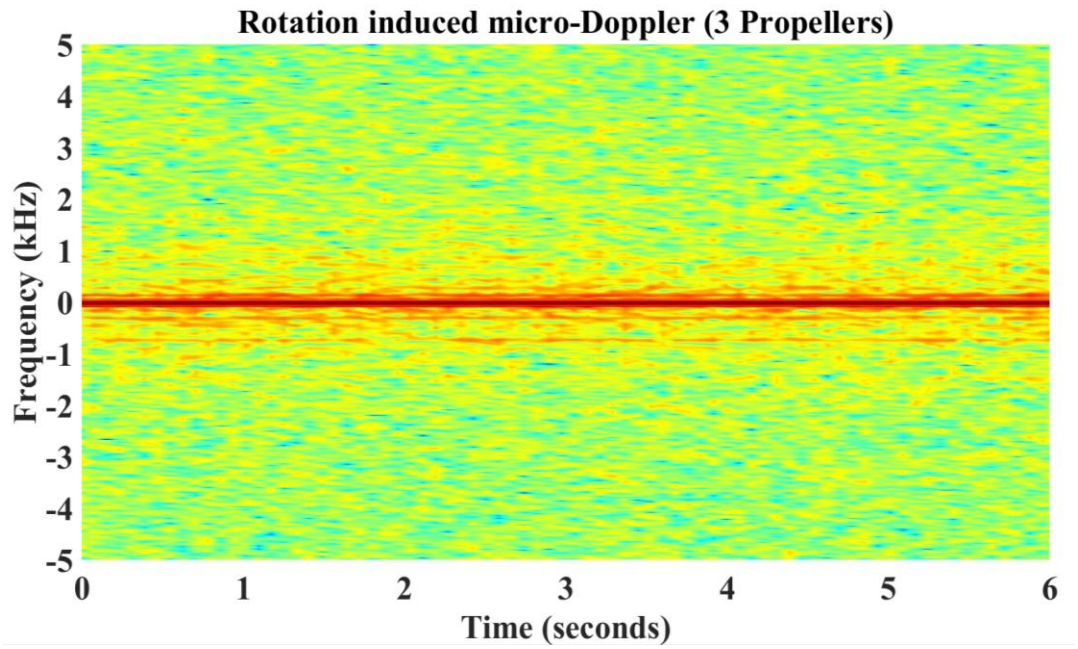

(c)

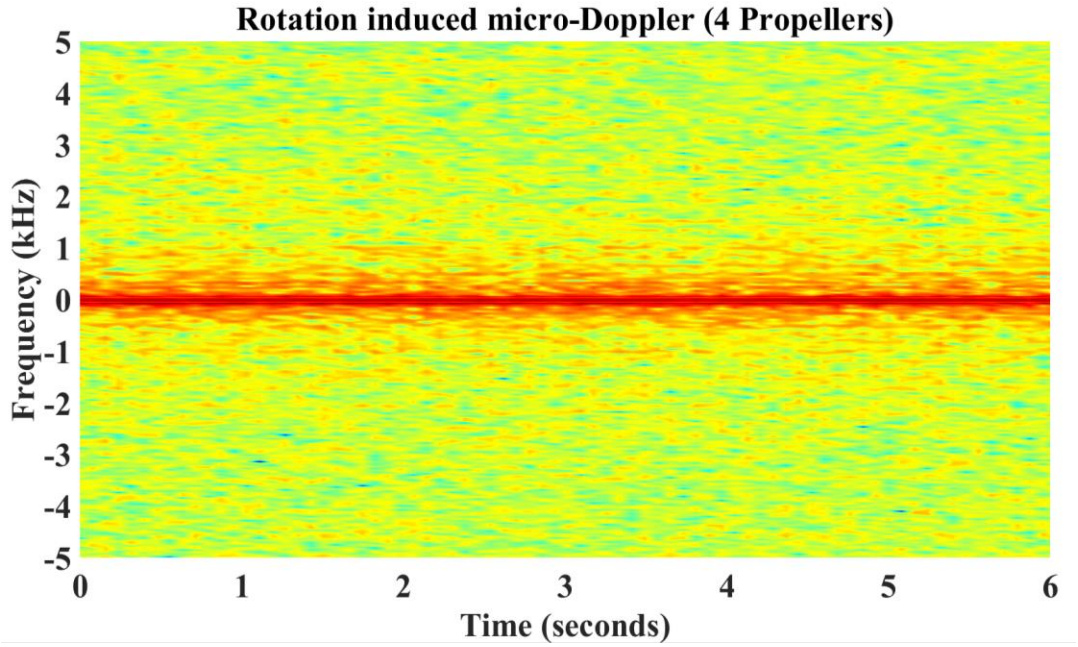

(d)

Figure 5.9. Spectrograms of the Rotation Induced Micro-Doppler when the Quadcopter is made to have (a) No Propellers, (b) One Propeller, (b) Three Propellers, and (d) Four Propellers.

5.3 Micro-Doppler Modulations from Quadcopter in Flight

In this section, the quadcopter is made to hover in front of the radar at a height of about 0.4 m and the micro-Doppler modulations caused by the rotation of blades together with back and forth, precession or sideways motion are recorded. Three distances are considered for measurements: 1.5 m, 2 m and 3 m. The quadcopter is suspended using a thin thread of very-low reflectivity to control the height at which it is flown. The suspended quadcopter is shown in figure 5.10.

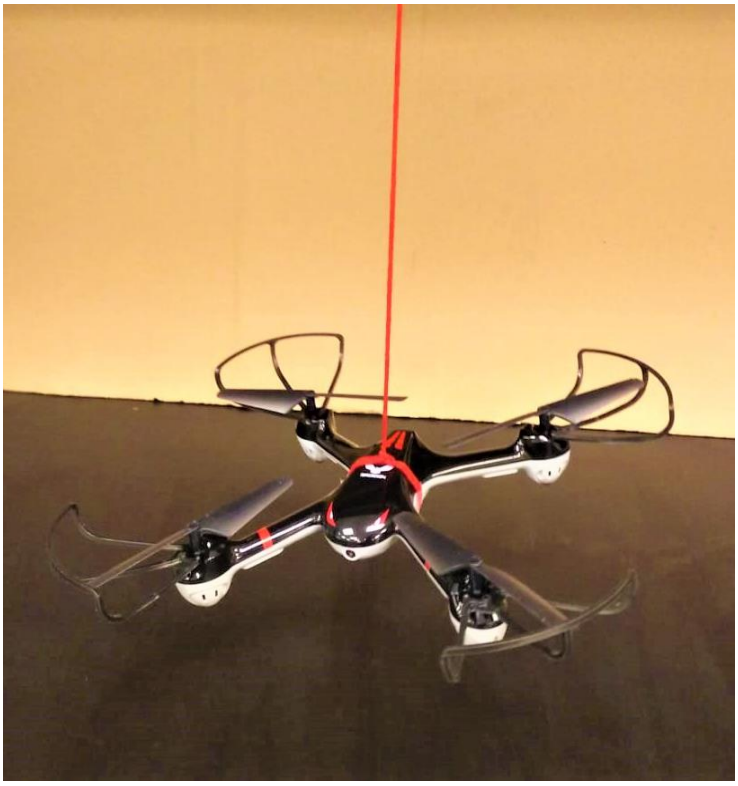

Figure 5.10. Quadcopter Suspended with a Thread of very-low Reflectivity.

5.3.1 Quadcopter at 1.5 m

The spectrogram obtained for the stationary quadcopter with blades off is still the same as in figure 5.5. When the blades are rotating and the quadcopter hovers with a back and forth motion, the spectrogram obtained is as shown in figure 5.11.

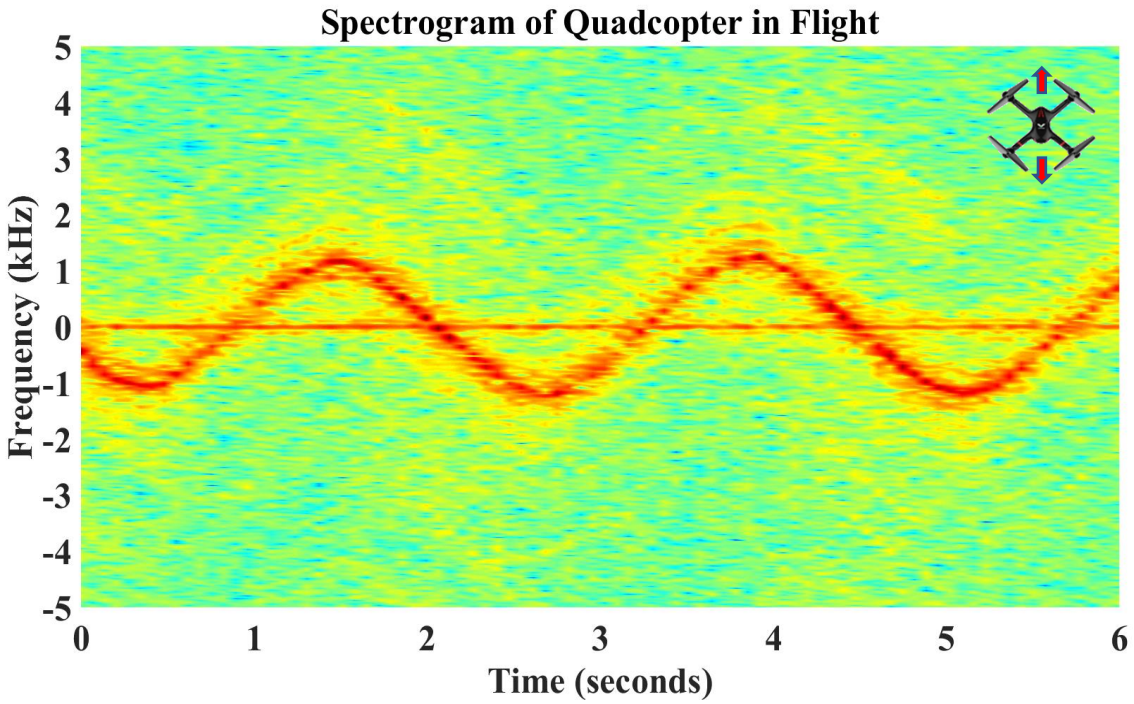

Figure 5.11. Spectrogram of Hovering Quadcopter with Back and Forth Motion.

In the spectrogram, the center line appears due to the reflections from the stationary background due to the operation in indoor environment. Although absorbers are used, as the SNR of the received signals are very low, it is difficult to get rid of the background clutter. However, this problem is not expected to be present in the actual quadcopter tracking scenarios where the operation happens in the outdoor environment. As seen in figure 5.4, the signal received from this stationary background is around -100 dBm, while the noise floor is around -120 dBm. Thus, 20 dB is subtracted from the center of the spectrogram to remove the effect of background reflections. The spectrogram obtained after such a modification is shown in figure 5.12. Since the background reflections are dominantly seen in all measurements because of the low power capabilities of the THz system, resulting in low SNR, stationary peak subtraction is done for all the measurement results shown hereafter.

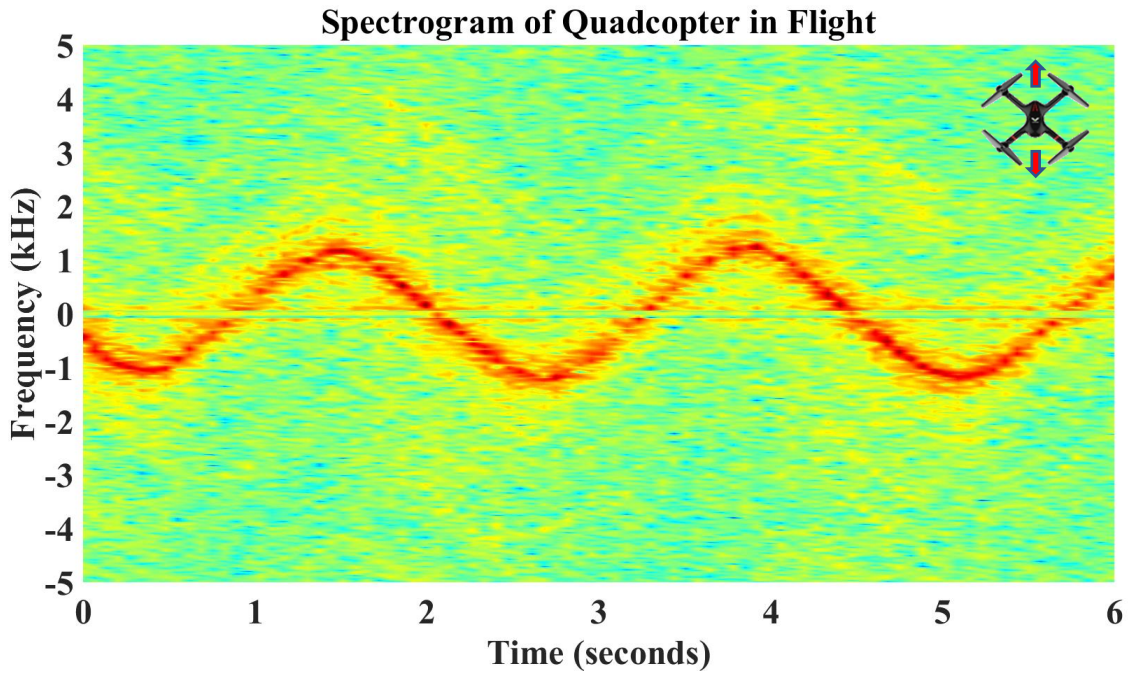

Figure 5.12. Spectrogram of the Hovering Quadcopter with Back and Forth Motion after Stationary Peak Subtraction.

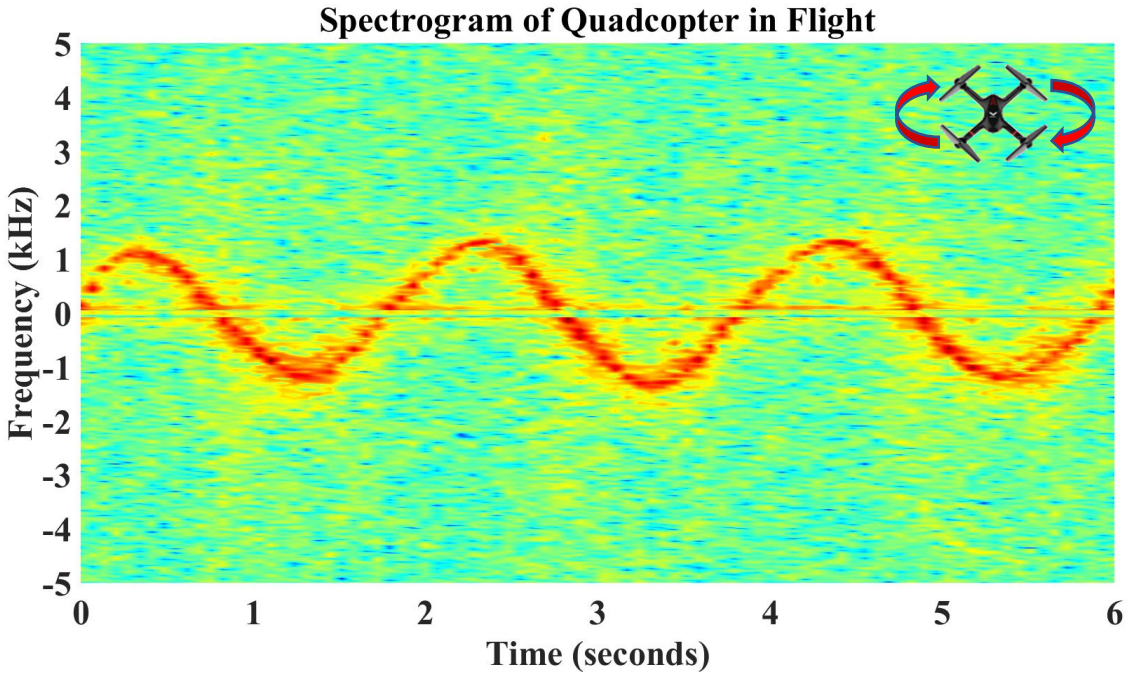

Figure 5.13. Spectrogram of the Hovering Quadcopter with Precession Motion after Stationary Peak Subtraction.

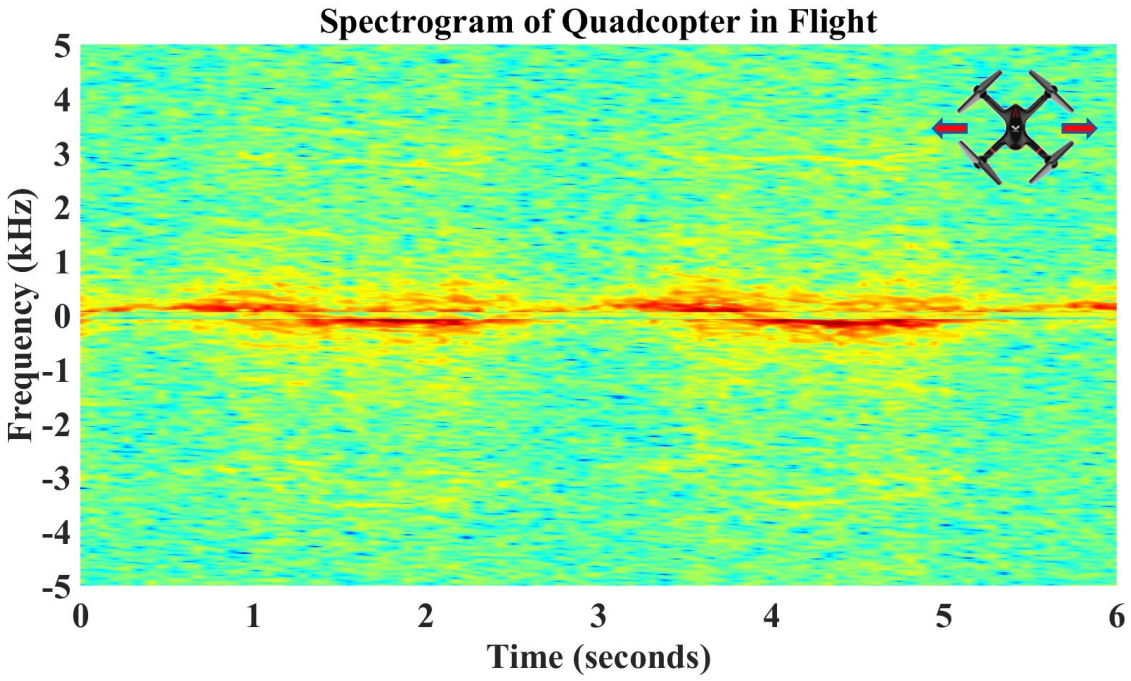

Figure 5.14. Spectrogram of the Hovering Quadcopter with Sideways Motion after Stationary Peak Subtraction.

The micro-Doppler modulations for precession and sideways motion after peak subtraction are shown in figures 5.13 and 5.14 respectively. While the back and forth motion and the precession motion induce additional sinusoidal modulation, the sideways motion does not induce additional modulation as it is perpendicular to the direction of the radar signal. As such, only the modulation due to rotation of the blades is seen. This modulation appears as a frequency spread along the sine wave and will not be present for the targets which do not have any rotational micromotions, such as birds. If the blades of the quadcopter are turned off and all these three motions are repeated manually, it would be tantamount to the case of considering the modulations from targets without rotation. To demonstrate this, the quadcopter is turned off and the spectrograms are obtained for the three cases as shown in figures 5.15 (a), (b) and (c).

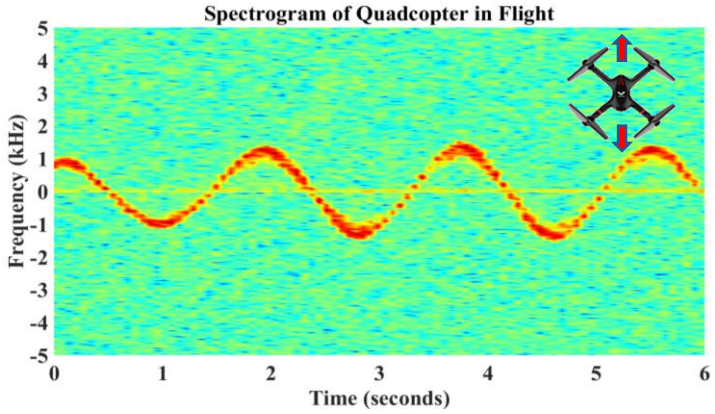

(a)

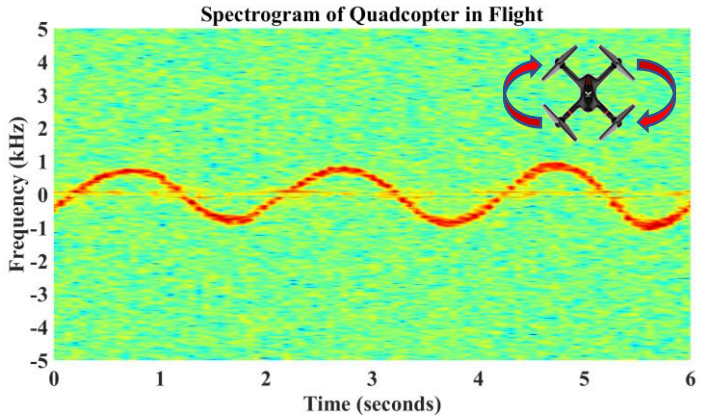

(b)

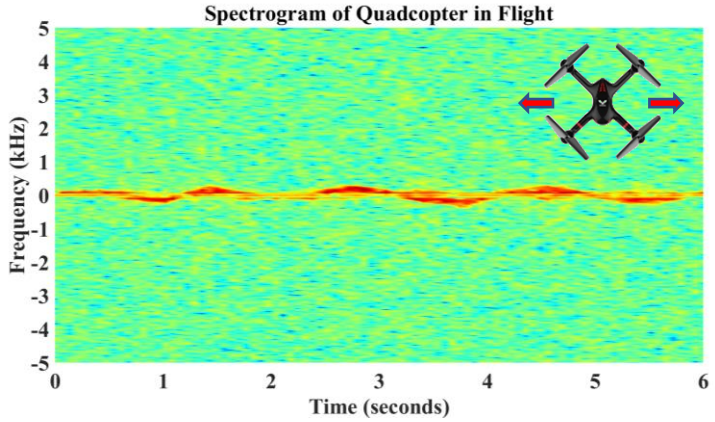

(c)

Figure 5.15. Spectrograms of the Quadcopter with Blades off: (a) Back and Forth, (b) Precession, (c) Sideways.

In practical scenarios, it might not always be the case that the quadcopter is always hovering in front of the radar. It might be out of the FoV of the radar at one instant, and might come into the FoV after some time. To demonstrate this, the quadcopter is made to move from out of FoV of the radar, into the FoV of the radar and the corresponding spectrograms are plotted in figures 5.16 (a), (b) and (c).

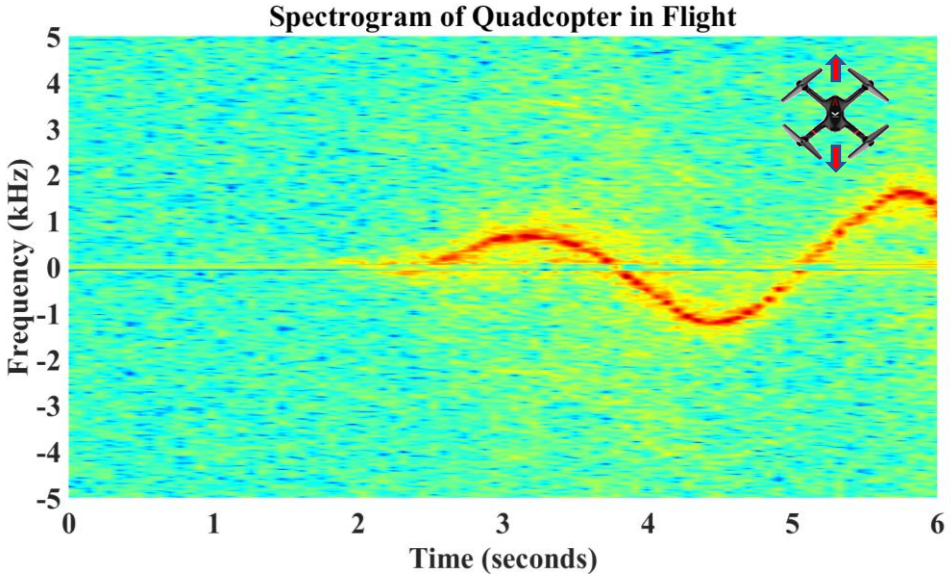

(a)

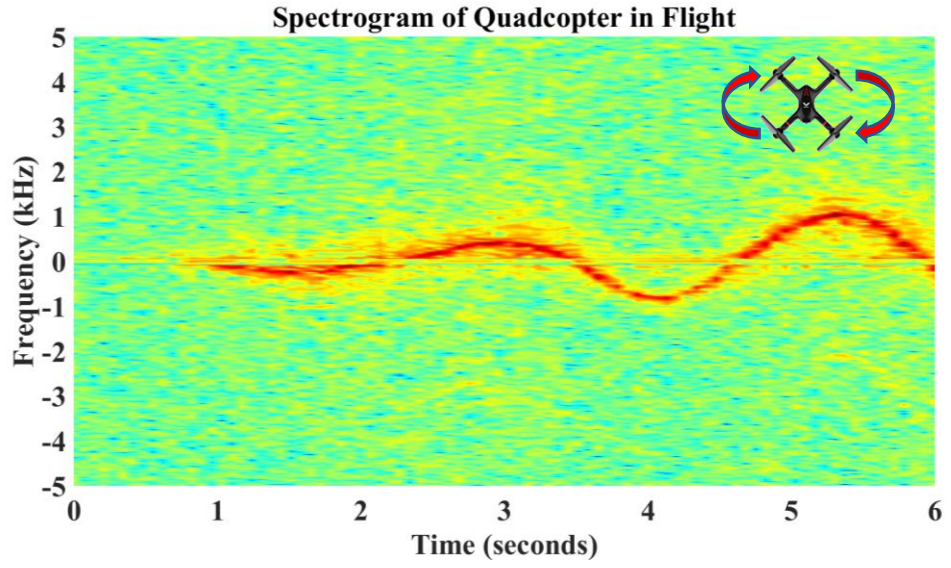

(b)

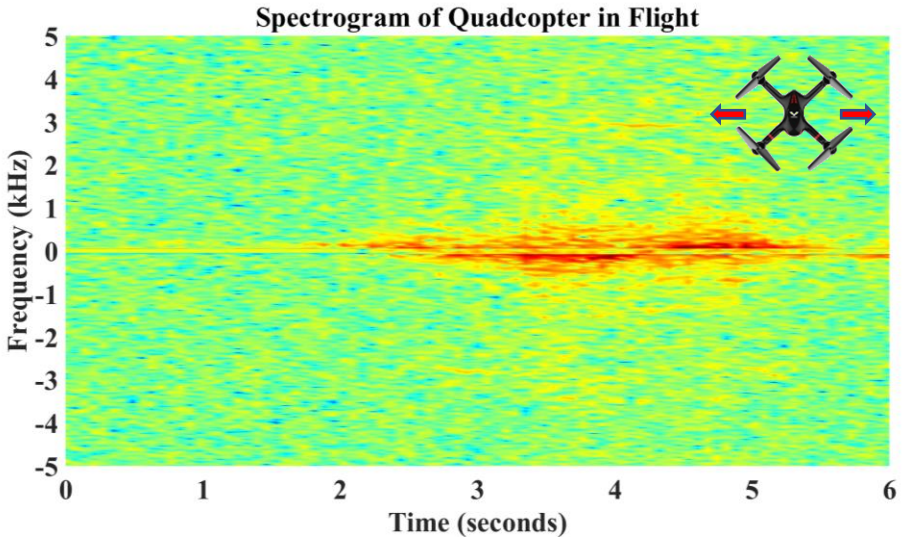

(c)

Figure 5.16. Spectrograms of the Quadcopter with Blades on entering the FoV from out of FoV for (a) Back and Forth, (b) Precession and (c) Sideways Motions.

If the blades are turned off and the quadcopter is made to enter the FoV manually, the obtained spectrogram will have much lower frequency spread. The additional modulations caused by the rotational micromotions will not be seen when the blades are off and this feature can be used for discerning between birds and quadcopters. This is shown in figures 5.17 (a), (b) and (c) respectively.

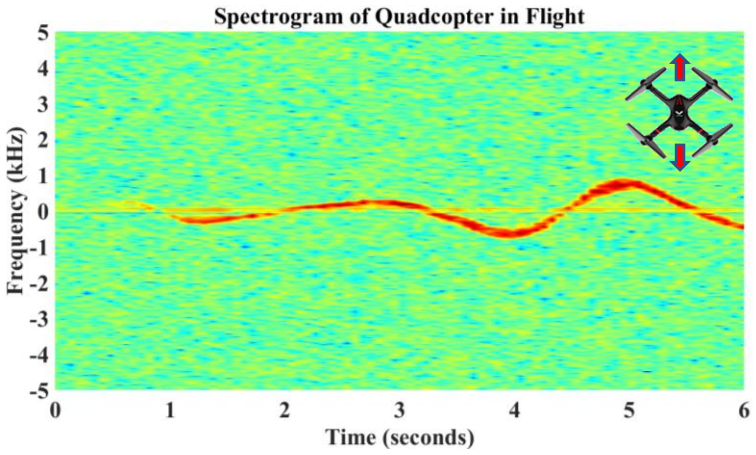

(a)

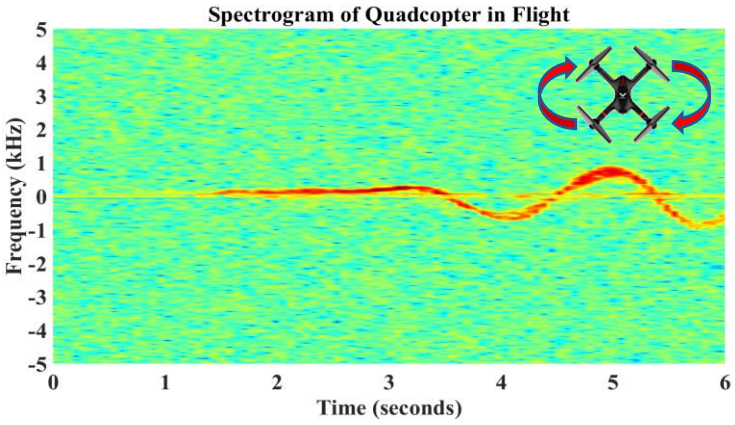

(b)

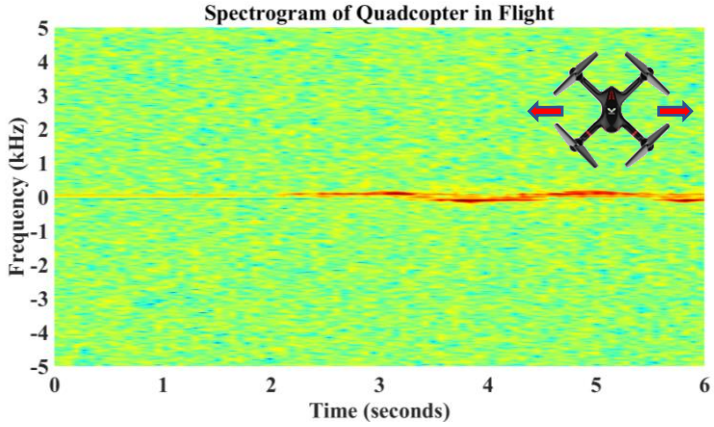

(c)

Figure 5.17. Spectrograms of the Quadcopter with Blades off entering the FoV from out of FoV for (a) Back and Forth, (b) Precession and (c) Sideways Motions.

5.3.2 Quadcopter at 2m and 3m from the Radar

The entire process is repeated for the distances of 2 m and 3 m, and the measurement results are presented in the next section. It will be seen that as the distance from the radar increases, the loss of signal power due to longer propagation path increases and results in lowering the frequency spread due to rotational micromotion. This is due to the low power handling capability of the THz system. The corresponding spectrograms for the 3 motions for the cases when blades are on and off are shown in figures 5.18 to 5.21.

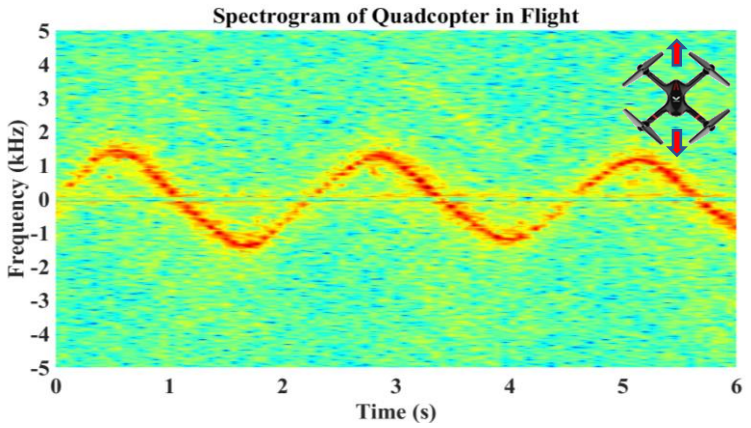

(a)

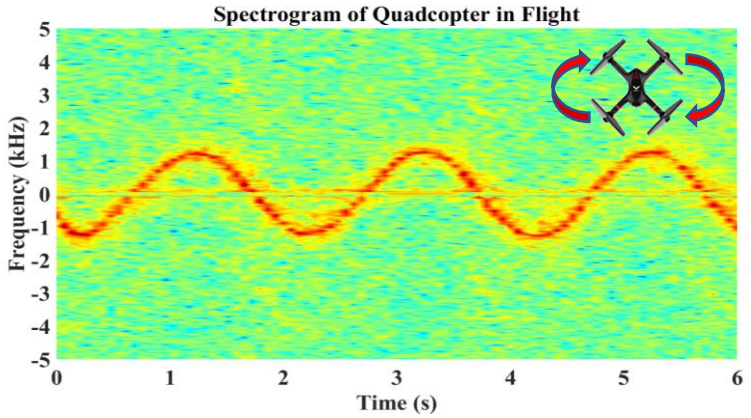

(b)

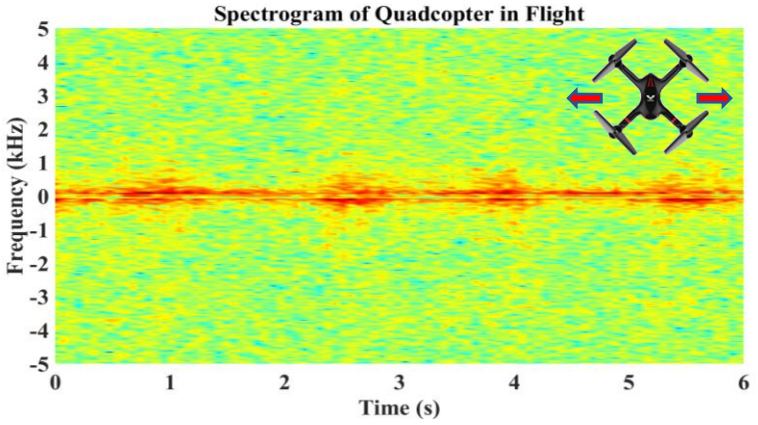

(c)

Figure 5.18. Spectrogram of the Quadcopter at 2m with Blades on for (a) Back and Forth, (b) Precession and (c) Sideways Motions.

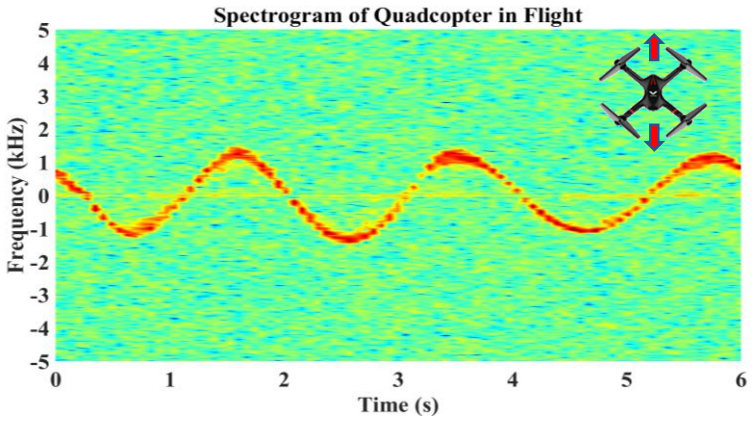

(a)

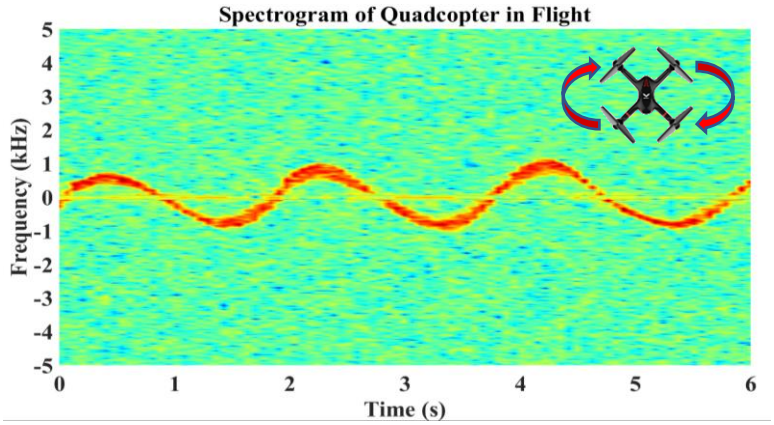

(b)

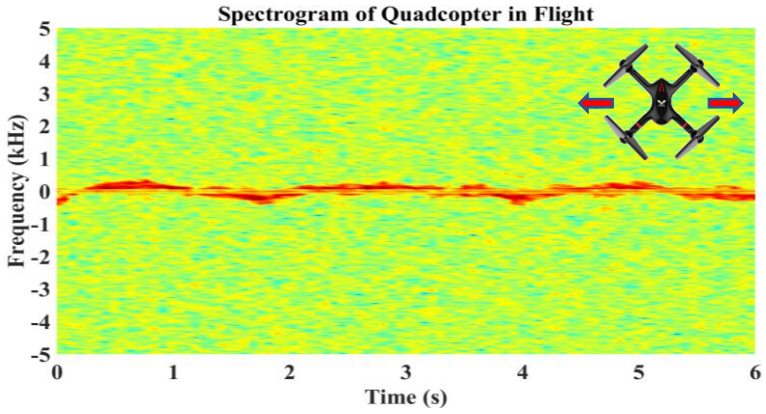

(c)

Figure 5.19. Spectrogram of the Quadcopter at 2m with Blades off for (a) Back and Forth, (b) Precession and (c) Sideways Motions.

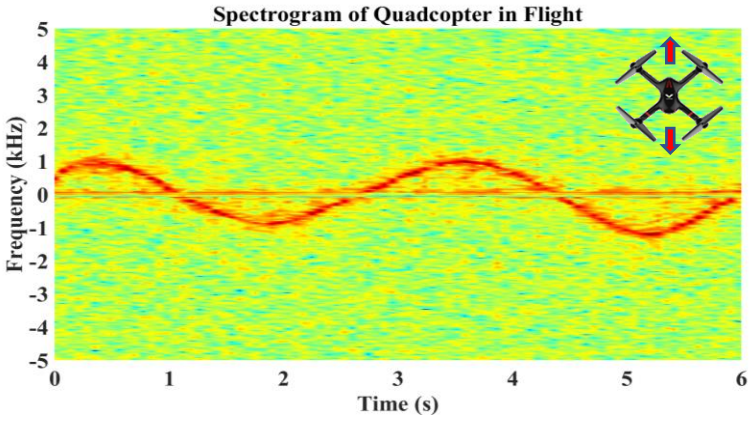

(a)

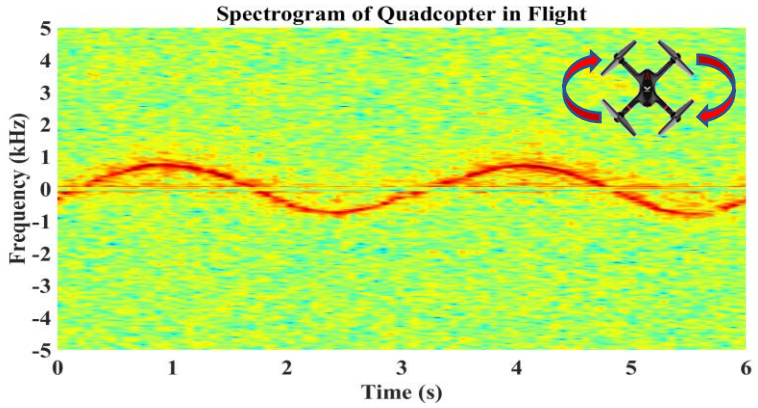

(b)

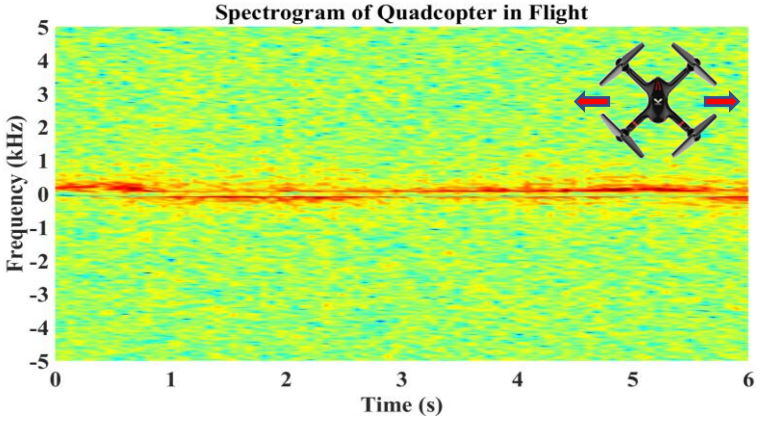

(c)

Figure 5.20. Spectrogram of the Quadcopter at 3m with Blades on for (a) Back and Forth, (b) Precession and (c) Sideways Motions.

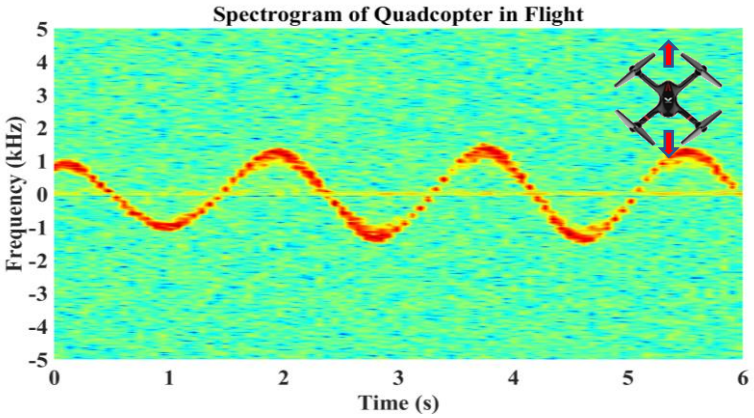

(a)

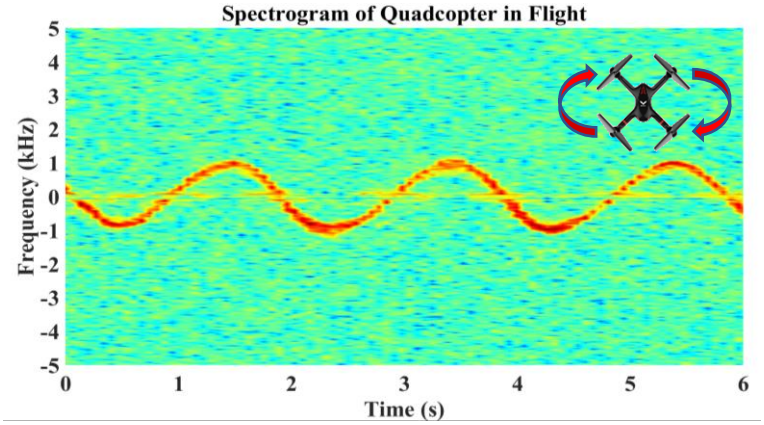

(b)

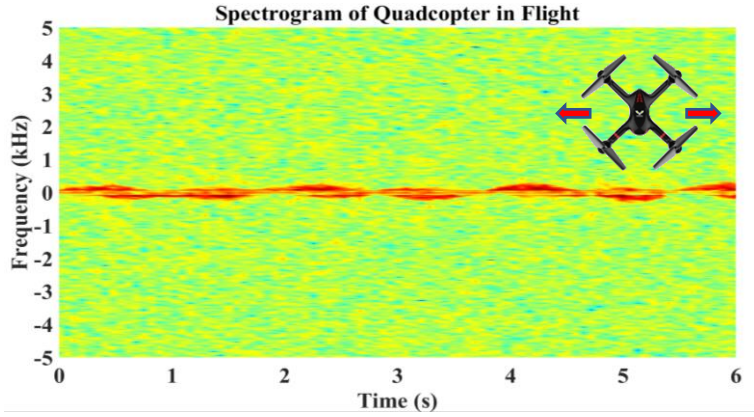

(c)

Figure 5.21. Spectrogram of the Quadcopter at 3m with Blades off for (a) Back and Forth, (b) Precession and (c) Sideways Motions.

The spectrograms of the quadcopter entering the FoV of the radar from out of its FoV also follow the similar trends as in figures 5.18 to 5.21 and thus not shown here. The difference in the frequency spread between the case when the quadcopter blades are on and when the quadcopter blades are off is analyzed to discern the quadcopters from other targets without rotational motion. Two methods have been used for the analysis and both the methods provide promising results for the characterization of quadcopters.

In the first method, the average power in the spectrogram is calculated for each case, and a comparison graph is plotted. The average power in the spectrogram is considerably higher when the blades are on as compared to when the blades of off. The graphs are shown in figure 5.22. Since the power levels are in negative dBm, the graphs are shown upside down. The black line marks the lowest power level when the blades are on which is greater than the case when the blades are off for all the three motions. The decrease in the power level of the received signal is seen to be pronounced at 3m where the power levels drop drastically. This is again due to the low power handling capability of the THz systems and needs to be addressed in the future work.

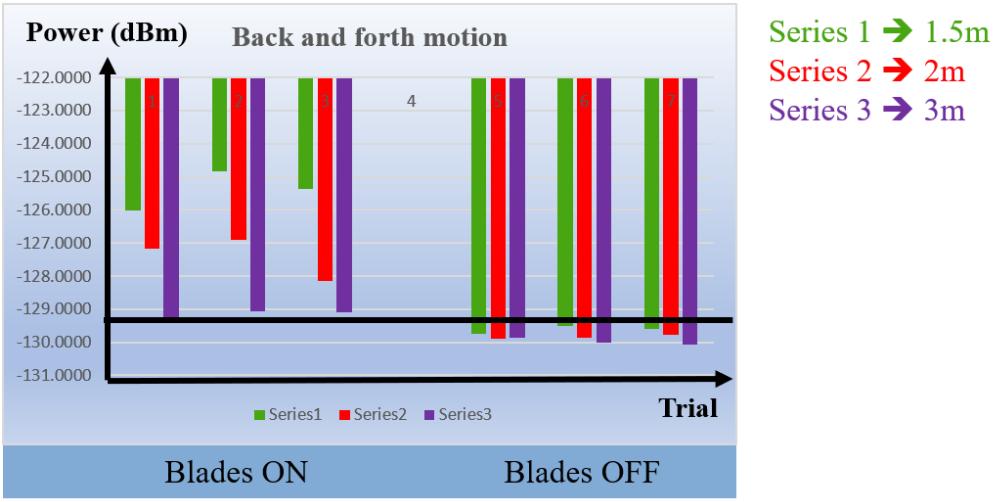

(a)

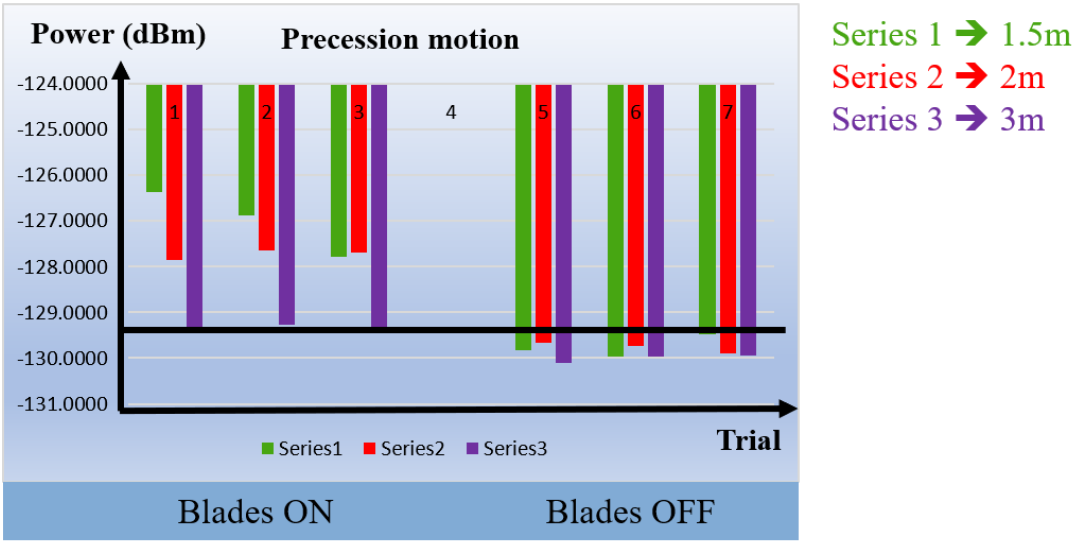

(b)

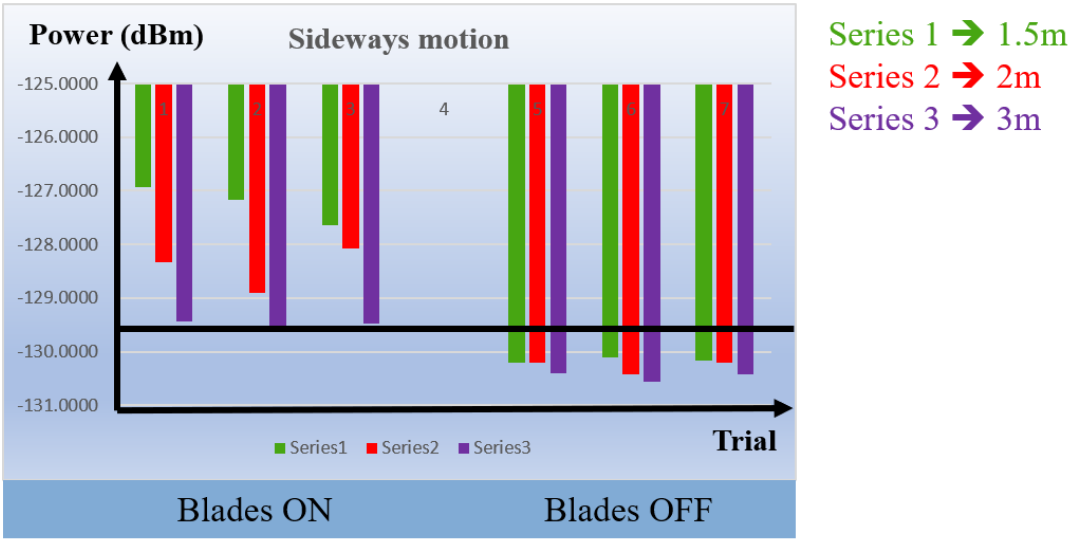

(c)

Figure 5.22. Graphs for Comparing the Average Power in the Spectrogram when the Quadcopter has Blades on and Blades off at 1.5 m, 2 m and 3 m, for (a) Back and Forth, (b) Precession and (c) Sideways Motions.

The second method uses the variance of the spectrum to quantify the frequency spread. A gaussian beam is fitted on to the data in each cross section of the frequency

spectrum and the average variance is calculated. An arbitrary duration of 1 s is considered for the variance calculation as was done for the calculation of the average power in the spectrogram. A higher variance is achieved for the case with blades on as compared to the case with blades off as expected. These values are plotted in the graphs for each of the three motions as shown in figure 5.23.

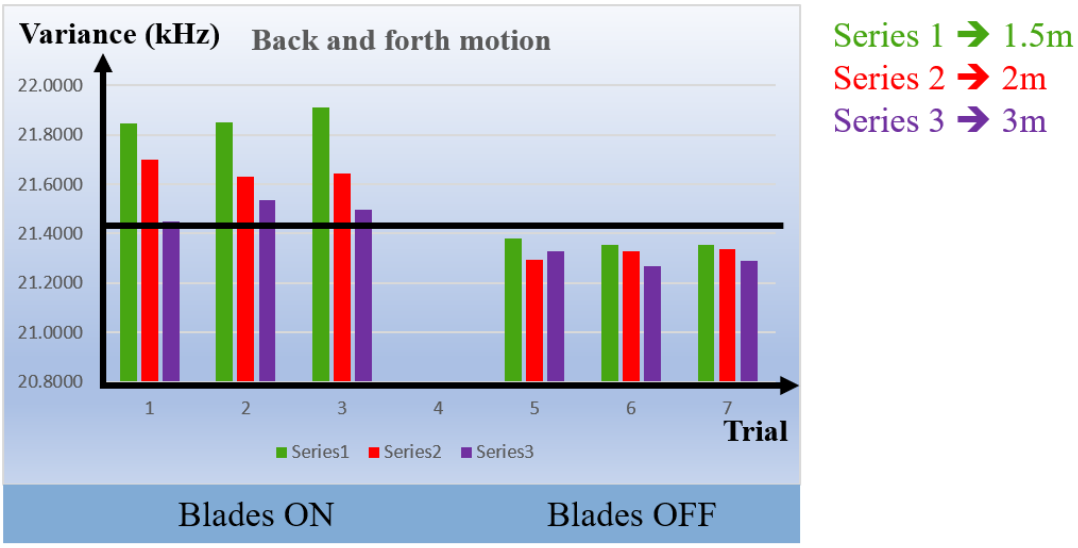

(a)

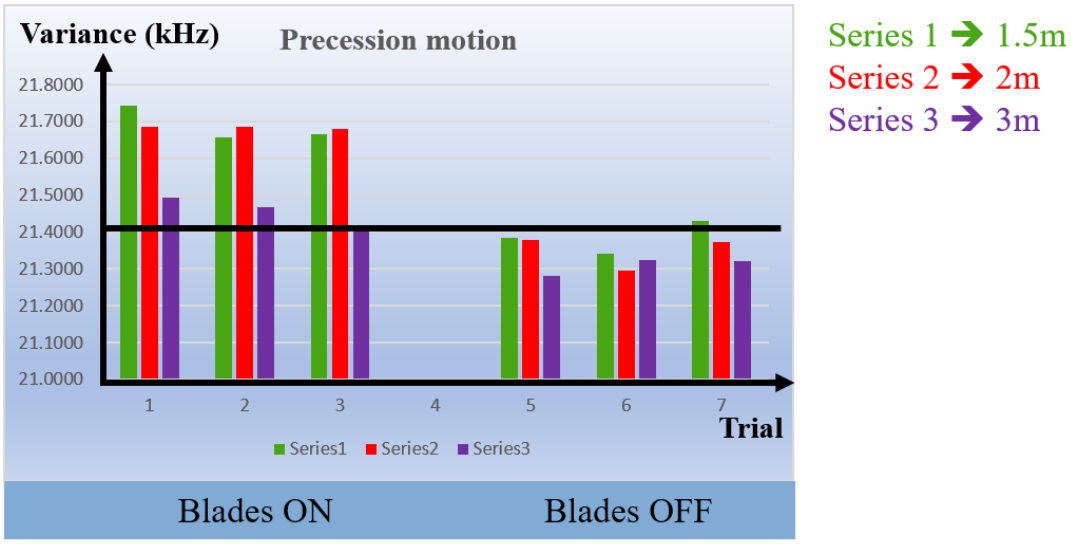

(b)

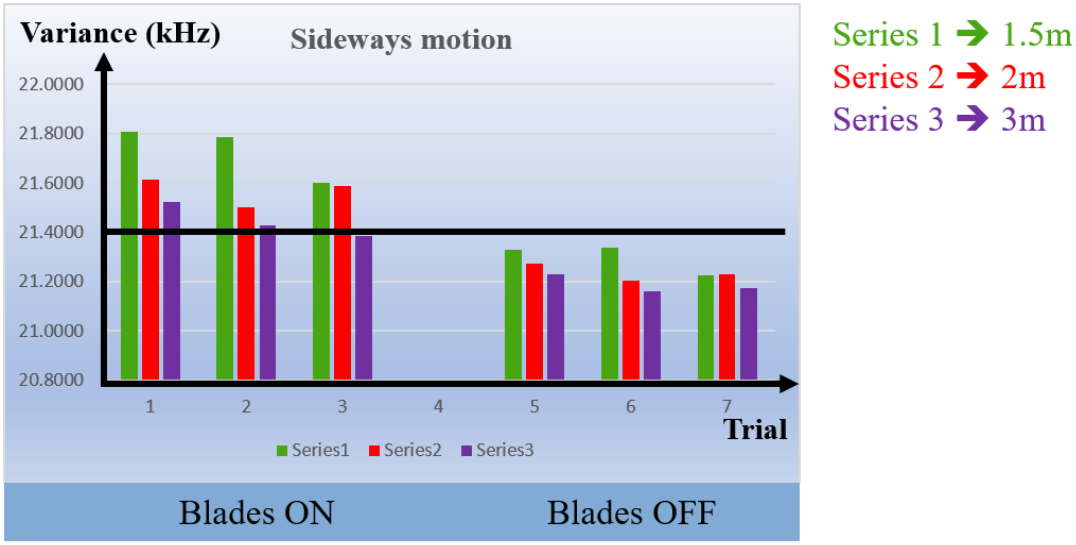

(c)

Figure 5.23. Graphs for Comparing the Average Variance of the Spectrogram when the Quadcopter has Blades on and Blades off at 1.5 m, 2 m and 3 m, for (a) Back and Forth, (b) Precession and (c) Sideways Motions.

5.4 Conclusions

The analysis indicates that by using the average power and the variance data, the quadcopters can be distinguished from birds and other targets that do not have the rotational micromotions. However, both these analysis methods depend on the power of the received signal. This makes the power and variance values of the case with blades on at 3 m close to the values with blades off at 1.5 m. So, if the distance increases, the power and the variance values for the case when blades are on decrease further and might lead to ambiguous results, and thus, puts a limit on the maximum distance for successful operation of the current system. As a result, a more robust analysis method must be developed which does not depend on the power levels. One such method calculates the variance of a normalized Gaussian curve. This will be considered for future work.

CHAPTER 6

SUMMARY AND FUTURE WORK

6.1 Summary

In this work, a THz micro-Doppler radar is designed for detecting and characterizing the quadcopters, or any multicopter in general, based on their micromotions. A summary of the radar-based detection schemes is presented, and the advantages of using the radar-based detection techniques is outlined. THz systems offer the advantages of higher resolution than the microwave systems, which is beneficial for the extraction of micro-Doppler features. As a result, the radar was designed to operate at a low-THz frequency of 270 GHz using continuous-wave Doppler radar principles in a monostatic configuration. A 15 GHz RF signal was generated by Rhode and Schwarz VNA and upconverted to 270 GHz using a frequency extender. A DROCON X708W quadcopter was used as the target for measurements. It is an X4 configuration quadcopter containing four two-blade propellers. The reflected signal from the quadcopter was down converted to 279 MHz for display and analysis. Two of the micromotions of the quadcopters are particularly focused: one is the vibrational and the other is the rotational micromotion, as these are the two motions that separate the quadcopters from other targets.

Since the micro-Doppler modulations are time varying, they cannot be analyzed using Fourier transforms. Time-frequency analysis methods must be used which have good resolution in both time and frequency. A linear time-frequency transform, the short-time Fourier transform (STFT) was used in this work to analyze the micro-Doppler modulations. Theoretical analysis of the micro-Doppler modulations induced by vibrational and

rotational micromotions is presented along with the analytical equations used to calculate these modulations. A point scatterer model was used to model a single propeller of the quadcopter and using Matlab, and the modulations induced by the rotation of propellers were plotted in the time-frequency domain. The back and forth/ precession motion and the rotational micromotions were first analyzed separately, and then, the effect of both these motions together was studied.

A Matlab code has been developed using SCPI commands to automate the measurement process exploiting the remote-control feature of the VNA and the signal analyzer. The measurements were carried out for detecting the micro-Doppler modulations due to vibrational and rotational micromotions seen in quadcopters using the THz micro-Doppler radar. The modulations induced when the quadcopter is stationary and when it is in flight are shown using various spectrograms. It is shown that the vibration induced micromotions cannot be detected at distances longer than 0.5 m using the power levels employed in the system and thus, only the micro-Doppler modulations induced by the rotational micromotion when the drone is hovering in front of the radar are presented. Three distances were considered for measurement; 1.5 m, 2 m and 3 m along with three types of motions the drone can have while hovering; the back and forth motion, the precession motion and the sideways motion. Spectrograms were obtained for each case and a comparison of the situations when the blades of the quadcopter are on and when the blades of the quadcopter are off is also provided. Two methods were used to characterize frequency spread induced by the rotational micromotion of the blades of the quadcopter; the first method used the average power in the spectrum at a particular instant of time while the second method used the variance of the spectrum at any given time. It was shown

through bar graphs that using both methods, a higher power or variance is obtained when the propellers are on as compared to when the propellers are off. Thus, either the average power or the variance data could be used to distinguish the quadcopter from targets which do not have rotational micromotions. The challenges with the existing measurement methodology were also outlined and suggestions were made for improvements of current techniques.

6.2 Future Work

The most important challenge with the use of THz system is the low power handling capability of the system. In all the measurements, the peak power of the received signal is around -85 dBm and this decreases as the distance from the radar increases. The quadcopters are characterized by small radar cross sections which reduces the reflections from them when they are used as the targets. Along with this, since most of the commonly used quadcopters have a plastic or carbon fiber body, which are not as reflective as the conducting materials, there is additional loss of signal power as it propagates from the radar to the quadcopter and back to the radar. An effective solution would be to use high power sources such as the vacuum electronic devices which can generate powers up to 1 kW at 300 GHz using variants of backward wave oscillators (BWO) called the clinotron and orotron [39].

The second problem occurs due to the design of the propeller blades. As the blades are curved in shape with the radius of curvature increasing towards the tip of the blades, the tips of the blades are flat which makes them appear as thin lines with negligible cross sections to the radar. This, combined with the low operating power, leads to the loss of the reflections from these parts of the blades, and it was evidenced in the measurement results

of this work as well. While the theoretical analysis predicted around 13 kHz of frequency shift, the frequency shift was of the order of few kHz in the measured spectrogram. Since the tips of the blades have the highest velocity and are responsible for the maximum frequency shift, loss of signals from these parts of the blades lowers the detectable frequency shift. The signals are lost within the noise floor of the signal analyzer and become undetectable. This is the reason for the reduced frequency shift from the rotational micromotion in the measurements. However, a very good correlation was achieved between the theoretical and practical results for the back and forth and the precession motion. In both cases, the frequency shift is around 1 kHz. Thus, the future work will focus on viewing the propellers of the quadcopter at an angle, rather than looking at the propellers directly. The down conversion of the 270 GHz signal to 279 MHz generated intermodulation products at about ±13 kHz from the center frequency. As a result, the measurement span was restricted to 10 kHz in this work. Filtering techniques will be employed in the future work to eliminate these products so that higher power components of the reflected signal can be traced.

The measurements are limited by the operating speeds of the VNA and the signal analyzer and thus, using just the short-time Fourier transform is not enough to extract the micro-Doppler modulations caused by rotation. Bilinear time-frequency transforms will be considered in the future to extract these components.

Finally, the analysis used for distinguishing the quadcopters from other targets with not rotational micromotions, relies on the received signal power. Future work will focus on eliminating the power dependency and developing more sophisticated analysis methods.

REFERENCES

[1] V. C. Chen, F. Li, S.-S. Ho, and H. Wechsler, "Analysis of Micro-Doppler Signatures," *IEEE Proceedings – Radar, Sonar and Navigation*, vol. 150, no. 4, pp. 271-276, 2003.

[2] V. C. Chen, F. Li, S.-S. Ho, and H. Wechsler, "Micro-Doppler effect in radar: phenomenon, model and simulation study," IEEE transactions on Aerospace and Electronic Systems, vol. 32, no. 1, pp. 2-21, 2006.

[3] T. Sparr, and B. Krane, "Micro-Doppler Analysis of Vibrating Targets in SAR," *IEEE Proceedings – Radar, Sonar and Navigation*, vol. 150, no. 4, pp. 277-283, 2003.

[4] P. Suresh, T. Thayaparan, T. Obulesu, and K. Venkataramaniah, "Extracting Micro-Doppler Radar Signatures from Rotating Targets using Fourier – Bessel Transform and Time – Frequency Analysis," *IEEE Transactions on Geoscience and Remote Sensing*, vol. 52, no. 6, pp. 3204-3210, 2014.

[5] I. Djurovic, V. Popovic-Bugarin, and M. Simeunovic, "The STFT – Based Estimator of Micro-Doppler Parameters," *IEEE Transactions on Aerospace and Electronic Systems*, vol. 53, no. 3, pp. 1273-1283, 2017.

[6] H. Gao, L. Xie, S. Wen, and Y. Kuang, "Micro-Doppler Signature Extraction from Ballistic Target with Micromotions," *IEEE Transactions on Aerospace and Electronic Systems*, vol. 46, no. 4, pp. 1969-1982, 2010.

[7] T. Thayaparan, S. Abrol, E. Riseborough, L. Stankovic, D. Lamothe, and G. Duff, "Analysis of Radar micro-Doppler Signatures from Experimental Helicopter and Human Data," *IET Radar, Sonar & Navigation*, vol. 1, no. 4, pp. 288-299, 2007.

[8] B. Karlsson, "Modeling Multicopter Radar Return," Master's thesis, Chalmers University of Technology, Gothenberg, Sweden, 2017.

[9] A. K. Singh, and Y. H. Kim, "Automatic Measurement of Blade Length and Rotation Rate of Drone using W-Band Micro-Doppler Radar," *IEEE Sensors Journal*, vol. 18, no. 5, pp. 1895-1902, 2018.

[10] L. Ren *et al*., "Short-Time State-Space Method for Micro-Doppler Identification of Walking Subject using UWB Impulse Doppler Radar," *IEEE Transactions on Microwave Theory and Techniques*, vol. PP, no. 99, pp. 1-14, 2018.

[11] R. D. E. Marchetti, F. Norouzian, M. Gashinova, and M. Cherniakov, "Micro-Doppler Signature of Pedestrian walking on spot at low-terahertz frequencies," *International Conference on Radar Systems*, 2018.

[12] P. H. Siegel, "Terahertz Technology," *IEEE Transactions on Microwave Theory and Techniques*, vol. 50, no. 3, pp. 910-928, 2002.

[13] Y. S. Lee, *Principles of Terahertz Science and Technology*. Taylor and Francis, 2012.

[14] G. C. Trichopoulos, "Antennas for Terahertz Applications: Focal Plane Arrays and On-chip Non-Contact Measurement Probes", Ph.D. dissertation, OSU, Columbus, OH, USA, 2013.

[15] E. R. Brown, "Fundamentals of Terrestrial Millimeter-Wave and THz Remote Sensing", *International Journal of High Speed Electronics and Systems*, vol. 13, pp. 995-1098, 2003.

[16] H. B. Liu, H. Zhong, N. Karpowicz, Y. Chen, and X. C. Zhang, "Terahertz Spectroscopy and Imaging for Defense and Security Applications," *Proceedings of IEEE*, vol. 95, no. 8, pp.1514-1527, 2007.

[17] C. Baker *et al*., "Detection of Concealed Explosives at a Distance Using Terahertz Technology," *Proceedings of IEEE*, vol. 95, no. 8, pp. 1559-1565, 2007.

[18] B. St. Peter *et al*., "Development and Testing of a Single Freq THz imaging system for breast cancer detection," *IEEE Journal of Biomedical and Health Informatics*, vol. 17, no. 4, pp. 785-797, 2013.

[19] H. Breitenbom *et al*., "Terahertz Spectral Imaging and Thermal Sensing for Biomedical Applications," *42nd International Conference on Infrared, Millimeter, and Terahertz Waves (IRMMW-THz)*, 2017.

[20] D. M. Hailu, D. Saeedkia, "Novel Applications of Terahertz Technology for the Plastic Industry," *41st International Conference on Infrared, Millimeter, and Terahertz Waves (IRMMW-THz)*, 2016.

[21] K. C. Huang, Z. Wang, "Terahertz Terabit Wireless Communication," *IEEE Microwave Magazine*, vol. 12, no. 4, pp. 108-116, 2011.

[22] V. Petrov *et al*., "Terahertz Band Communications: Applications, Research Challenges, and Standardization Activities," *8th International Congress on Ultra-Modern Telecommunications and Control Systems and Workshops (ICUMT)*, 2016.

[23] P. de Maagt, "Terahertz, Technology for space and earth applications," *First European Conference on Antennas and Propagation*, 2006.

[24] T.K. Sarkar, M. S. Palma, and E. L. Mokole, "Echoing Across the Years: A History of Early Radar Evolution," *IEEE Microwave Magazine*, vol. 17, no. 10, pp. 46-50, 2016.

[25] M. I. Skolnik, *Introduction to Radar Systems*. McGraw – Hill, 2001.

[26] F. E. Nathanson, J. P. Reilly, M. N. Cohen, *Radar Design Principles: Signal Processing and the Environment*. McGraw – Hill, 1991.

[27] M. I. Skolnik, *Radar Handbook*. McGraw – Hill, 2008.

[28] F. B. Berger, "The Nature of Doppler Velocity Measurement," *IRE Transactions on Aeronautical and Navigational Electronics*, vol. ANE-4, no. 3, pp. 103-112, 1957.

[29] M. A, Richards, J. Scheer, W.A. Holm, *Principles of Modern Radar. Volume1, Basic Principles*. SciTech Pub., 2010.

[30] C. A. Balanis, *Antenna Theory: Analysis and Design*. John Wiley & Sons, 2016.

[31] S. Ramalingam, C. A. Balanis, C.R. Birtcher, S. Pandi, H. N. Shaman, "Axially Modulated Cylindrical Metasurface Leaky-Wave Antennas," *IEEE Antennas and Wireless Propagation Letters*, vol. 17, no. 1, pp. 130-133, 2018.

[32] F. Yang, Y. Rahmat-Samii, "Microstrip Antennas Integrated with Electromagnetic Band-Gap (EBG) Structures: A Low Mutual Coupling Design for Array Applications," *IEEE Transactions on Antennas and Propagation*, vol. 51, no. 10, pp. 2936-2946, 2003.

[33] S. Doughty, K. Woodbridge, and C. Baker, "Characterization of a Multistatic Radar System," *Proceedings of 3rd European Radar Conference*, 2006.

[34] *Navy Electricity and Electronics Training Series: Module 18 – Radar Principles*. 1998.

[35] *R&S ZVA, R&S ZVB, R&S ZVT Operating Manual*, Rhode and Schwarz, Germany, 2016.

[36] *VNA Extension Modules Operating Manual*, Virginia Diodes, Inc., Charlottesville, VA, 2018.

[37] J. R. Moon, "A survey of bird flight data relevant to radar tracking systems," Radar, 2002.

[38] L. Cohen, *Time-Frequency Analysis*. Prentice-Hall, 1995.

[39] J.H. Bookse *et al*., "Vacuum Electronic High Power Terahertz Sources," *IEEE Transactions on Terahertz Science and Technology*, vol. 1, no. 1, pp. 54-75, 2011.

APPENDIX A

MATLAB CODE FOR REMOTE CONTROL OF SIGNAL ANALYZER

```
%************************************************************************%
%************************************************************************%
% This code can ne used to connect to any signal or spectrum analyzer and
% extract the data from it. Here the analyzer used is Keysight N9020A.
% The code also mimics the signal analyzer screen dynamically updating
% the data as seen on the analyzer.
% The spectrum data obtained from each sweep is stored in memory and the
% time-frequency representation of the entire measurement duration is
% finally plotted.
% A waterfall plot can also be plotted to see the variations over time.
%************************************************************************%
%************************************************************************%

clc
close all
clear all

% To clear the instruments in memory
instrument = instrfind;
if ~isempty(instrument);
    fclose(instrument);
    delete(instrument);
    clear i1;
end

N9020A_sa = visa ('ni', 'TCPIP0::169.254.2.208::inst0::INSTR');

set(N9020A_sa, 'InputBufferSize', 1e6);
fopen(N9020A_sa);
Identity = query(N9020A_sa, '*IDN?')
fprintf(N9020A_sa, '*RST');
fprintf(N9020A_sa, ':FORM:DATA REAL,32');

% Setting the center frequency, span, reference level
fprintf(N9020A_sa, ':FREQ:CENT 279.002106 MHz'); % Previously used 279.00135,
278.996, 278.9977 278.999 LO drift
freq_cent = str2double(query(N9020A_sa,':FREQ:CENT?'));
fprintf('Center Frequency: %.5f MHz\n', freq_cent/1e6);
fprintf(N9020A_sa, ':FREQ:SPAN 12 kHz');
freq_span = str2double(query(N9020A_sa,':FREQ:SPAN?'));
fprintf('Frequency span: %d kHz\n', freq_span/1e3);
fprintf(N9020A_sa, ':DISP:WIND:TRAC:Y:RLEV -50');
ref_lev = str2double(query(N9020A_sa, ':DISP:WIND:TRAC:Y:RLEV?'));
fprintf('Reference Level: %d\n', ref_lev);
```

```
% To find RBW, VBW and sweep time
fprintf(N9020A_sa, ':BAND:RES 50 Hz');
rbw = str2double(query(N9020A_sa, ':BAND:RES?'));
fprintf('Resolution Bandwidth: %d Hz\n', rbw);
fprintf(N9020A_sa, ':BAND:Video 50 Hz');
vbw = str2double(query(N9020A_sa, ':BAND:VIDeo?'));
fprintf('Video Bandwidth: %d Hz\n', vbw);
swp_time = str2double(query(N9020A_sa, ':SWE:TIME?'));
fprintf('Sweep Time: %.3f ms\n',round(swp_time*1000,3));

% To find/set the number of sweep points
% fprintf(E4440A_sa, ':SWE:POIN 201');
num_pts = str2double(query(N9020A_sa, ':SWE:POIN?'));
fprintf('Number of Sweep Points: %d\n', num_pts);

% freq_axis = (freq_cent - freq_span/2 : freq_span/(num_pts-1): freq_cent +
freq_span/2)/1e6;
freq_axis = (-freq_span/2: freq_span/(num_pts-1): freq_span/2)/1e3;
fstart = (- freq_span/2)/1e3;
fstop = (freq_span/2)/1e3;

% To select the mode, format and to get the entire trace
fprintf(N9020A_sa, ':INIT:CONT OFF'); % To put the instrument in continuous mode
fprintf(N9020A_sa, ':INIT:IMM;*wai'); % To start a sweep and wait till it finishes
fprintf(N9020A_sa, ':FORM:BORD SWAP'); % To swap from Little Endian and Big
Endian

figure (1) % Used to mimic the screen of the spectrum analyzer
ph = plot(1:num_pts, ref_lev*ones(1,length(freq_axis))); % To create a plot handle and
draw a line at the reference level
xlim([1 num_pts]);
ylim([ref_lev-140 ref_lev]);
grid on;
curr_fig = gcf;
set(findall(curr_fig, '-property', 'FontSize'),'FontSize', 10, 'fontWeight', 'bold');
title('Swept SA Trace', 'fontweight', 'bold', 'fontsize', 14);
xlabel('Frequency Point Index', 'fontweight', 'bold', 'fontsize', 12);
ylabel('Amplitude (dBm)', 'fontweight', 'bold', 'fontsize', 12);

num_traces = 100;
spectrum = zeros(num_traces,num_pts);

tic;

for i=1:num_traces % Indicates the number of traces that will be acquired
```

```
    fprintf(N9020A_sa, ':TRAC? TRACE1');
    data = binblockread(N9020A_sa, 'float32');
    spectrum(i,:) = data;
    fscanf(N9020A_sa);
    set(ph,'Ydata', data);
    drawnow;
    fprintf(N9020A_sa, ':INIT:IMM; *wai'); % To start a sweep and wait till it finishes
end
Elapsed_time = toc % tic - toc: gives the total time the code has run

time_axis = 0e-3:Elapsed_time/(num_traces-1): Elapsed_time;

figure('units','normalized','outerposition',[0 0 1 1])
surf(time_axis, freq_axis, spectrum') % To get a surface plot
curr_fig = gca;
set(findall(curr_fig, '-property', 'FontSize'),'FontSize', 16, 'fontWeight', 'bold');
title(Spectrogram of the Quadcopter, 'fontweight', 'bold', 'fontsize', 18);
xlabel('Time (seconds)', 'fontweight', 'bold', 'fontsize', 16);
ylabel('Frequency (kHz)', 'fontweight', 'bold', 'fontsize', 16);
zlabel('Amplitude (dBm)', 'fontweight', 'bold', 'fontsize', 16);
view(2);
shading interp;
colormap jet;
xlim([0 round(Elapsed_time)-1])
ylim([fstart fstop])
curr_fig.YTick = ([fstart: 1:  fstop]);

figure(3); % 3-D waterfall plot of all acquired traces
waterfall(freq_axis, 1:num_traces, spectrum);
curr_fig = gcf;
set(findall(curr_fig, '-property', 'FontSize'),'FontSize', 10, 'fontWeight', 'bold');
title('Spectrogram of the Quadcopter, 'fontweight', 'bold', 'fontsize', 18);
xlabel('Frequency (MHz)', 'fontweight', 'bold', 'fontsize', 16);
ylabel('Trace Number', 'fontweight', 'bold', 'fontsize', 16);
zlabel('Amplitude (dBm)', 'fontweight', 'bold', 'fontsize', 16);
axis tight;

fclose(N9020A_sa);
delete(N9020A_sa);
clear E4440A_sa;
```

APPENDIX B

MATLAB CODE FOR CALCULATION OF MICRO-DOPPLER MODULATION INDUCED BY ROTATIONAL MICROMOTION TOGETHER WITH THE BACK AND FORTH MOTION, USING A SINGLE PROPELLER POINT SCATTERER MODEL

```
%*************************************************************************%
%*************************************************************************%
% This code calculates the instantaneous frequency shift caused by the
% rotation of the blades based on the position of the blades as they rotate
% on their axis.
% It also includes the modulation induced by the back and forth motion od
% the quadcopter body as it hovers.
%*************************************************************************%
%*************************************************************************%

clc
close all
clear all

format long;
%Inputs needed
vel1 = 1000; % rpm
vel2 = 0.2; % speed of back and forth motion
distance = 1; % distance to the front tip of the blade in meter
fv = vel2;
Dv = 1;

v = vel1*2*pi/60*6.9e-2;
f0 = 270e9;
c = 3e8;
t = linspace(0,360,601);
t1 = 0:6:90;
t2 = 84:-6:6;

% 0 to 90 degrees
lv1 = 7e-2*sind(t1);
lh1 = 7e-2*cosd(t1);    %or fliplr(lv1)
a1 = distance + 7e-2 - lh1;
theta_a1 = atand(lv1./a1); %angle made by radar signal to the horizontal
theta_a2 = 180 - t1-theta_a1;
theta_x1 = 360 - 90 - theta_a2; % actual angle between radar dignal and direction of
motion of target

% 90 to 180 degrees
lv2 = 7e-2*sind(t2);
lh2 = 7e-2*cosd(t2);    %or fliplr(lv1)
a2 = distance + 7e-2 + lh2;
theta_b1 = atand(lv2./a2); %angle made by radar signal to the horizontal
theta_b2 = 180 - t2-theta_b1;
```

```
theta_x2 = 90 + theta_b2; % actual angle between radar dignal and direction of motion of
target

% 180 to 270 degrees
lv3 = 7e-2*sind(t1);
lh3 = 7e-2*cosd(t1);    %or fliplr(lv1)
a3 = distance + 7e-2 + lh3;
theta_c1 = atand(lv3./a3); %angle made by radar signal to the horizontal
theta_c2 = 180 - t1-theta_c1;
theta_x3 = 90 - theta_c2; % actual angle between radar dignal and direction of motion of
target

% 270 to 360 degrees
lv4 = 7e-2*sind(t2);
lh4 = 7e-2*cosd(t2);    %or fliplr(lv1)
a4 = distance + 7e-2 - lh4;
theta_d1 = atand(lv4./a4); %angle made by radar signal to the horizontal
theta_d2 = 180 - t2-theta_d1;
theta_x4 = theta_d2 - 90; % actual angle between radar dignal and direction of motion of
target

time_axis = 0e-3:1e-3:600e-3;

figure('units','normalized','outerposition',[0 0 1 1]);
hold on;

for a = 0:v/30:v

   for b = 0e-3:1e-3:14e-3
      fd1 = (2*a*f0/c).*cosd(theta_x1);
   end

   for b = 16e-3:1e-3:30e-3
      fd2 = (2*a*f0/c).*cosd(theta_x2);
   end

   for b = 31e-3:1e-3:45e-3
      fd3 = (2*a*f0/c).*cosd(theta_x3);
   end

   for b = 46e-3:1e-3:60e-3
      fd4 = (2*a*f0/c).*cosd(theta_x4);
   end

% fd = 2*.5*270e9/3e8*10.*sind(t);
```

```
fd = 4*pi*f0*fv*Dv/c*cosd(2*pi*fv*t);


fda = [fd1,fd2,fd3,fd4];
fd_a = repmat(fda,1,10);
fd_a_plot = [fd_a fd1(1)]+fd;
fdb = [fd3,fd4,fd1,fd2];
fd_b = repmat(fdb,1,10);
fd_b_plot = [fd_b fd1(1)]+fd;


plot(time_axis,fd_a_plot/1e3, 'Linewidth', 4);
current_fig = gca;
set(findall(current_fig, '-property', 'FontSize'),'FontSize', 20, 'fontWeight', 'bold');
title('Spectrogram showing m-D features of Quadcopter Blades', 'fontweight', 'bold',
'fontsize', 22);
xlabel('Time (seconds)', 'fontweight', 'bold', 'fontsize', 20);
ylabel('Frequency (kHz)', 'fontweight', 'bold', 'fontsize', 20);
%ylim([-15e3 15e3]);
% comet(time_axis, fd_a_plot);

plot(time_axis,fd_b_plot/1e3, 'Linewidth', 4);
current_fig = gca;
set(findall(current_fig, '-property', 'FontSize'),'FontSize', 20, 'fontWeight', 'bold');
title('Spectrogram showing m-D features of Quadcopter Blades', 'fontweight', 'bold',
'fontsize', 22);
xlabel('Time (seconds)', 'fontweight', 'bold', 'fontsize', 20);
ylabel('Frequency (kHz)', 'fontweight', 'bold', 'fontsize', 20);
colormap jet;
% comet(time_axis, fd_b_plot);
%ylim([-15e3 15e3]);
end
```